

# Fluids – Lecture 1 Notes

## 1. Formation of Lifting Flow

Reading: Anderson 4.5 – 4.6

## Formation of Lifting Flow

### Conservation of Circulation — Kelvin's Theorem

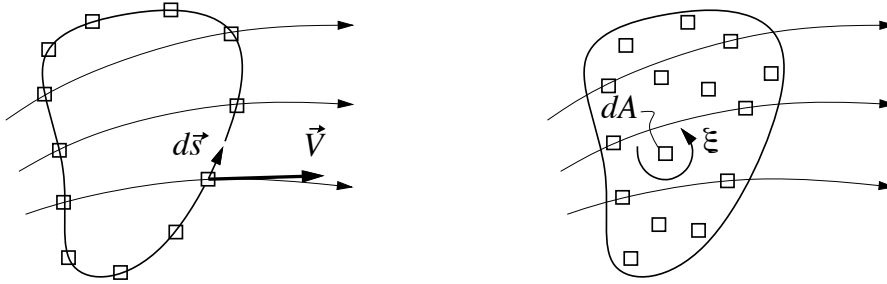
The circulation about any closed circuit is defined to be

$$\Gamma \equiv - \oint \vec{V} \cdot d\vec{s} = - \iint \vec{\xi} \cdot \hat{n} dA$$

where  $d\vec{s}$  is an arc length element of the circuit, and  $\vec{V}$  is the local flow velocity. The equivalent vorticity area integral form follows from Stokes Theorem. In 2-D, this second form is

$$\Gamma = - \iint \xi dA \quad (\text{In 2-D})$$

To investigate the formation of a lifting flow about an airfoil, we now consider the circulation  $\Gamma$  about a circuit demarked by fluid elements which are drifting with the flow (a fine smoke ring would constitute such a circuit). Because both the shape of the circuit and the velocities



seen by the circuit will in general change in time, there is the possibility that  $\Gamma(t)$  will change in time as well. The rate of change of this circulation is

$$\frac{d\Gamma}{dt} = - \frac{d}{dt} \iint \xi dA = - \iint \frac{D}{Dt} (\xi dA)$$

where the substantial derivative has been invoked because we are seeking a time rate of change in a frame moving with the fluid. For low speed 2-D flows where density is effectively constant, the area  $dA$  of a fluid element cannot change because of conservation of mass. Hence we have

$$\frac{d\Gamma}{dt} = - \iint \frac{D\xi}{Dt} dA$$

But by the 2-D Helmholtz Theorem,

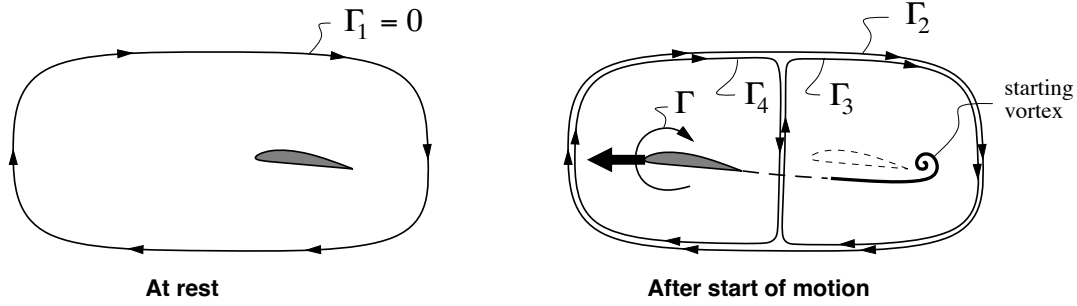
$$\frac{D\xi}{Dt} = 0$$

which then leads to *Kelvin's Circulation Theorem*.

$$\frac{d\Gamma}{dt} = 0 \quad (\text{for a drifting circuit})$$

### The Starting Vortex

Consider an airfoil initially at rest. Since  $\vec{V} = 0$ , the circulation  $\Gamma_1$  about the circuit around



the airfoil must be zero as well. When the airfoil is set into motion, it will develop a nonzero circulation,  $\Gamma_4$  in the figure. Experimental flow observations show that a *starting vortex* of circulation  $\Gamma_3$  is shed from the trailing edge. This shedding is associated with the Kutta condition being satisfied for every instant in time. The vortex is swept downstream as seen by an observer on the airfoil.

By construction of the circuits, we have

$$\Gamma_2 = \Gamma_3 + \Gamma_4$$

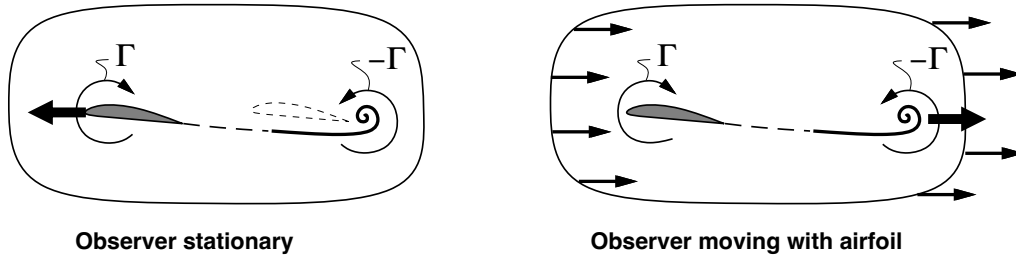
and by Kelvin's Theorem this overall  $\Gamma_2$  must be the same as the outer circuit's  $\Gamma_1$  before the airfoil started to move.

$$\Gamma_2 = \Gamma_1 = 0$$

Therefore, the airfoil and the starting vortex must have equal and opposite circulations.

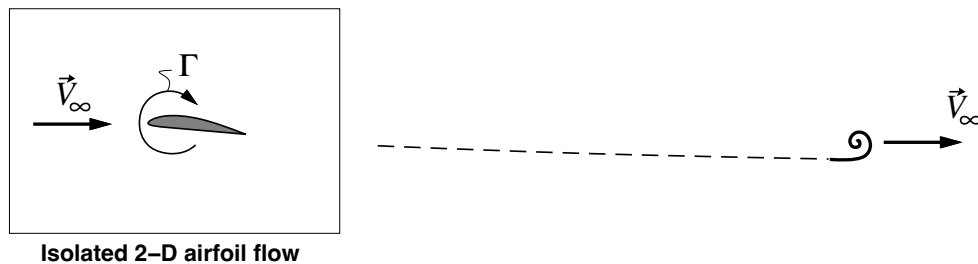
$$\Gamma_3 = -\Gamma_4$$

It's important to note that circulation about any circuit is the same to any non-rotating observer. Hence, Kelvin's Theorem applies to in both stationary and moving frames of reference. The airfoil and the starting vortex also have the same equal and opposite circulations in either frame.



### Established Steady Flow

A long time after the start of motion, the starting vortex is very far downstream behind the airfoil, and has no influence on the flowfield about the airfoil. We therefore disregard the shed starting vortex when considering any steady 2-D airfoil flow. Shed vortices must still be considered when analyzing *unsteady* airfoil flows. These are beyond scope here.



# Fluids – Lecture 2 Notes

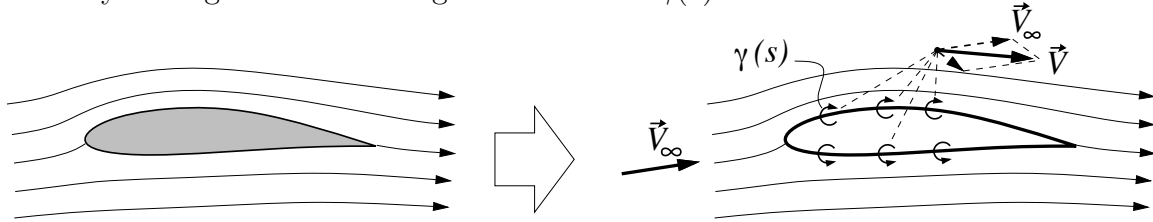
1. Airfoil Vortex Sheet Models
2. Thin-Airfoil Analysis Problem

Reading: Anderson 4.4, 4.7

## Airfoil Vortex Sheet Models

### Surface Vortex Sheet Model

An accurate means of representing the flow about an airfoil in a uniform flow is to place a vortex sheet on the airfoil surface. The total velocity  $\vec{V}(x, z)$ , which is the vector sum of the freestream velocity and the vortex-sheet velocity, can be forced parallel to the airfoil surface by suitably setting the sheet strength distribution  $\gamma(s)$ .

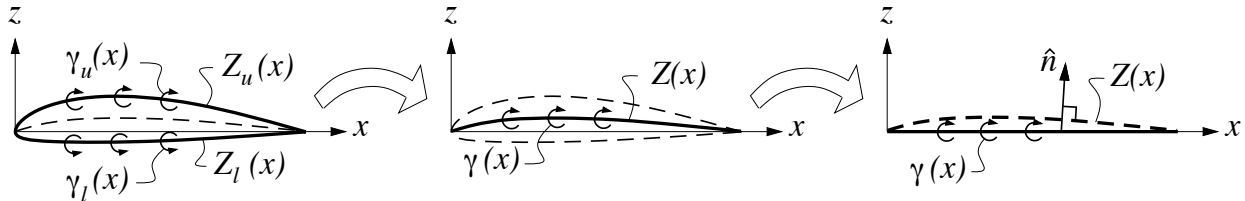


A panel method is normally used to numerically compute  $\gamma(s)$ . By using a sufficient number of panels, this result can be made as accurate as needed. The main drawback of such numerical calculations is that they give limited insight into how the flow is influenced by changes in the angle of attack or the airfoil geometry. Such insight, which is important for effective aerodynamic design and engineering, is much better provided by simple approximate analytic solutions. The panel method can still be used for accuracy when it's needed.

### Single Vortex Sheet Model

In order to simplify the problem sufficiently to allow analytic solution, we make the following assumptions and approximations:

- 1) The airfoil is assumed to be *thin*, with small maximum camber and thickness relative to the chord, and is assumed to operate at a small angle of attack,  $\alpha \ll 1$ .
- 2) The upper and lower vortex sheets are superimposed together into a single vortex sheet  $\gamma = \gamma_u + \gamma_\ell$ , which is placed on the  $x$  axis rather than on the curved mean camber line  $Z = (Z_u + Z_\ell)/2$ .



- 3) The flow-tangency condition  $\vec{V} \cdot \hat{n} = 0$  is applied on the  $x$ -axis at  $z = 0$ , rather than on the camber line at  $z = Z$ . But the normal vector  $\hat{n}$  is normal to the actual camber line shape, as shown in the figure.

- 4) Small-angle approximations are assumed. The freestream velocity is then written as follows.

$$\vec{V}_\infty = V_\infty [(\cos \alpha)\hat{i} + (\sin \alpha)\hat{k}] \simeq V_\infty (\hat{i} + \alpha\hat{k})$$

On the  $x$ -axis where the vortex sheet lies, the sheet's velocity  $w(x)$ , which is strictly in the  $z$ -direction, is given by integrating all the contributions along the sheet.

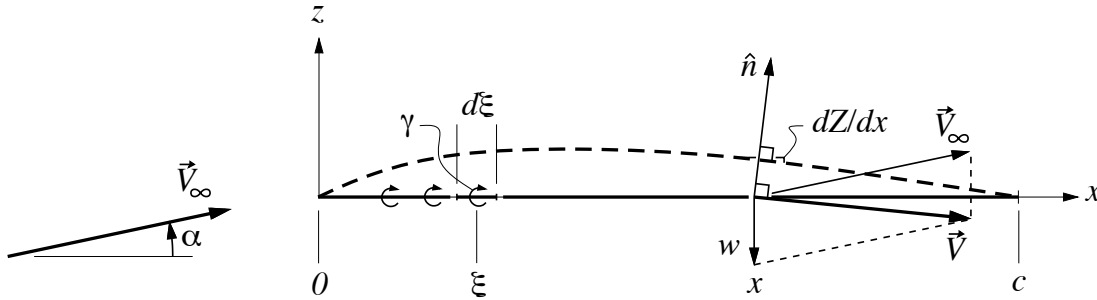
$$w(x) = - \int_0^c \frac{\gamma(\xi) d\xi}{2\pi(x - \xi)}$$

Adding this to the freestream velocity then gives the total velocity.

$$\vec{V}(x, 0) = \vec{V}_\infty + w\hat{k} \simeq V_\infty\hat{i} + \left( V_\infty\alpha - \int_0^c \frac{\gamma(\xi) d\xi}{2\pi(x - \xi)} \right) \hat{k} \quad (1)$$

The normal unit vector is obtained from the slope of the camberline shape  $Z(x)$ .

$$\vec{n}(x) = -\frac{dZ}{dx}\hat{i} + \hat{k} \quad , \quad \hat{n} = \frac{\vec{n}}{|\vec{n}|} \quad (2)$$



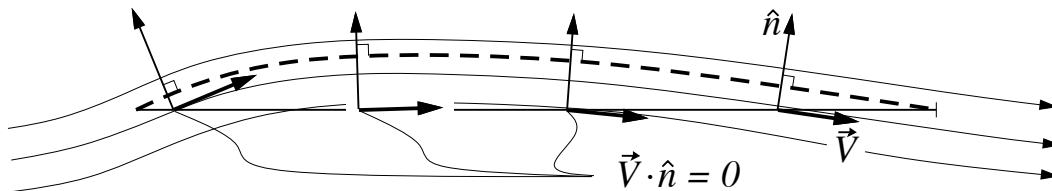
To force the total velocity to be parallel to the camberline, we now apply the flow tangency condition  $\vec{V} \cdot \hat{n} = 0$ . Performing this dot product between (1) and (2), and removing the unnecessary factor  $1/|\vec{n}|$  gives the *fundamental equation of thin airfoil theory*.

$$V_\infty \left( \alpha - \frac{dZ}{dx} \right) - \int_0^c \frac{\gamma(\xi) d\xi}{2\pi(x - \xi)} = 0 \quad (\text{for } 0 < x < c) \quad (3)$$

## Thin-Airfoil Analysis Problem

### Flow tangency imposition

For a given camberline shape  $Z(x)$  and angle of attack  $\alpha$ , we now seek to determine the vortex strength distribution  $\gamma(x)$  such that the fundamental equation (3) is satisfied at every  $x$  location. As shown in the figure, this will result in the total velocity  $\vec{V}$  at every  $x$ -location to be approximately parallel to the local camberline, producing a physically-correct flow about this camberline. The thinner the airfoil, the closer the camberline is to the  $x$ -axis where the flow tangency is actually imposed, and the more accurate the approximation becomes. Compared to typical airfoils, the height of the camberline in the figure is exaggerated severalfold for the sake of illustration.



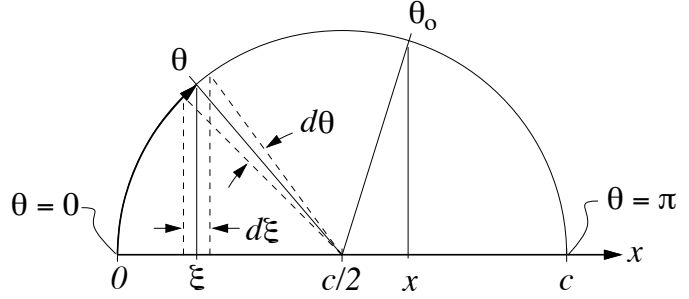
### Coordinate transformation

To enable solution of equation (3), it is necessary to first perform a trigonometric substitution for the coordinate  $x$ , and the dummy variable of integration  $\xi$ .

$$x = \frac{c}{2} (1 - \cos \theta_o)$$

$$\xi = \frac{c}{2} (1 - \cos \theta)$$

$$d\xi = \frac{c}{2} \sin \theta d\theta$$



As shown in the figure,  $\theta$  runs from 0 at the leading edge, to  $\pi$  at the trailing edge. Since  $x$  and  $\theta$  are interchangeable, functions of  $x$  can now be treated as functions of  $\theta$ . Equation (3) then becomes

$$\frac{1}{2\pi} \int_0^\pi \frac{\gamma(\theta) \sin \theta d\theta}{\cos \theta - \cos \theta_o} = V_\infty \left( \alpha - \frac{dZ}{dx} \right) \quad (\text{for } 0 < \theta_o < \pi) \quad (4)$$

where the known camberline slope  $dZ/dx$  is now considered a function of  $\theta_o$ . This is an *integral equation* which must be solved for the unknown  $\gamma(\theta)$  distribution, with the additional requirement that it satisfy the Kutta condition at the trailing edge point,

$$\gamma(\pi) = 0$$

### Symmetric airfoil case

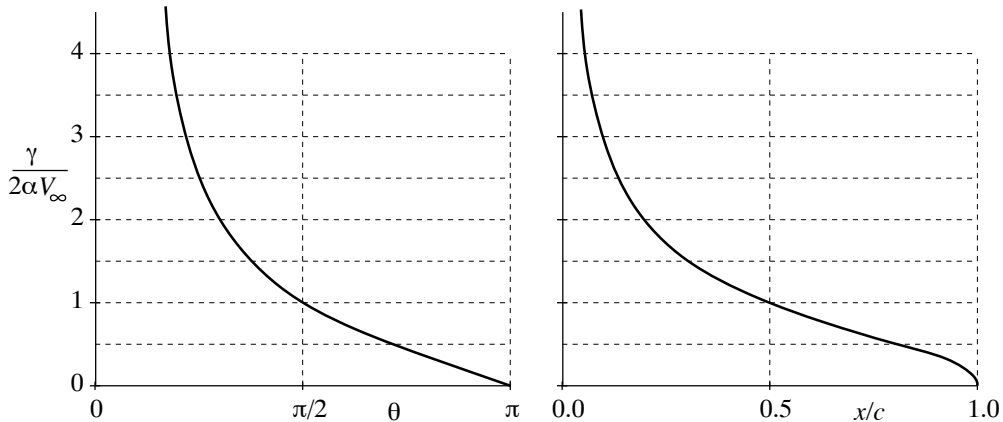
In practice, the camberline slope  $dZ/dx$  can have any arbitrary distribution along the chord. For simplicity, we will first consider a *symmetric airfoil*. This has a flat camberline, with  $Z = 0$  and  $dZ/dx = 0$ . Equation (4) then simplifies to

$$\frac{1}{2\pi} \int_0^\pi \frac{\gamma(\theta) \sin \theta d\theta}{\cos \theta - \cos \theta_o} = V_\infty \alpha \quad (\text{for } 0 < \theta_o < \pi) \quad (5)$$

Solution of this equation is still formidable, and is beyond scope here. Let us simply state that the solution is

$$\gamma(\theta) = 2\alpha V_\infty \frac{1 + \cos \theta}{\sin \theta} \quad \text{or} \quad \gamma(x) = 2\alpha V_\infty \sqrt{\frac{c-x}{x}}$$

The shape of these distributions is shown in the figure below.



Note that at the trailing edge,  $\gamma = 0$  as required by the Kutta condition, and that at the leading edge  $\gamma \rightarrow \infty$ . The latter is of course not physical, although the singularity is weak (integrable), and the integrated results for  $c_\ell$  and  $c_m$  are in fact valid.

The load distribution  $p_\ell - p_u$  is obtained using the Bernoulli equation, together with the tangential velocity jump properties across the vortex sheet.

$$p_\ell - p_u = \left( p_o - \frac{1}{2}\rho V_\ell^2 \right) - \left( p_o - \frac{1}{2}\rho V_u^2 \right) = \rho \frac{1}{2} (V_u + V_\ell) (V_u - V_\ell) = \rho V_\infty \gamma$$

The lift/span on an element  $d\xi$  of the sheet is

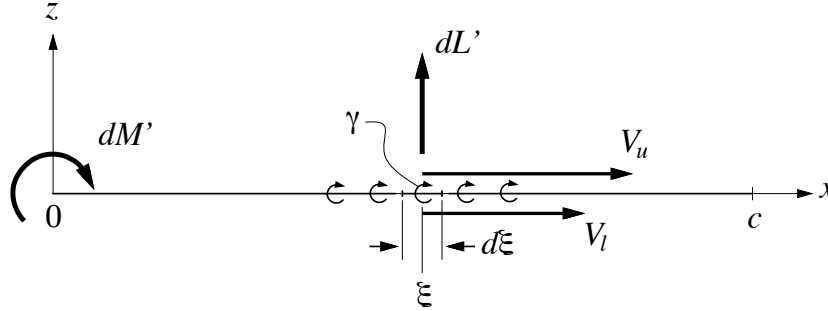
$$dL' = (p_\ell - p_u) d\xi = \rho V_\infty \gamma d\xi$$

and the total lift/span is then obtained by integrating this load distribution.

$$L' = \rho V_\infty \int_0^c \gamma(\xi) d\xi$$

The integral is also seen to be the overall circulation, making this lift result consistent with the Kutta-Joukowski Theorem.

$$\Gamma = \int_0^c \gamma(\xi) d\xi \quad , \quad L' = \rho V_\infty \Gamma$$



The actual integration of the loading or sheet strength is most easily performed in the trigonometric coordinate  $\theta$ . By direct substitution, we have

$$\Gamma = \frac{c}{2} \int_0^\pi \gamma(\theta) \sin \theta d\theta = \alpha c V_\infty \int_0^\pi (1 + \cos \theta) d\theta = \pi \alpha c V_\infty$$

The lift/span is then

$$L' = \rho V_\infty \Gamma = \pi \alpha c \rho V_\infty^2$$

and the corresponding lift coefficient is

$$c_\ell = \frac{L'}{\frac{1}{2}\rho V_\infty^2 c} = 2\pi \alpha$$

This is a very important result, showing that the lift is proportional to the angle of attack, with a *lift slope* of

$$\frac{dc_\ell}{d\alpha} = 2\pi$$

These results very closely match the results of more complex panel method calculations, as well as experimental data.

The pitching moment/span on the sheet element, taken about the leading edge, is obtained by weighting the lift by the moment arm  $\xi$ .

$$dM'_{\text{LE}} = -\xi dL' = -\rho V_{\infty} \gamma \xi d\xi$$

The overall moment/span is then

$$M'_{\text{LE}} = -\rho V_{\infty} \int_0^c \gamma \xi d\xi$$

We can again most easily integrate this in the trigonometric coordinate.

$$M'_{\text{LE}} = -\alpha \frac{c^2}{2} \rho V_{\infty}^2 \int_0^{\pi} (1 + \cos \theta)(1 - \cos \theta) d\theta = -\alpha \frac{c^2}{2} \rho V_{\infty}^2 \int_0^{\pi} (1 - \cos^2 \theta) d\theta = -\pi \alpha \frac{c^2}{4} \rho V_{\infty}^2$$

The moment coefficient about the leading edge point is

$$c_{m,\text{le}} = \frac{M'_{\text{LE}}}{\frac{1}{2} \rho V_{\infty}^2 c^2} = -\frac{\pi \alpha}{2} = -\frac{c_{\ell}}{4}$$

and the equivalent moment coefficient about the standard quarter-chord point at  $x/c = 1/4$  is

$$c_{m,c/4} = c_{m,\text{le}} + \frac{1}{4} c_{\ell} = 0$$

This very important result shows that a symmetric airfoil has zero moment about the quarter-chord point, for any angle of attack.

# Fluids – Lecture 3 Notes

## 1. Thin-Airfoil Analysis Problem (continued)

Reading: Anderson 4.8

### Cambered airfoil case

We now consider the case where the camberline  $Z(x)$  is nonzero. The general thin airfoil equation, which is a statement of flow tangency on the camberline, was derived previously.

$$\frac{1}{2\pi} \int_0^\pi \frac{\gamma(\theta) \sin \theta d\theta}{\cos \theta - \cos \theta_o} = V_\infty \left( \alpha - \frac{dZ}{dx} \right) \quad (\text{for } 0 < \theta_o < \pi) \quad (1)$$

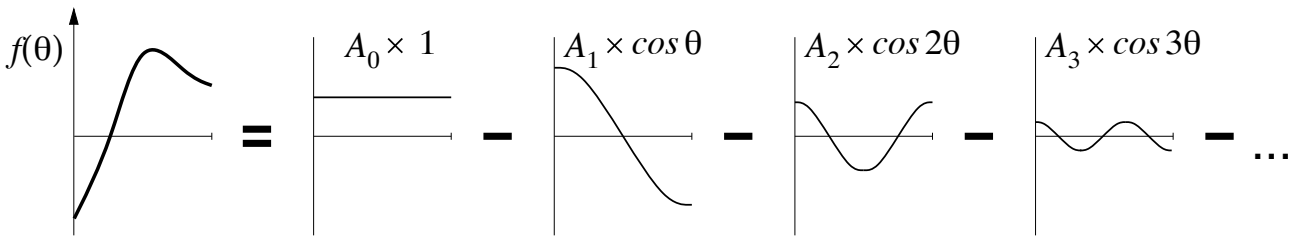
For an arbitrary camberline shape  $Z(x)$ , the slope  $dZ/dx$  varies along the chord, and in the equation it is negated and shifted by the constant  $\alpha$ . Let us consider this combination to be some general function of  $\theta_o$ .

$$\alpha - \frac{dZ}{dx} \equiv f(\theta_o)$$

For the purpose of computation, any such function can be conveniently represented or approximated by a *Fourier cosine series*,

$$f(\theta_o) = A_0 - \sum_{n=1}^N A_n \cos n\theta_o$$

which is illustrated in the figure. The negative sign in front of the sum could be absorbed into all the  $A_n$  coefficients, but is left outside for later algebraic simplicity.



The overall summation can be made arbitrarily close to a known  $f(\theta_o)$  by making  $N$  sufficiently large (i.e. using sufficiently many terms). The required coefficients  $A_0, A_1, \dots, A_N$  are computed one by one using *Fourier analysis*, which is the evaluation of the following integrals.

$$\begin{aligned} A_0 &= \frac{1}{\pi} \int_0^\pi f(\theta) d\theta \\ -A_1 &= \frac{2}{\pi} \int_0^\pi f(\theta) \cos \theta d\theta \\ -A_2 &= \frac{2}{\pi} \int_0^\pi f(\theta) \cos 2\theta d\theta \\ &\vdots \\ -A_N &= \frac{2}{\pi} \int_0^\pi f(\theta) \cos N\theta d\theta \end{aligned}$$



For the particular  $f(\theta_o)$  used here, these integrals become

$$A_0 = \alpha - \frac{1}{\pi} \int_0^\pi \frac{dZ}{dx} d\theta$$

$$A_n = \frac{2}{\pi} \int_0^\pi \frac{dZ}{dx} \cos n\theta d\theta \quad (n = 1, 2, \dots)$$

In practice, the integrals can be evaluated either analytically or numerically. If  $dZ/dx$  is smooth, then the higher  $A_n$  coefficients will rapidly decrease, and at some point the remainder can be discarded (the series truncated) with little loss of accuracy.

Replacing  $\alpha - dZ/dx$  in equation (1) with its Fourier series gives the integral equation

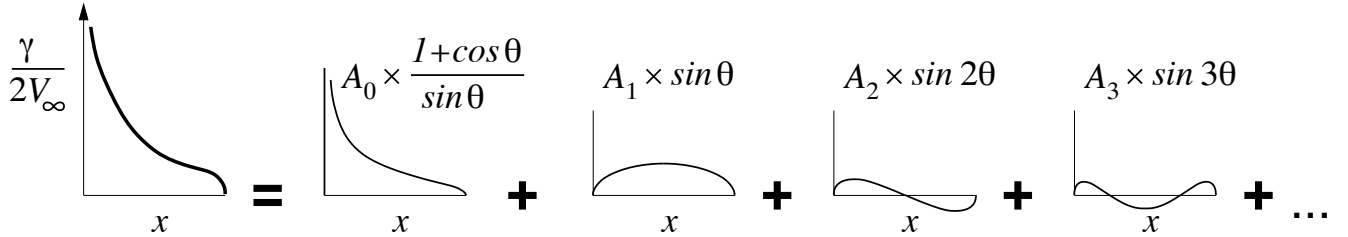
$$\frac{1}{2\pi} \int_0^\pi \frac{\gamma(\theta) \sin \theta d\theta}{\cos \theta - \cos \theta_o} = V_\infty \left( A_0 - \sum_{n=1}^N A_n \cos n\theta_o \right) \quad (2)$$

which is to be solved for the unknown  $\gamma(\theta)$  distribution. As before, the solution of this integral equation is beyond scope here. Again, let us simply state the solution.

$$\gamma(\theta) = 2V_\infty \left( A_0 \frac{1 + \cos \theta}{\sin \theta} + \sum_{n=1}^N A_n \sin n\theta \right)$$

The leading term is the same as for the zero-camber case, but with  $A_0$  replacing  $\alpha$ . The remaining coefficients  $A_1, \dots, A_N$  in the summation depend only on the shape of the camberline, and in particular are independent of  $\alpha$ .

The figure shows the contributions of the various terms towards  $\gamma$ , all plotted versus the physical  $x$  coordinate rather than versus  $\theta$ . Note that here the coefficients  $A_0, A_1 \dots A_N$  have



already been determined, and are now merely used to construct  $\gamma(\theta)$  by simple summation of the series. This  $\gamma(\theta)$  will now be integrated to obtain the lift force and moment.

### Force calculation

The circulation and lift/span are computed in the same manner as with the symmetric airfoil case.

$$\Gamma = \int_0^c \gamma(\xi) d\xi \quad , \quad L' = \rho V_\infty \Gamma$$

The integral is again most easily performed in the trigonometric coordinate  $\theta$ .

$$\Gamma = \frac{c}{2} \int_0^\pi \gamma(\theta) \sin \theta d\theta = cV_\infty \left[ A_0 \int_0^\pi (1 + \cos \theta) d\theta + \sum_{n=1}^N A_n \int_0^\pi \sin n\theta \sin \theta d\theta \right]$$

The first integral in the brackets is easily evaluated.

$$\int_0^\pi (1 + \cos \theta) d\theta = \pi$$

The integrals inside the summation can be evaluated by using the *orthogonality property* of the sine functions.

$$\int_0^\pi \sin n\theta \sin m\theta d\theta = \begin{cases} \pi/2 & (\text{if } n = m) \\ 0 & (\text{if } n \neq m) \end{cases}$$

We see that only the  $n = 1$  integral inside the summation evaluates to  $\pi/2$ , and all the others are zero. The final result is

$$\begin{aligned} \Gamma &= c V_\infty \left( \pi A_0 + \frac{\pi}{2} A_1 \right) \\ L' &= \rho V_\infty \Gamma = \rho V_\infty^2 c \pi \left( A_0 + \frac{1}{2} A_1 \right) \\ c_\ell &= \frac{L'}{\frac{1}{2} \rho V_\infty^2 c} = \pi (2A_0 + A_1) \end{aligned}$$

It's informative to substitute the previously-obtained expressions for  $A_0$  and  $A_1$ , giving

$$c_\ell = 2\pi \left[ \alpha - \frac{1}{\pi} \int_0^\pi \frac{dZ}{dx} (1 - \cos \theta_o) d\theta_o \right]$$

The integral term inside the brackets depends only on the camberline shape, and is independent of the angle of attack. Hence the lift slope is

$$\frac{dc_\ell}{d\alpha} = 2\pi$$

which is the same as for the symmetrical airfoil case. We therefore reach the important conclusion that camber has no influence on the lift slope. A terse and convenient way to represent the  $c_l(\alpha)$  function is therefore

$$c_\ell = \frac{dc_\ell}{d\alpha} (\alpha - \alpha_{L=0})$$

where  $\alpha_{L=0}$  is called the *zero-lift angle*, which depends only on the camberline shape.

$$\alpha_{L=0} = \frac{1}{\pi} \int_0^\pi \frac{dZ}{dx} (1 - \cos \theta_o) d\theta_o$$

The moment/span about the leading edge is again computed using the trigonometric coordinate.

$$M'_{LE} = -\rho V_\infty \int_0^c \gamma \xi d\xi = -\rho V_\infty \frac{c^2}{4} \int_0^\pi \gamma(\theta) (1 - \cos \theta) \sin \theta d\theta = -\rho V_\infty^2 \frac{c^2}{4} \pi \left( A_0 + A_1 - \frac{1}{2} A_2 \right)$$

The moment/span and corresponding moment coefficient about the  $x = c/4$  quarter-chord point are

$$\begin{aligned} M'_{c/4} &= M'_{LE} + \frac{c}{4} L' = \rho V_\infty^2 \frac{c^2}{4} \frac{\pi}{2} (A_2 - A_1) \\ c_{m,c/4} &= \frac{M'_{c/4}}{\frac{1}{2} \rho V_\infty^2 c^2} = \frac{\pi}{4} (A_2 - A_1) \end{aligned}$$

An important result is that this  $c_{m,c/4}$  depends only on the camberline shape, but not on the angle of attack. Therefore, the quarter-chord location is the *aerodynamic center* for any airfoil, defined as the location about which the moment is independent of  $\alpha$ , or

$$\frac{dc_{m,c/4}}{d\alpha} = 0$$

## Summary

For airfoil analysis, Thin Airfoil Theory takes in the following inputs:

- $\alpha$       angle of attack
- $dZ/dx$    camberline slope distribution along chord

The outputs are:

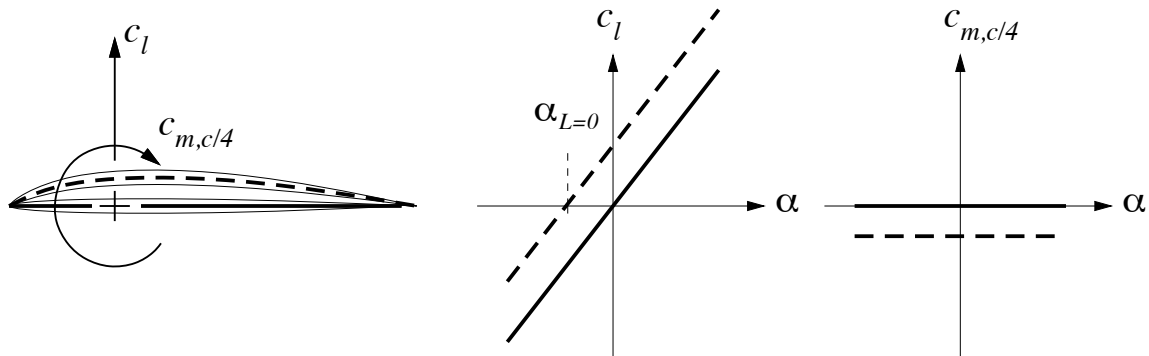
- $c_\ell$     lift coefficient
- $c_m$     moment coefficient, about  $c/4$  or any other location

The information propagates as follows.

$$\alpha, \frac{dZ}{dx}(\theta_o) \xrightarrow{\text{Fourier analysis}} A_0, A_1 \dots A_N \xrightarrow{\text{series summing}} \gamma(\theta) \xrightarrow{\text{chordwise integration}} c_\ell, c_m$$

The Fourier coefficients  $A_n$  and the vortex sheet strength distribution  $\gamma(\theta)$  are intermediate results.

The influence of camber on the airfoil  $c_\ell(\alpha)$  and  $c_{m,c/4}(\alpha)$  curves is illustrated in the figure.



These results are subject to the assumptions inherent in thin airfoil theory. In practice, they are surprisingly accurate even for relatively thick or highly-cambered airfoils. It appears to be better at predicting trends (with camber,  $\alpha$ , etc) than absolute numbers. When used merely as a conceptual framework for understanding airfoil behavior rather than for quantitative predictions, thin airfoil theory is highly applicable to almost any airfoil.

# Fluids – Lecture 4 Notes

## 1. Thin Airfoil Theory Application: Analysis Example

Reading: Anderson 4.8, 4.9

### Analysis Example

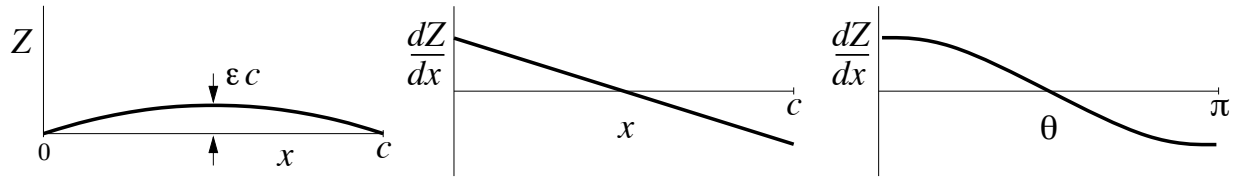
#### Airfoil camberline definition

Consider a thin airfoil with a simple parabolic-arc camberline, with a maximum camber height  $\varepsilon c$ .

$$Z(x) = 4\varepsilon x \left(1 - \frac{x}{c}\right)$$

The camberline slope is then a linear function in  $x$ , or a cosine function in  $\theta$ .

$$\frac{dZ}{dx} = 4\varepsilon \left(1 - 2\frac{x}{c}\right) = 4\varepsilon \cos \theta_o$$



#### Fourier coefficient calculation

Substituting the above  $dZ/dx$  into the general expressions for the Fourier coefficients gives

$$A_0 = \alpha - \frac{1}{\pi} \int_0^\pi \frac{dZ}{dx} d\theta = \alpha - \frac{1}{\pi} \int_0^\pi 4\varepsilon \cos \theta d\theta$$

$$A_n = \frac{2}{\pi} \int_0^\pi \frac{dZ}{dx} \cos n\theta d\theta = \frac{2}{\pi} \int_0^\pi 4\varepsilon \cos \theta \cos n\theta d\theta$$

The integral in the  $A_0$  expression easily evaluates to zero. The integral in the  $A_n$  expression can be evaluated by using the *orthogonality property* of the cosine functions.

$$\int_0^\pi \cos n\theta \cos m\theta d\theta = \begin{cases} \pi & (\text{if } n = m = 0) \\ \pi/2 & (\text{if } n = m \neq 0) \\ 0 & (\text{if } n \neq m) \end{cases}$$

For our case we have  $m = 1$ , and then set  $n = 1, 2, 3, \dots$  to evaluate  $A_1, A_2, A_3, \dots$ . The final results are

$$\begin{aligned} A_0 &= \alpha \\ A_1 &= 4\varepsilon \\ A_2 &= 0 \\ A_3 &= 0 \\ &\vdots \end{aligned}$$

so only  $A_0$  and  $A_1$  are nonzero for this case.

### Lift and moment coefficients

The coefficients can now be computed directly using their general expressions derived previously.

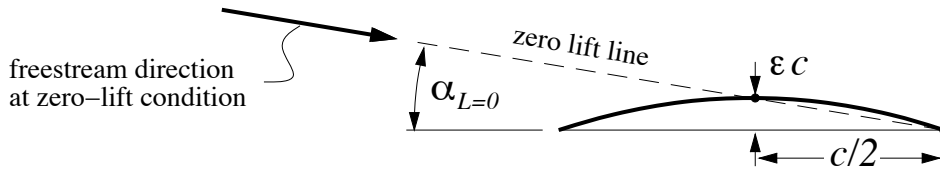
$$c_\ell = \pi(2A_0 + A_1) = 2\pi(\alpha + 2\varepsilon)$$

$$c_{m,c/4} = \frac{\pi}{4}(A_2 - A_1) = -\pi\varepsilon$$

From the  $c_\ell(\alpha)$  expression above, the zero-lift angle is seen to be

$$\alpha_{L=0} = -2\varepsilon$$

which is also the angle of the *zero lift line*. In the present case of a parabolic camber line, the zero lift line passes through the maximum-camber point and the trailing edge point.



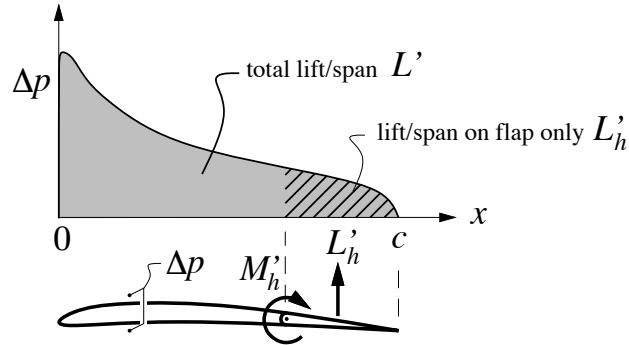
As a possible shortcut, the zero-lift angle could also have been computed directly from its explicit equation derived earlier.

$$\alpha_{L=0} = \frac{1}{\pi} \int_0^\pi \frac{dZ}{dx} (1 - \cos \theta_o) d\theta_o = \frac{1}{\pi} \int_0^\pi 4\varepsilon \cos \theta_o (1 - \cos \theta_o) d\theta_o = -2\varepsilon$$

But this integral is just the combination of the integrals for  $A_0$  and  $A_1$ , so there is no real simplification here.

### Surface loading (further details)

In many applications, obtaining just the  $c_\ell$  and  $c_m$  of the entire airfoil is sufficient. But in some cases, we may also want to know the force and moment on only a portion of the airfoil. For example, the force and moment on a flap are of considerable interest, since the flap hinge and flap control linkage must be designed to withstand these loads. We therefore need to know how the loading  $\Delta p(x)$  is distributed over the chord, and over the flap in particular.



The loading  $\Delta p$  is directly related to the vortex sheet strength  $\gamma(x)$ , and can also be given in terms of the dimensionless pressure coefficient.

$$\Delta p(x) = \rho V_\infty \gamma(x) = \frac{1}{2} \rho V_\infty^2 \Delta C_p(x) \quad (1)$$

The general expression for the sheet strength, obtained previously, is

$$\gamma(\theta) = 2V_\infty \left( A_0 \frac{1 + \cos \theta}{\sin \theta} + \sum_{n=1}^N A_n \sin n\theta \right)$$

Substituting the Fourier coefficients obtained for the present case gives

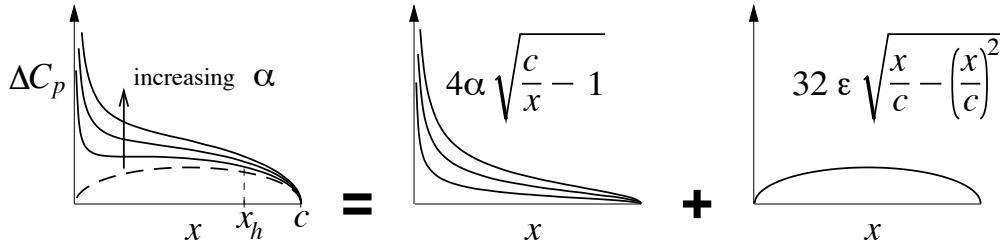
$$\begin{aligned} \gamma(\theta) &= 2V_\infty \left( \alpha \frac{1 + \cos \theta}{\sin \theta} + 4\varepsilon \sin \theta \right) \\ \text{or} \quad \Delta C_p(\theta) &= 2 \frac{\gamma(\theta)}{V_\infty} = 4\alpha \frac{1 + \cos \theta}{\sin \theta} + 16\varepsilon \sin \theta \end{aligned}$$

The integration of  $\Delta C_p$  over the flap can be conveniently performed in the  $\theta$  coordinate as usual, using the above expression. But it is also of some interest to examine this distribution in the physical  $x$  coordinate. The relevant relations between  $\theta$  and  $x$  are

$$\begin{aligned} \cos \theta &= 1 - 2x/c \\ \sin \theta &= \sqrt{1 - \cos^2 \theta} = \sqrt{1 - (1 - 2x/c)^2} = 2\sqrt{x/c - (x/c)^2} \end{aligned}$$

which can be substituted into the above  $\Delta C_p(\theta)$  expression to put it in terms of  $x$ .

$$\Delta C_p(x) = 4\alpha \sqrt{\frac{c}{x} - 1} + 32\varepsilon \sqrt{\frac{x}{c} - \left(\frac{x}{c}\right)^2}$$



Define  $x_h$  as the location of the flap hinge, so the flap extends from  $x = x_h$ , to the trailing edge at  $x = c$ . The corresponding  $\theta$  locations are  $\theta = \arccos(1 - 2x_h/c) \equiv \theta_h$ , and  $\theta = \pi$ , respectively. The load/span and moment/span coefficients on the flap hinge can now be computed by integrating the pressure loading.

$$\begin{aligned} c_{\ell_h} &\equiv \frac{L'_h}{\frac{1}{2}\rho V_\infty^2 c} = \frac{1}{c} \int_{x_h}^c \Delta C_p(x) dx = \frac{1}{2} \int_{\theta_h}^{\pi} \Delta C_p(\theta) \sin \theta d\theta \\ c_{m_h} &\equiv \frac{M'_h}{\frac{1}{2}\rho V_\infty^2 c^2} = \frac{1}{c^2} \int_{x_h}^c \Delta C_p(x) (x_h - x) dx = \frac{1}{4} \int_{\theta_h}^{\pi} \Delta C_p(\theta) (\cos \theta - \cos \theta_h) \sin \theta d\theta \end{aligned}$$

Here, integrations in  $\theta$  are simpler, but still somewhat tedious, and are best left for computer-based symbolic or numerical integration methods.

# Fluids – Lecture 5 Notes

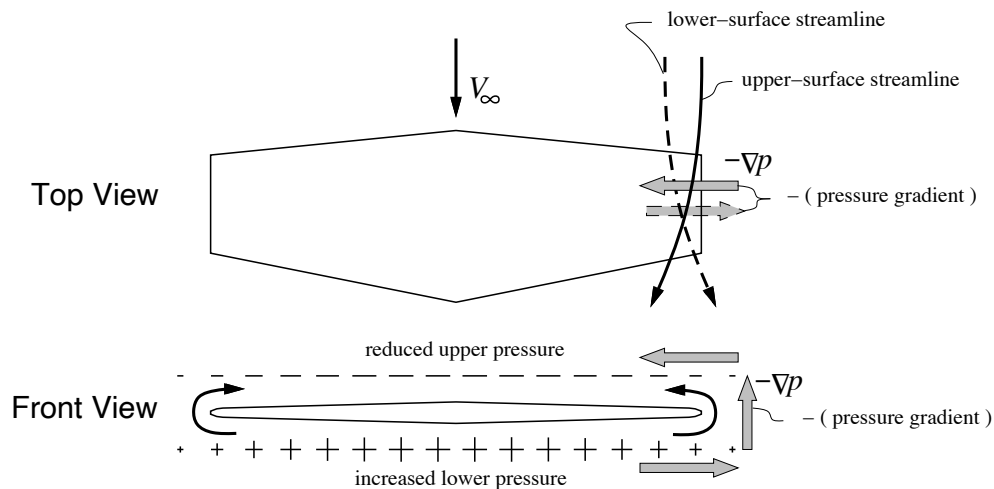
1. Introduction to 3-D Wings
2. 2-D and 3-D Coefficients

Reading: Anderson 5.1

## Introduction to 3-D Wings

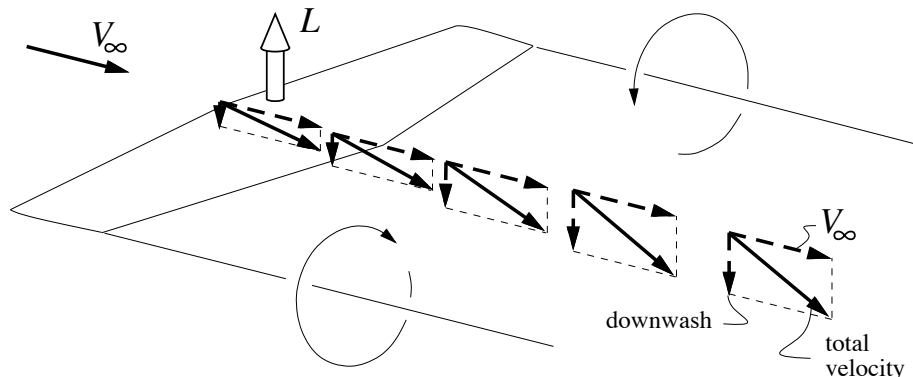
A 2-D airfoil can be considered as a wing of infinite span, with each spanwise location identical. In contrast, on a 3-D finite-span wing, the presence of wingtips introduces spanwise flow variations, a number of important new physical effects.

Spanwise flow. An upward-lifting wing must on average have a pressure difference between its upper and lower surfaces. Outside of the wingtips, this pressure difference must disappear. Consequently, fluid particles which approach the wingtip above the wing are subjected to a spanwise pressure gradient which causes them to curve towards the wing center. Fluid particles which approach below the wing will curve away from the wing center. Particles close to the tip will tend to flow around the tip edge, from the lower to the upper surface.



Trailing vortices. The flow curling around the tip forms a *tip vortex*, which then trails downstream, and can be easily made visible with smoke visualization.

Downwash. The velocity field associated with the two trailing vortices is mostly downward (opposite to lift direction) directly behind the wing, and upward outside the tip vortices. The downwash can also be viewed as the result of the lifting wing “pushing down” on the air, which results in the air having added downward momentum directly behind the wing.



Induced angle and lift reduction. There is a nonzero downwash velocity  $-w$  at the wing itself ( $w$  is positive up). In other words, the wing operates in its own downwash. The apparent freestream velocity which the wing sees is therefore tilted by the *induced angle*

$$\alpha_i = \arctan \frac{-w}{V_\infty} \simeq \frac{-w}{V_\infty}$$

where the small-angle approximation is justified since

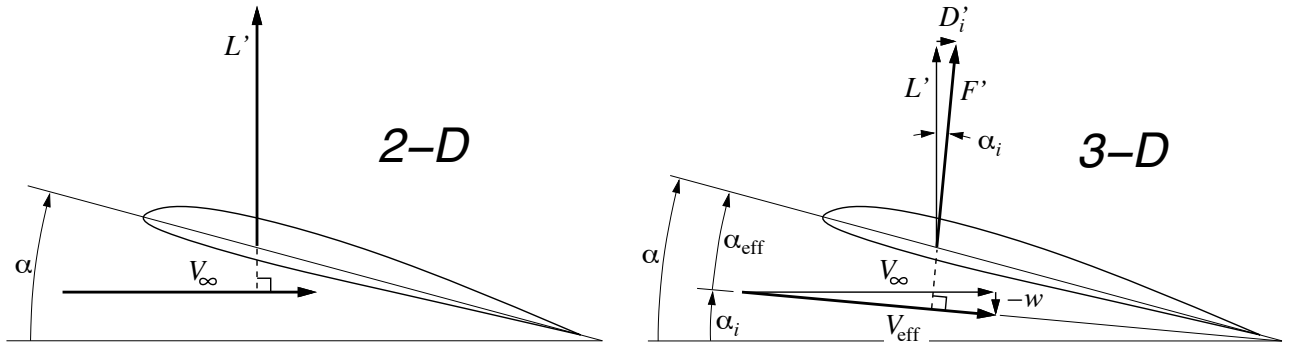
$$|w| \ll V_\infty$$

for typical wings. The effective angle of attack that the 3-D wing sees is significantly reduced from the geometric angle of attack  $\alpha$ ,

$$\alpha_{\text{eff}} = \alpha - \alpha_i$$

while the net effective freestream speed  $V_{\text{eff}}$  is nearly the same as the freestream speed.

$$V_{\text{eff}} = \sqrt{V_\infty^2 + w^2} \simeq V_\infty$$



Because  $\alpha_{\text{eff}} < \alpha$ , the lift generated by the 3-D wing is less than if the downwash and induced angle were absent, as in the 2-D case. In practice, this means that the 3-D wing has to operate at a greater geometric  $\alpha$  to achieve the same lift/span as the 2-D wing.

Induced drag. As the figure above shows, the tilt caused by the downwash velocity also tilts the lift force by the same angle  $\alpha_i$ . The lifting force/span produced by the wing is

$$F' = \rho V_\infty \Gamma$$

which can be resolved into lift and drag components aligned with to the true freestream velocity vector  $\vec{V}_\infty$ . Making our usual small-angle approximations, we have

$$\begin{aligned} L' &= F' \cos \alpha_i \simeq F' = \rho V_\infty \Gamma \\ D'_i &= F' \sin \alpha_i \simeq F' \alpha_i = -\rho w \Gamma \end{aligned}$$

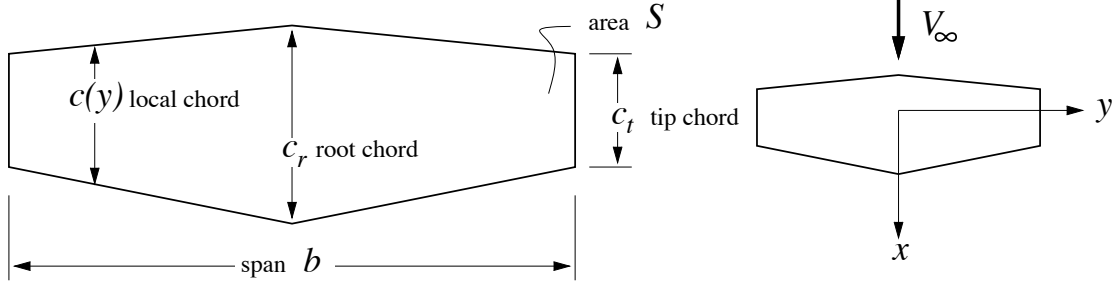
A very important consequence of the tilting of the lift force is the appearance of *induced drag*  $D'_i$ , which forms a very large fraction to the total drag on most aircraft. This induced drag is a form of *pressure drag*, and is completely unrelated to the viscous shear forces on the surface. Therefore, a lifting 3-D wing has nonzero induced drag even in inviscid flow, and is not subject to d'Alembert's Paradox.



## 2-D and 3-D Coefficients

### Geometric parameters

The figure shows standard wing dimension terminology, and the standard coordinate system.



Several other relevant geometric parameters can be defined. One is the *average chord*  $c_{\text{avg}}$ , which is a simple average of the local chord  $c(y)$ .

$$c_{\text{avg}} = \frac{1}{b} \int_{-b/2}^{b/2} c(y) dy = \frac{S}{b}$$

Another one is the *mean aerodynamic chord*  $\bar{c}$ , which is the root-mean-square average.

$$\bar{c}^2 = \frac{1}{b} \int_{-b/2}^{b/2} [c(y)]^2 dy$$

For a rectangular wing,  $c_{\text{avg}}$  and  $\bar{c}$  are the same, and usually differ only slightly for most tapered wings. Either choice is appropriate if consistently followed. Another important geometric parameter is the *aspect ratio*, defined as follows.

$$AR = \frac{b^2}{S} = \frac{b}{c_{\text{avg}}}$$

### Overall forces and moments

The overall forces and moments can be defined simply by integrating the appropriate unit-span quantities.

$$\begin{aligned} L &= \int_{-b/2}^{b/2} L'(y) dy = \int_{-b/2}^{b/2} \rho V_{\infty} \Gamma(y) dy \\ D_i &= \int_{-b/2}^{b/2} D'_i(y) dy = \int_{-b/2}^{b/2} -\rho w(y) \Gamma(y) dy \\ D_p &= \int_{-b/2}^{b/2} D'_p(y) dy \\ M_{c/4} &= \int_{-b/2}^{b/2} M'_{c/4}(y) dy \end{aligned}$$

Here,  $D'_p(y)$  is the local profile drag/span.

### Overall force and moment coefficients

Defining overall force and moment coefficients first requires selection of a suitable reference area and chord. Commonly-used choices are

$$S_{\text{ref}} = S \quad , \quad c_{\text{ref}} = c_{\text{avg}} \quad \text{or} \quad c_{\text{ref}} = \bar{c}$$

The overall coefficients are then defined as follows.

$$\begin{aligned}
C_L &= \frac{L}{\frac{1}{2}\rho V_\infty^2 S_{\text{ref}}} \\
C_{Di} &= \frac{D_i}{\frac{1}{2}\rho V_\infty^2 S_{\text{ref}}} \\
C_{Dp} &= \frac{D_p}{\frac{1}{2}\rho V_\infty^2 S_{\text{ref}}} \\
C_{M,c/4} &= \frac{M_{c/4}}{\frac{1}{2}\rho V_\infty^2 S_{\text{ref}} c_{\text{ref}}}
\end{aligned}$$

It is also useful to relate the overall and local lift, profile drag, and moment coefficients. Using the relations

$$\begin{aligned}
L'(y) &= \frac{1}{2}\rho V_\infty^2 c(y) c_\ell(y) \\
D'_p(y) &= \frac{1}{2}\rho V_\infty^2 c(y) c_{d_p}(y) \\
M'_{c,4}(y) &= \frac{1}{2}\rho V_\infty^2 [c(y)]^2 c_{m,c/4}(y)
\end{aligned}$$

we have

$$\begin{aligned}
C_L &= \frac{1}{S_{\text{ref}}} \int_{-b/2}^{b/2} c_\ell(y) c(y) dy \\
C_{Dp} &= \frac{1}{S_{\text{ref}}} \int_{-b/2}^{b/2} c_{d_p}(y) c(y) dy \\
C_{M,c/4} &= \frac{1}{S_{\text{ref}} c_{\text{ref}}} \int_{-b/2}^{b/2} c_{m,c/4}(y) [c(y)]^2 dy
\end{aligned}$$

Therefore, the overall  $C_L$  and  $C_{Dp}$  can be seen to be the chord-weighted average of the local  $c_\ell(y)$  and  $c_{d_p}(y)$ . In many situations, and especially in preliminary design, a common approximation is to assume that local lift and profile drag coefficients do not vary across the span, and therefore

$$\begin{aligned}
C_L &\simeq c_\ell \simeq \text{constant in } y \\
C_{Dp} &\simeq c_{d_p} \simeq \text{constant in } y
\end{aligned}$$

Once the planform chord distribution  $c(y)$  is fixed, the more exact integral definitions can be used.

### Total drag

The total drag on a wing is the sum of profile and induced drags.

$$\begin{aligned}
D &= D_p + D_i \\
\text{or} \quad C_D &= C_{Dp} + C_{Di} \simeq c_{d_p}(c_\ell) + C_{Di}
\end{aligned}$$

In the last approximation, the  $c_{d_p}(c_\ell)$  function is a 2-D airfoil drag polar, obtained from airfoil data or calculations. The induced drag coefficient  $C_{Di}$  will be considered in the next several lectures.

# Fluids – Lecture 6 Notes

1. 3-D Vortex Filaments
2. Lifting-Line Theory

Reading: Anderson 5.1

## 3-D Vortex Filaments

### General 3-D vortex

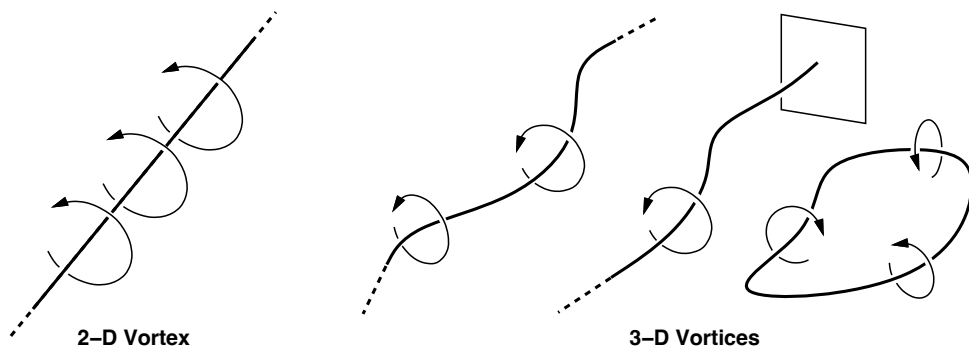
A 2-D vortex, which we have examined previously, can be considered as a 3-D vortex which is straight and extending to  $\pm\infty$ . Its velocity field is

$$V_\theta = \frac{\Gamma}{2\pi r} \quad V_r = 0 \quad V_z = 0 \quad (2\text{-D vortex})$$

In contrast, a general 3-D vortex can take any arbitrary shape. However, it is subject to the *Helmholtz Vortex Theorems*:

- 1) The strength  $\Gamma$  of the vortex is constant all along its length
- 2) The vortex cannot end inside the fluid. It must either
  - a) extend to  $\pm\infty$ , or
  - b) end at a solid boundary, or
  - c) form a closed loop.

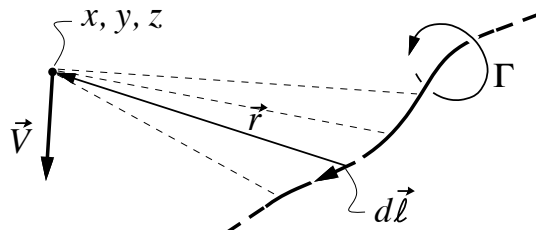
Proofs of these theorems are beyond scope here. However, they are easy to apply in flow modeling situations.



The velocity field of a vortex of general shape is given by the *Biot-Savart Law*.

$$\vec{V}(x, y, z) = \frac{\Gamma}{4\pi} \int_{-\infty}^{+\infty} \frac{d\vec{\ell} \times \vec{r}}{|\vec{r}|^3} \quad (\text{general 3-D vortex})$$

The integration is performed along the entire length of the vortex, with  $\vec{r}$  extending from the point of integration to the field point  $x, y, z$ . The arc length element  $d\vec{\ell}$  points along the filament, in the direction of positive  $\Gamma$  by right hand rule.

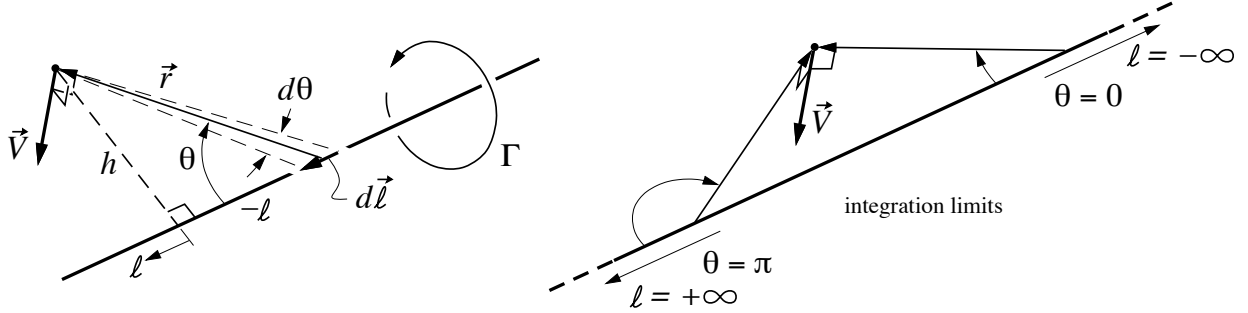


### Straight-vortex case

As a check, we can perform the Biot-Savart integral for the case of a straight vortex. Define  $h$  as the nearest perpendicular distance of the field point from the vortex line, and  $\theta$  as the angle between the vortex line and the radius vector  $\vec{r}$ . We then have

$$\begin{aligned} r \equiv |\vec{r}| &= \frac{h}{\sin \theta} \\ \ell &= -\frac{h}{\tan \theta} \\ d\ell &= \frac{h}{\sin^2 \theta} d\theta \\ d\vec{\ell} \times \vec{r} &= (d\ell r \sin \theta) \hat{\theta} \end{aligned}$$

where  $\hat{\theta}$  is the unit vector in the tangential direction.



The Biot-Savart integral can now be recast and evaluated as follows.

$$\vec{V} = \frac{\Gamma}{4\pi h} \hat{\theta} \int_0^\pi \sin \theta d\theta = \frac{\Gamma}{2\pi h} \hat{\theta}$$

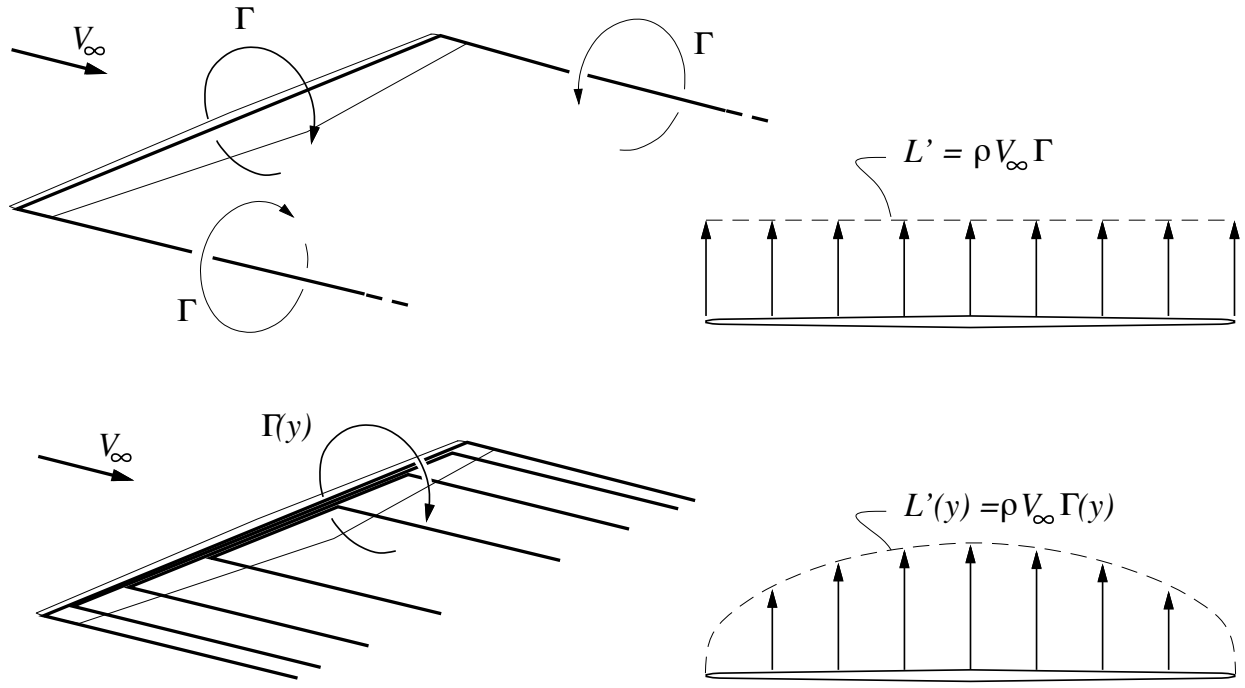
As expected, this recovers the 2-D vortex flowfield  $V_\theta = \Gamma/2\pi h$  for this particular case.

## Lifting-Line Theory

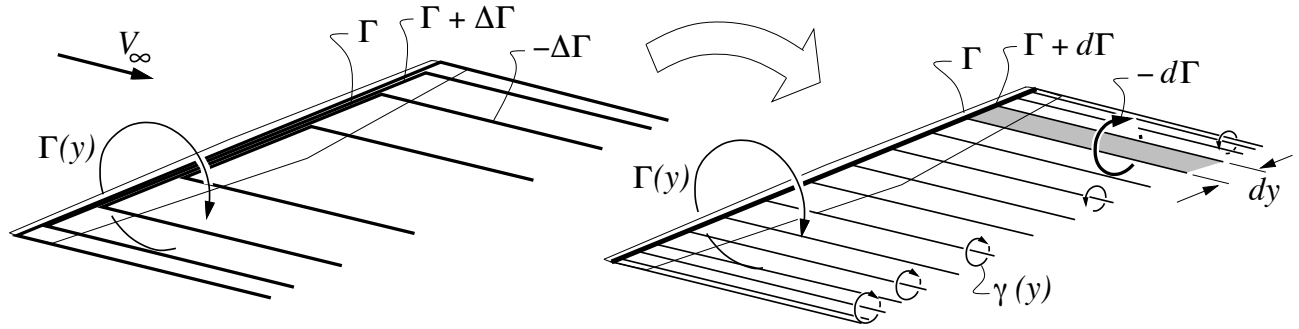
### Wing vortex model

A very simple model for the flowfield about lifting wing is the superposition of a freestream flow and a *horseshoe vortex*. The horseshoe vortex consists of three segments: a *bound vortex* spanning the wing, connected to two *trailing vortices* at each wing tip. As required by Helmholtz's vortex theorems, the circulation  $\Gamma$  is constant along the entire vortex line, and the vortex line extends downstream to infinity. Although this model qualitatively reproduces the observed tip vortices, it is not well suited for accurate prediction of overall wing lift and induced drag. The main deficiency is that its local lift/span  $L' = \rho V_\infty \Gamma$  is constant across the span, which is not very realistic. On a real wing,  $L'$  always falls gradually to zero at the tips. Another deficiency is that the induced drag predicted by this model is wildly inaccurate, when compared to more refined models or experimental data.

A better flowfield model employs multiple distributed horseshoe vortices as shown in the figure. Each horseshoe vortex has a constant strength along its length and hence obeys Helmholtz's theorem. Spreading the trailing vortices across the span rather than all at the tip allows a nonuniform spanwise circulation  $\Gamma(y)$  and corresponding loading  $L'(y)$  to be represented.



The figure shows only a few horseshoe vortices on the wing, but one can conceptually subdivide these into more and more vortices of decreasing strength, which in the limit become a *trailing vortex sheet* with strength  $\gamma(y)$ . The strength of the sheet can be determined by



considering a small change of circulation  $d\Gamma$  between spanwise stations  $y$  and  $y + dy$ . By Helmholtz's theorem, the  $dy$ -wide sheet strip trailing between those two stations must have a circulation  $-d\Gamma$ . This then gives the local sheet strength  $\gamma(y)$ .

$$\gamma dy = -d\Gamma$$

or

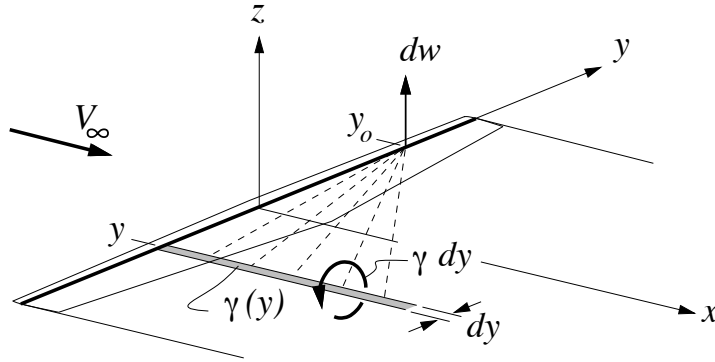
$$\gamma = -\frac{d\Gamma}{dy}$$

### Downwash distribution

The trailing vortex sheet will have a downwash distribution  $w(y)$  along the span. Consider a  $dy$ -wide strip of the sheet at location  $y$ , which forms a semi-infinite straight vortex with circulation  $\gamma dy$ . The velocity of this vortex at some other location  $y_o$  on the  $y$ -axis is

$$dw = \frac{\gamma dy}{4\pi(y_o - y)} = -\frac{(d\Gamma/dy) dy}{4\pi(y_o - y)}$$

where  $w$  is now defined positive up, in the  $+z$  direction. The factor of  $4\pi$  rather than  $2\pi$  appears because the strip is a semi-infinite vortex, with half the velocity contribution of a doubly-infinite vortex.



Integrating over all the wake strips gives the overall vertical velocity distribution of the whole trailing sheet.

$$w(y_o) = -\frac{1}{4\pi} \int_{-b/2}^{b/2} \frac{d\Gamma}{dy} \frac{dy}{y_o - y}$$

The induced angle distribution is therefore

$$\alpha_i(y_o) = \frac{-w(y_o)}{V_\infty} = \frac{1}{4\pi V_\infty} \int_{-b/2}^{b/2} \frac{d\Gamma}{dy} \frac{dy}{y_o - y}$$

which is defined positive down, as before.

We have obtained an important result, namely a quantitative relation between the circulation distribution  $\Gamma(y_o)$ , which gives the lift, and the downwash angle distribution  $\alpha_i(y_o)$ , which will give the lift slope and the induced drag of the wing. The required analysis and calculation method used to obtain the lift and induced drag will be addressed in the subsequent lectures.

# Fluids – Lecture 7 Notes

## 1. Elliptical Lift Distribution

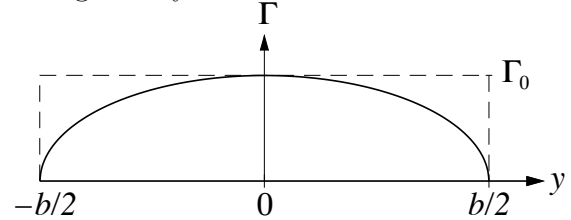
Reading: Anderson 5.3.1

### Elliptical Lift Distribution

#### Definition and lift calculation

Consider an elliptical spanwise circulation distribution given by

$$\Gamma(y) = \Gamma_0 \sqrt{1 - \left(\frac{2y}{b}\right)^2}$$



where  $\Gamma_0$  is the circulation at the wing center at  $y = 0$ . The overall lift on the wing is the integral of the corresponding lift/span distribution  $L'(y) = \rho V_\infty \Gamma(y)$ .

$$L = \int_{-b/2}^{b/2} L'(y) dy = \int_{-b/2}^{b/2} \rho V_\infty \Gamma_0 \sqrt{1 - \left(\frac{2y}{b}\right)^2} dy = \frac{\pi}{4} \rho V_\infty \Gamma_0 b$$

The integral can be evaluated via integral tables, or by inspection by noting that the area under an ellipse is  $\pi/4$  times the area of the enclosing rectangle.

#### Downwash calculation

Computation of the downwash first requires knowing the trailing vortex sheet strength, which is minus the derivative of the circulation.

$$\gamma(y) = -\frac{d\Gamma}{dy} = \frac{4\Gamma_0}{b^2} \frac{y}{\sqrt{1 - (2y/b)^2}}$$

The downwash at some location  $y_o$  is then

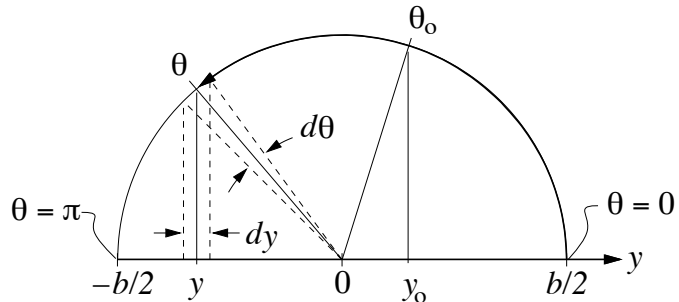
$$w(y_o) = \frac{1}{4\pi} \int_{-b/2}^{b/2} \frac{\gamma(y) dy}{y_o - y} = \frac{\Gamma_0}{\pi b^2} \int_{-b/2}^{b/2} \frac{y}{\sqrt{1 - (2y/b)^2}} \frac{dy}{y_o - y}$$

As in thin airfoil theory, the mathematical problem is considerably simplified by making the trigonometric substitution

$$y_o = \frac{b}{2} \cos \theta_o$$

$$y = \frac{b}{2} \cos \theta$$

$$dy = -\frac{b}{2} \sin \theta d\theta$$



The downwash integral then becomes

$$w(\theta_o) = -\frac{\Gamma_0}{2\pi b} \int_{\pi}^0 \frac{\cos \theta}{\cos \theta_o - \cos \theta} d\theta = \frac{\Gamma_0}{2\pi b} \int_0^{\pi} \frac{\cos \theta}{\cos \theta_o - \cos \theta} d\theta$$

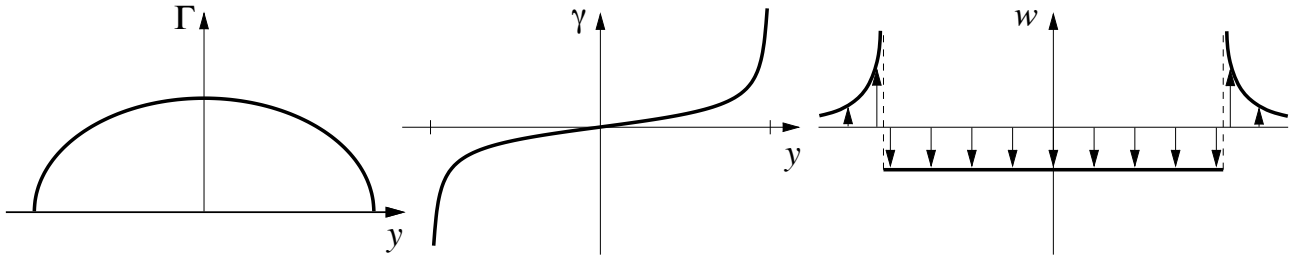
This can be evaluated using the known tabulated integral

$$\int_0^\pi \frac{\cos n\theta}{\cos \theta - \cos \theta_o} d\theta = \frac{\pi \sin n\theta_o}{\sin \theta_o}$$

for any  $\theta_o = 0 \dots \pi$ , and any integer  $n$ . Our case corresponds to  $n = 1$ , and hence

$$w(\theta_o) = \frac{\Gamma_0}{2\pi b} \left( -\frac{\pi \sin \theta_o}{\sin \theta_o} \right) = -\frac{\Gamma_0}{2b}$$

We have the somewhat surprising result that the downwash is uniform over the span of a wing with an elliptical circulation distribution. There is a sharp upwash just outboard of the tips which rapidly dies off with distance, but this doesn't impact the flow angles seen by the wing itself.



From the earlier lift expression above we have

$$\Gamma_0 = \frac{4L}{\rho V_\infty b \pi}$$

which allows elimination of  $\Gamma_0$  from the  $w$  result to give a somewhat more convenient expression.

$$w = -\frac{2L}{\rho V_\infty b^2 \pi}$$

### Induced angles

Because  $w$  is uniform across the span, the induced angles are uniform as well.

$$\alpha_i = -\frac{w}{V_\infty} = \frac{\Gamma_0}{2bV_\infty} = \frac{L}{\frac{1}{2}\rho V_\infty^2 b^2 \pi}$$

We can also use the definition of the overall lift coefficient

$$C_L \equiv \frac{L}{\frac{1}{2}\rho V_\infty^2 S}$$

to obtain yet a third expression for the induced angle.

$$\alpha_i = \frac{S C_L}{b^2 \pi} = \frac{C_L}{\pi AR}$$

### Induced drag

Because  $\alpha_i$  for the elliptically-loaded wing is constant along the span, all the lift vectors along



the span are tilted by the same amount, making the calculation of induced drag relatively simple.

$$D_i = \int_{-b/2}^{b/2} L'(y) \alpha_i dy = \alpha_i \int_{-b/2}^{b/2} L'(y) dy = \alpha_i L$$

Substituting for  $\alpha_i$  in terms of the lift itself gives

$$D_i = \frac{(L/b)^2}{\frac{1}{2}\rho V_\infty^2 \pi}$$

Dividing by  $\frac{1}{2}\rho V_\infty^2 S$  gives the equivalent dimensionless relation.

$$C_{Di} = \frac{C_L^2}{\pi AR}$$

The dimensional and dimensionless forms for induced drag above are both useful. Which one would be used in practice depends on the design or analysis application at hand.

### Total wing drag

The overall wing drag is equal to the profile drag plus the induced drag.

$$\begin{aligned} D &= D_p + D_i \\ \text{or} \quad C_D &= C_{Dp} + C_{Di} \end{aligned}$$

The profile drag coefficient is the chord-weighted average of the local  $c_d(y)$ .

$$C_{Dp} = \frac{1}{S} \int_{-b/2}^{b/2} c_d(y) c(y) dy$$

Here  $c_d$  is the 2-D airfoil viscous airfoil drag, and is usually known in the form of a  $c_d(c_\ell; Re)$  drag polar from wind tunnel data or from calculations. In general,  $c_d(y)$  will vary across the span, although a very common approximation is to simply assume that it's constant, and determined using the overall wing  $C_L$ , and the Reynolds number based on the average chord.

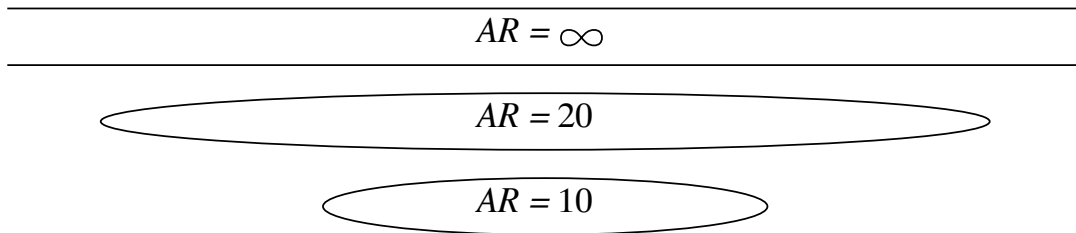
$$c_d \simeq c_d(C_L; Re_{\text{avg}}) \quad , \quad Re_{\text{avg}} = \frac{V_\infty c_{\text{avg}}}{\nu}$$

In this case  $C_{Dp} = c_d$ , and together with the induced drag result the total drag coefficient can then be computed as follows.

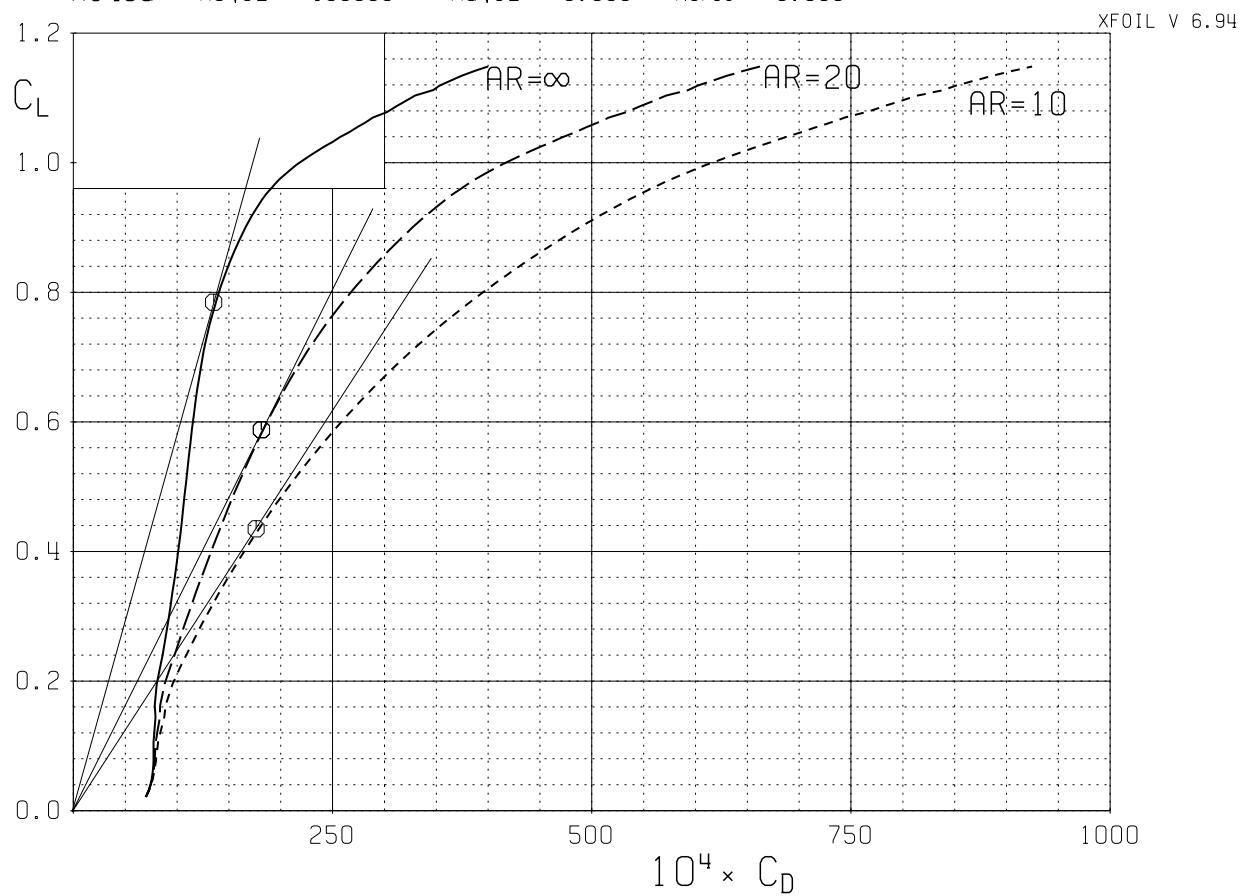
$$C_D(C_L; Re_{\text{avg}}) = c_d(C_L; Re_{\text{avg}}) + \frac{C_L^2}{\pi AR}$$

The figure shows a typical  $C_D(C_L)$  polar plot for one Reynolds number and two aspect ratios,  $AR = 20$  and  $AR = 10$ , together with the 2-D  $c_d(C_L)$  curve, which can be viewed as the limiting  $AR = \infty$  case. Note that this polar corresponds to the *entire wing*, rather than to just one 2-D airfoil section. Two features are immediately apparent:

- 1) The maximum lift/drag ratio  $(C_L/C_D)_{\text{max}}$ , indicated by the slope of the tangent line, decreases considerably as  $AR$  is decreased. Since  $C_L/C_D$  is a critical aircraft performance parameter, especially for range or duration, this indicates the importance of large aspect ratio.
- 2) The  $C_L$  at which the maximum  $C_L/C_D$  ratio is reached decreases as  $AR$  decreases. This implies that for a given wing loading, the aircraft with the smaller aspect ratio must be flown faster to attain its best range or duration.



AG40d	$Re_{\sqrt{CL}} = 100000$	$Ma_{\sqrt{CL}} = 0.000$	$N_{crit} = 9.000$
AG40d	$Re_{\sqrt{CL}} = 100000$	$Ma_{\sqrt{CL}} = 0.000$	$N_{crit} = 9.000$
AG40d	$Re_{\sqrt{CL}} = 100000$	$Ma_{\sqrt{CL}} = 0.000$	$N_{crit} = 9.000$



# Fluids – Lecture 8 Notes

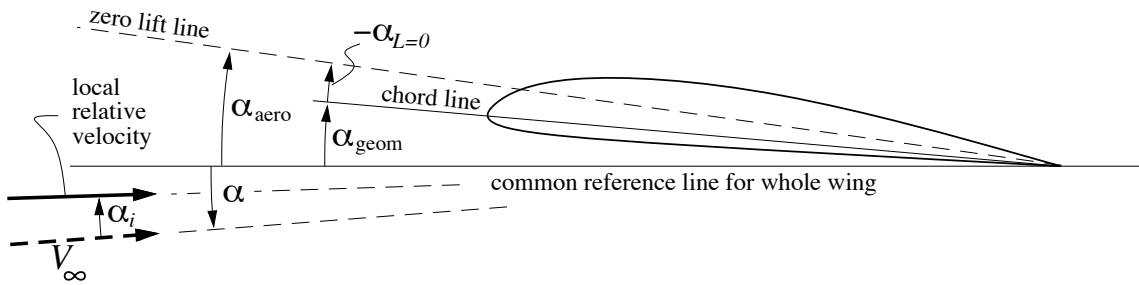
1. Wing Geometry
2. Wing Design Problem

Reading: Anderson 5.3.2, 5.3.3

## Wing Geometry

### Chord and twist

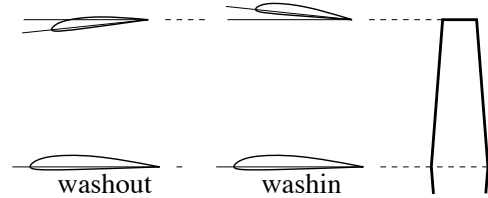
The chord distribution is given by the  $c(y)$  function. Each spanwise station also has a local *geometric twist* angle  $\alpha_{\text{geom}}(y)$ , measured from some reference line which is common to the whole wing. The freestream angle  $\alpha$  is also defined from this same common reference line. The choice of the reference line for all these angles is arbitrary. A typical choice might be the fuselage axis line, or the the wing-center chord line.



How the geometric twist varies across the span is loosely described by the terms *washout* and *washin*:

Washout:  $\alpha_{\text{geom}}(y)$  decreases towards the tip.

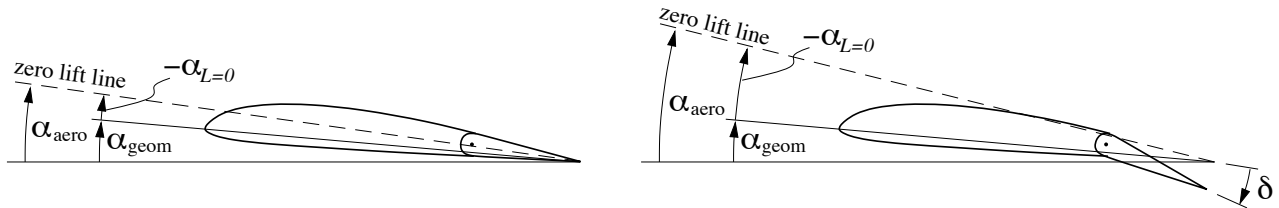
Washin :  $\alpha_{\text{geom}}(y)$  increases towards the tip.



If the wing has a spanwise-varying camber, the local zero-lift angle  $\alpha_{L=0}(y)$  will also vary. It is useful to define an overall *aerodynamic twist* angle as

$$\alpha_{\text{aero}}(y) \equiv \alpha_{\text{geom}}(y) - \alpha_{L=0}(y)$$

The local  $\alpha_{L=0}(y)$  and hence  $\alpha_{\text{aero}}(y)$  can be changed by a flap deflection  $\delta$ .



### Local loading/angle relations

The local lift/span can be given either in terms of the local circulation  $\Gamma(y)$ , or the local chord- $c_\ell$  product.

$$L'(y) = \rho V_\infty \Gamma(y)$$

$$L'(y) = \frac{1}{2} \rho V_\infty^2 c(y) c_\ell(y)$$

Equating these gives the circulation in terms of the chord and  $c_\ell$ .

$$\Gamma(y) = \frac{1}{2} V_\infty c(y) c_\ell(y) \quad (1)$$

Assuming the airfoils are not stalled, the local  $c_\ell$  is proportional to the angle between the local relative velocity and the zero lift line.

$$c_\ell(y) = a_o [\alpha + \alpha_{\text{aero}}(y) - \alpha_i(y)] \quad (2)$$

The constant of proportionality  $a_o = dc_\ell/d\alpha$  is nearly  $2\pi$  for thin airfoils, but is somewhat larger for thick airfoils. It can be obtained from either experimental data or calculation.

Finally, the relation between  $\alpha_i$  at any one location  $y_o$ , and the entire spanwise circulation distribution, was obtained previously using the Biot-Savart law.

$$\alpha_i(y_o) = \frac{1}{4\pi V_\infty} \int_{-b/2}^{b/2} \frac{d\Gamma}{dy} \frac{dy}{y_o - y} \quad (3)$$

Equations (1), (2), and (3) form the basis of wing analysis and design. The general analysis problem is rather complicated and is somewhat beyond scope here. However, the design problem is simpler, and an example design problem is considered next.

## Wing Design Problem

### Elliptic loading

A typical basic wing design problem is to determine the geometry of a wing so that it will have some specified load (or circulation) distribution  $\Gamma(y)$ . As an example, consider the simple case where the span  $b$  and flight speed  $V_\infty$  are given, and the circulation is to be elliptic.

$$\Gamma(y) = \Gamma_0 \sqrt{1 - \left(\frac{2y}{b}\right)^2}$$

Although we don't yet know what the wing looks like, we do already know its lift and induced drag from  $\Gamma(y)$  alone. From previous results,

$$L = \frac{\pi}{4} \rho V_\infty \Gamma_0 b, \quad D_i = \frac{(L/b)^2}{\frac{1}{2} \rho V_\infty^2 \pi}$$

### Planform definition

The wing chord distribution, or planform, is partially given by equation (1). This now becomes

$$c(y) c_\ell(y) = \frac{2\Gamma_0}{V_\infty} \sqrt{1 - \left(\frac{2y}{b}\right)^2}$$

which states only that the  $c \times c_\ell$  product must be elliptic. How  $c$  or  $c_\ell$  vary individually is not determined, but rather must be chosen by the designer. The possibilities are unlimited, but it's useful to consider two particularly simple choices.

**Choice 1:** Pick a spanwise constant  $c_\ell$ . In this case the chord distribution must be elliptic,

$$c(y) = c_0 \sqrt{1 - \left(\frac{2y}{b}\right)^2}$$

$$c_0 = \frac{2\Gamma_0}{V_\infty c_\ell}$$

where  $c_0$  is the center chord. Such a wing is aerodynamically attractive, but the curved outlines may be impractical for construction.

**Choice 2:** Pick a simple constant wing chord,  $c(y) = c$ . Using equation (1) again we have

$$c_\ell(y) = c_{\ell_0} \sqrt{1 - \left(\frac{2y}{b}\right)^2}$$

$$c_{\ell_0} = \frac{2\Gamma_0}{V_\infty c}$$

where  $c_{\ell_0}$  is the wing-center lift coefficient.

### Aerodynamic twist definition

Whatever choice is made for either  $c(y)$  or  $c_\ell(y)$ , the required corresponding wing twist distribution can now be obtained. We have determined earlier that for the elliptic loading case, equation (3) produces a spanwise-constant induced angle, given by

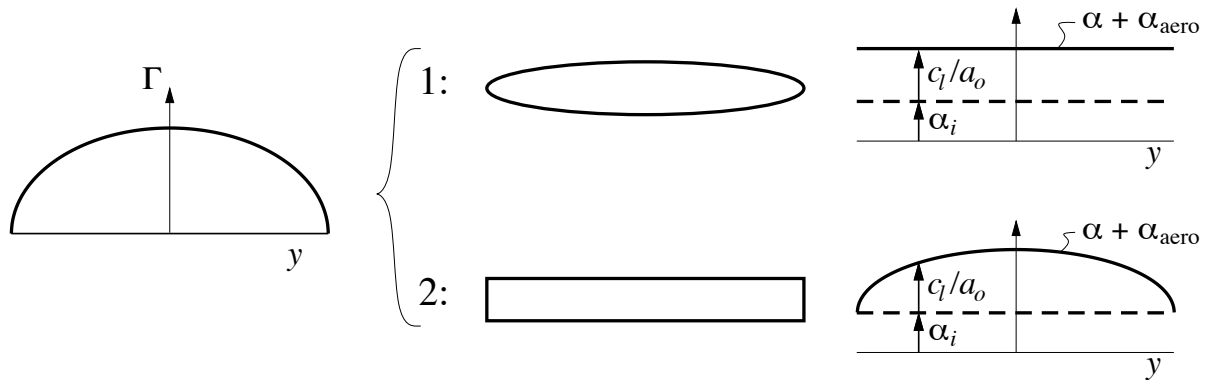
$$\alpha_i(y) = \frac{\Gamma_0}{2bV_\infty} \quad (\text{spanwise constant})$$

although a non-constant  $\alpha_i$  does not present any complications. The aerodynamic twist distribution is then given by rearranging equation (2).

$$\alpha + \alpha_{\text{aero}}(y) = \frac{c_\ell(y)}{a_o} + \alpha_i(y)$$

Only the sum  $\alpha + \alpha_{\text{aero}}(y)$  is defined at this point, since it is the relevant angle which directly affects the lift. How this sum is split up between  $\alpha_{\text{aero}}(y)$  and  $\alpha$  is arbitrary, and will be defined as a final step.

The figure shows the two design choices described here, and the resulting wing shapes and aerodynamic twist distributions. Note that the elliptic-planform wing is *aerodynamically flat*, meaning that it has a constant aerodynamic twist (i.e. the zero-lift lines at all spanwise locations are parallel). In contrast, the “simple” constant chord wing has not turned out so simple after all, with an elliptic aerodynamic twist distribution.



### Geometric twist definition

Definition of the geometric wing twist requires that the airfoil be selected, possibly varying across the span. This selection fixes the  $\alpha_{L=0}(y)$  distribution,

$$\text{given airfoil} \longrightarrow \alpha_{L=0}(y)$$

which in turn determines the required geometric twist, apart from the constant  $\alpha$  offset.

$$\alpha + \alpha_{\text{geom}}(y) = \frac{c_\ell(y)}{a_o} + \alpha_i(y) + \alpha_{L=0}(y) \quad (4)$$

### Reference line selection

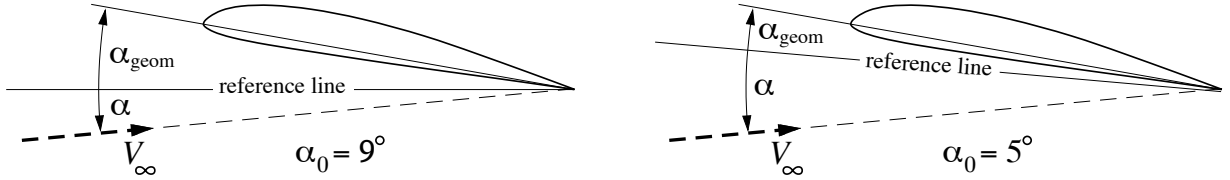
The overall angle of attack  $\alpha$  is finally determined by selection of a common angle reference line for the whole wing. A convenient choice is to set the geometric twist angle at the wing center  $y = 0$  to take on some specific value, say  $\alpha_{\text{geom}}(0) = \alpha_0$ . Applying equation (4) at  $y = 0$  then defines  $\alpha$ .

$$\alpha = \frac{c_\ell(0)}{a_o} + \alpha_i(0) + \alpha_{L=0}(0) - \alpha_0$$

When this  $\alpha$  is substituted into equation (4), the geometric twist distribution is finally obtained.

$$\alpha_{\text{geom}}(y) = \alpha_0 + \frac{c_\ell(y) - c_\ell(0)}{a_o} + \alpha_i(y) - \alpha_i(0) + \alpha_{L=0}(y) - \alpha_{L=0}(0)$$

It must be stressed that the choice of  $\alpha_0$  does not alter the wing twist, or the wing's orientation relative to the freestream velocity (i.e. the physical flow situation is unaffected). As shown in the figure, changing  $\alpha_0$  merely sets the arbitrary reference line at a different orientation on the wing/freestream combination. The flowfields are identical.



# Fluids – Lecture 9 Notes

## 1. General Wings

Reading: Anderson 5.3.2, 5.3.3

## General Wings

### General circulation distribution and downwash

The assumption of elliptic loading is too restrictive for the design of practical wings. A more general circulation distribution can be conveniently described by a *Fourier sine series*, in terms of the angle coordinate  $\theta$  defined earlier.

$$\Gamma(\theta) = 2bV_\infty \sum_{n=1}^N A_n \sin n\theta$$

This is a superposition of individual weighted component shapes  $\sin n\theta$ , shown in the figure plotted versus the physical coordinate  $y$ . The induced angle for this  $\Gamma$  distribution is

$$\frac{\Gamma}{2bV_\infty} = A_1 \times \sin \theta + A_2 \times \sin 2\theta + A_3 \times \sin 3\theta + \dots$$

evaluated by first noting that

$$\frac{d\Gamma}{dy} dy = \frac{d\Gamma}{d\theta} d\theta = 2bV_\infty \sum_{n=1}^N nA_n \cos n\theta d\theta$$

which is then substituted into the induced angle integral.

$$\alpha_i = \frac{1}{4\pi V_\infty} \int_{-b/2}^{b/2} \frac{d\Gamma}{dy} \frac{dy}{y_o - y} = \frac{1}{\pi} \sum_{n=1}^N nA_n \int_0^\pi \frac{\cos n\theta}{\cos \theta - \cos \theta_o} d\theta$$

This integral was evaluated earlier, which gives the final result.

$$\alpha_i(\theta_o) = \sum_{n=1}^N nA_n \frac{\sin n\theta_o}{\sin \theta_o}$$

Each component of  $\Gamma(\theta)$  has a corresponding component of  $\alpha_i(\theta)$ . The leading  $n = 1$  term

$$\alpha_i = A_1 \times 1 + A_2 \times \frac{\sin 2\theta}{\sin \theta} + A_3 \times \frac{\sin 3\theta}{\sin \theta} + \dots$$

is the same as the elliptic loading case, with the expected uniform induced angle. The remaining terms deviate the loading away from the elliptic distribution, and deviate the downwash away from the uniform distribution.

## Lift

We can now compute the lift for the general circulation distribution by integrating it across the span.

$$L = \int_{-b/2}^{b/2} \rho V_{\infty} \Gamma(y) dy$$

The integral is most easily evaluated using the  $\theta$  coordinate. With the substitutions

$$\begin{aligned} y &= \frac{b}{2} \cos \theta \\ dy &= -\frac{b}{2} \sin \theta d\theta \end{aligned}$$

we then have

$$L = \rho V_{\infty} \left[ 2bV_{\infty} \sum_{n=1}^N A_n \frac{b}{2} \int_0^{\pi} \sin n\theta \sin \theta d\theta \right]$$

All the integrals inside the summation are readily evaluated using the orthogonality property of the sine functions.

$$\int_0^{\pi} \sin n\theta \sin m\theta d\theta = \begin{cases} \pi/2 & (\text{if } n = m) \\ 0 & (\text{if } n \neq m) \end{cases}$$

For our case we have  $m = 1$ , and then consider  $n = 1, 2, 3, \dots$  for each term. Clearly, the  $n = 1$  integral evaluates to  $\pi/2$ , and the rest evaluate to zero. Therefore,

$$\begin{aligned} L &= \frac{\pi}{2} \rho V_{\infty}^2 b^2 A_1 \\ C_L &= \frac{L}{\frac{1}{2} \rho V_{\infty}^2 S} = \pi A_1 \frac{b^2}{S} = A_1 \pi AR \end{aligned}$$

Only the leading  $n = 1$  component of the circulation contributes to the lift. This is expected after examination of the component shapes for  $\Gamma(y)$ , which shows that only the  $n = 1$  shape has a nonzero area under it.

## Induced drag and span efficiency

The induced drag is also evaluated by spanwise integration.

$$D_i = \int_{-b/2}^{b/2} \rho V_{\infty} \Gamma(y) \alpha_i(y) dy$$

After switching from  $y$  to  $\theta$ , and substituting for  $\Gamma(\theta)$  and  $\alpha_i(\theta)$ , this evaluates to

$$D_i = \pi b^2 \frac{1}{2} \rho V_{\infty}^2 \left[ A_1^2 + 2A_2^2 + 3A_3^2 + \dots NA_N^2 \right] = \pi b^2 \frac{1}{2} \rho V_{\infty}^2 A_1^2 \left[ 1 + \sum_{n=2}^N n \left( \frac{A_n}{A_1} \right)^2 \right]$$

Although only the  $A_1$  part of the circulation contributes to lift, all the  $A_n$  parts contribute towards increasing the induced drag. We therefore conclude that the elliptic load distribution gives the smallest induced drag for a given lift and span.

A more convenient equation for the induced drag can be obtained by replacing  $A_1$  in terms of the lift. This gives

$$D_i = \frac{(L/b)^2}{\frac{1}{2} \rho V_{\infty}^2 \pi} [1 + \delta]$$



where

$$\delta \equiv \sum_{n=2}^N n \left( \frac{A_n}{A_1} \right)^2$$

can be thought of as a fractional induced drag penalty due to the presence of the higher  $n = 2, 3 \dots$  “non-elliptic” loading terms. It is traditional to define a *span efficiency*

$$e \equiv \frac{1}{1 + \delta}$$

so that the induced drag is finally given as

$$D_i = \frac{(L/b)^2}{\frac{1}{2}\rho V_\infty^2 \pi e}$$

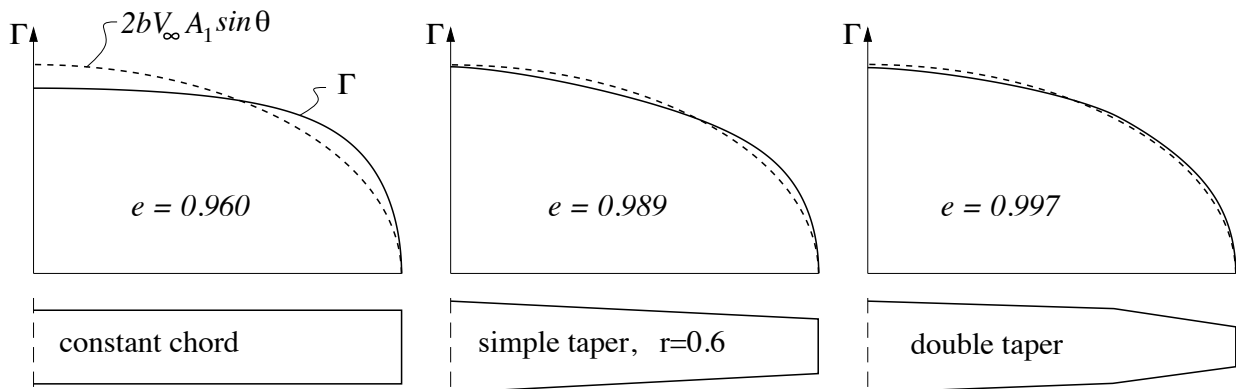
The corresponding induced drag coefficient is then easily obtained.

$$C_{Di} = \frac{C_L^2}{\pi e AR}$$

Because  $\delta$  is the sum of squares and hence non-negative, the span efficiency must be  $e \leq 1$ , and the actual induced drag is never less than the minimum drag corresponding to elliptic loading, for which  $\delta = 0$  and  $e = 1$ .

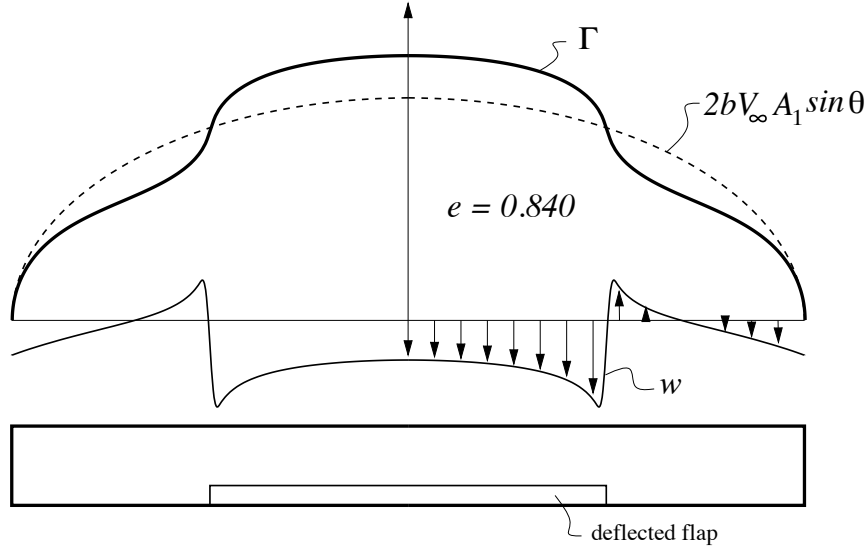
### Load distributions on typical planforms

The figure shows three wing planforms with no twist (constant  $\alpha_{\text{geom}}$ ), along with their computed circulation distributions at some nonzero lift. Also shown is the elliptic component of the circulation  $2bV_\infty A_1 \sin \theta$  as a dotted line. The difference between the two curves is the remaining  $n = 2, 3 \dots$  terms, which produce a nonzero  $\delta$ , and  $e < 1$ . Even the relatively crude constant-chord wing has an acceptable span efficiency, with only a 4% induced drag “penalty”. The loading on the double-taper wing is very nearly elliptic, and hence  $e \simeq 1$  for this case. Clearly, the complexity of a curved elliptic planform is hardly warranted.



### Effects of trailing edge flaps

Deflection of a part-span trailing edge flap will usually cause a significant distortion in the load distribution, producing a significant increase in induced drag. The figure shows the constant-chord wing case, with a central flap deflected downward  $15^\circ$ . The loading is strongly non-elliptic, and the span efficiency has decreased to 0.840. Note also the strongly non-uniform downwash distribution resulting from this distorted loading.



### Lift slope reduction

The downwash behind any finite wing modifies the wing's lift slope. Consider the  $c_\ell$ -angle relation at a typical spanwise location.

$$c_\ell = a_0 (\alpha + \alpha_{\text{aero}} - \alpha_i)$$

For a nearly-elliptic loading, we have  $c_\ell \simeq C_L$  and  $\alpha_i \simeq C_L / \pi e AR$

$$\begin{aligned} \text{giving} \quad C_L &= a_0 \left( \alpha + \alpha_{\text{aero}} - \frac{C_L}{\pi e AR} \right) \\ \text{or} \quad C_L &= \frac{a_0}{1 + \frac{a_0}{\pi e AR}} (\alpha + \alpha_{\text{aero}}) = a (\alpha + \alpha_{\text{aero}}) \end{aligned}$$

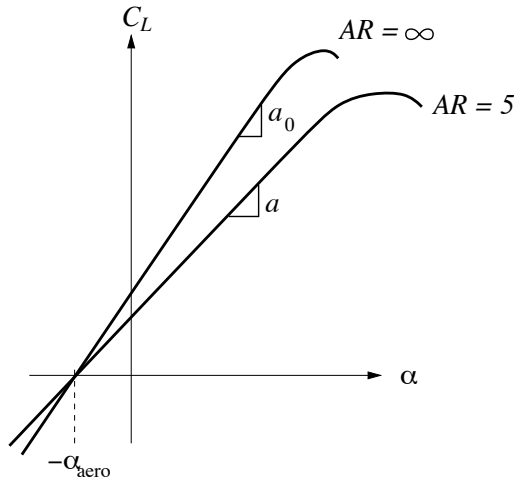
The lift slope is now

$$\frac{dC_L}{d\alpha} = \frac{a_0}{1 + \frac{a_0}{\pi e AR}} \equiv a$$

A common approximation is to assume that  $a_0 = 2\pi$  and  $e \simeq 1$ , in which case

$$a \simeq \frac{2\pi}{1 + 2/AR}$$

This slope  $a$  clearly decreases as  $AR$  is reduced. Low aspect ratio wings must therefore operate at higher angles of attack than high aspect ratio wings to reach the same  $C_L$ .



# Fluids – Lecture 10 Notes

1. Aircraft Performance Analysis
2. Parasite Drag Estimation

Reference: Hoerner,S.F., “Fluid-Dynamic Drag”, Ch 3.

## Aircraft Performance Analysis

### Drag breakdown

The drag on a subsonic aircraft can be broken down as follows.

$$D = D_o + D_p + D_i$$

where  $D_o$  = “parasite” drag of fuselage + tail + landing gear + ...  
 $D_p$  = wing profile drag  
 $D_i$  = induced drag

We now use the wing airfoil drag polar  $c_d(c_\ell; Re)$  to give the wing profile drag, and use lifting line to give the induced drag. The nondimensional total drag coefficient is then

$$\frac{D}{\frac{1}{2}\rho V^2 S} \equiv C_D = \frac{CDA_o}{S} + c_d(C_L; Re) + \frac{C_L^2}{\pi eAR} \quad (1)$$

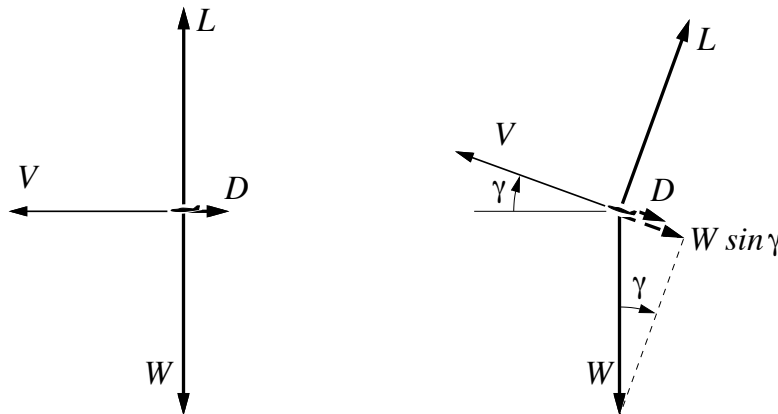
where the “ $\infty$ ” subscript on the flight speed  $V$  has been dropped. The parasite drag area  $CDA_o$  will be considered later.

### Flight power

The mechanical power  $P$  needed for constant-velocity flight is given by

$$\eta_p P = V (D + W \sin \gamma) \quad (2)$$

where  $W$  is the weight,  $\gamma$  is the *climb angle*, and  $\eta_p$  is the propulsive efficiency. If  $P$  is defined as the motor shaft power, then  $\eta_p$  is the propeller efficiency.



In level flight,  $\gamma = 0$ , and the power is

$$\eta_p P = V D = \frac{1}{2}\rho V^3 S C_D \quad (3)$$

The flight speed  $V$  is given by the Lift = Weight condition, together with the definition of the lift coefficient  $C_L$ .

$$L = \frac{1}{2} \rho V^2 S C_L = W$$

$$V = \left( \frac{2W/S}{\rho C_L} \right)^{1/2}$$

The ratio  $W/S$  is called the *wing loading*, and has the units of force/area, or pressure. The level-flight power equation (3) then takes the following form.

$$P = \frac{1}{\eta_p} \left( \frac{2W/S}{\rho} \right)^{1/2} W \frac{C_D}{C_L^{3/2}} \quad (4)$$

### Power dependencies

Equation (4) indicates how the level flight power depends on the quantities of interest. The following dependencies are particularly worthy to note:

$$P \sim \frac{1}{\eta_p}$$

$$P \sim \frac{1}{S^{1/2}}$$

$$P \sim W^{3/2}$$

$$P \sim \frac{C_D}{C_L^{3/2}}$$

Note the very strong effect of overall weight  $W$ . This indicates that to reduce flight power, considerable effort should be directed towards weight reduction if that's possible.

An important consideration is that the proportionality with each parameter assumes that all the other parameters are held fixed, which is difficult if not impossible to do in practice. For example, increasing the wing area  $S$  is likely to also increase the weight  $W$ , so the net influence on the flight power requires a closer analysis of the area-weight relation.

The flight power is seen to vary as the inverse of the ratio  $C_L^{3/2}/C_D$ , must be maximized to obtain minimum-power flight, or maximum-duration flight. But again, increasing the maximum achievable  $C_L^{3/2}/C_D$  will typically require changes in the other aircraft parameters.

### Drag and power polars

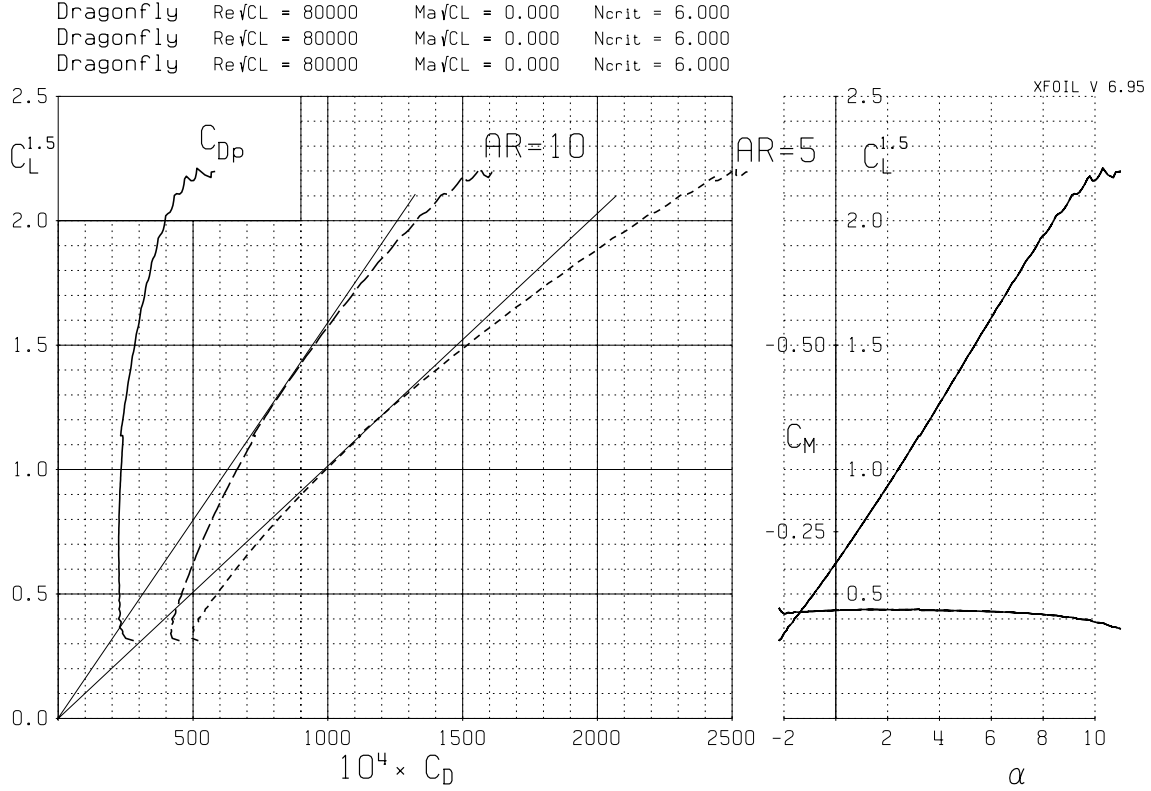
One convenient way to examine the aircraft's power-requirement characteristics is in a *power polar*. This is a variation on the more common drag polar, with the vertical  $C_L$  axis being replaced by  $C_L^{3/2}$ . An example power polar is shown below, showing three curves:

Only  $C_{Dp}$ , which assumes  $C_{Do} = 0$  and  $AR = \infty$ .

Total  $C_D$ , assuming  $C_{Do}S_o/S = 0.01$ , and  $eAR = 10$ .

Total  $C_D$ , assuming  $C_{Do}S_o/S = 0.01$ , and  $eAR = 5$ .

The slope of the line tangent to each polar curve indicates the maximum  $C_L^{3/2}/C_D$  value, and the point of contact gives the  $C_L$  at which this condition occurs. For the two example polars, we have:



For  $AR = 10$ :  $(C_L^{3/2}/C_D)_{\max} = 16.0$  at  $C_L \simeq 0.90$

For  $AR = 5$ :  $(C_L^{3/2}/C_D)_{\max} = 10.0$  at  $C_L \simeq 0.70$

The  $AR = 10$  aircraft can therefore be expected to have a power requirement which is lower by a factor of  $10.0/16.0 = 0.625$ . The expected duration is longer by the reciprocal factor  $16.0/10.0 = 1.6$ . But this assumes that the larger  $AR$  has no other adverse effect on the other important parameters affecting  $P$ , which is very unlikely.

### Maximum Speed

Maximum speed can also be estimated using the drag or power relations developed here. The level-flight power relation (3) at maximum power becomes

$$\eta_p P_{\max} = \frac{1}{2} \rho V_{\max}^3 S \left[ \frac{CDA_o}{S} + c_d(C_{L_{\min}}; Re_{\max}) + \frac{C_{L_{\min}}^2}{\pi e AR} \right]$$

where  $C_{L_{\min}} = \frac{2W/S}{\rho V_{\max}^2}$

This can be solved for  $V_{\max}$ , numerically or graphically if necessary. If one can assume that at maximum speed the induced drag is negligible, and  $c_d$  is some constant, then we have

$$V_{\max} \simeq \left[ \frac{2 \eta_p P_{\max}}{\rho (CDA_o + S c_d)} \right]^{1/3}$$

Alternatively, if the maximum thrust  $T_{\max}$  is known rather than the maximum power, the maximum velocity is obtained from the horizontal force balance.

$$T_{\max} = \frac{1}{2} \rho V_{\max}^2 S \left[ \frac{CDA_o}{S} + c_d(C_{L_{\min}}; Re_{\max}) + \frac{C_{L_{\min}}^2}{\pi e AR} \right]$$

$$V_{\max} \simeq \left[ \frac{2 T_{\max}}{\rho (CDA_o + S c_d)} \right]^{1/2}$$

## Parasite Drag Estimation

To estimate the total parasite drag  $D_o$ , it is commonly assumed that it is simply a summation of the estimated parasite drags of the various drag-producing components on the aircraft. For example,

$$D_o = D_{\text{fuselage}} + D_{\text{tail}} + D_{\text{gear}} + \dots$$

To make this summation applicable to any flight speed, we simply divide it by the flight dynamic pressure, to give a summation of the drag areas.

$$CDA_o \equiv \frac{D_o}{\frac{1}{2}\rho V^2} = CDA_{\text{fuselage}} + CDA_{\text{tail}} + CDA_{\text{gear}} + \dots \quad (5)$$

where

$$CDA_{\text{fuselage}} = \frac{D_{\text{fuselage}}}{\frac{1}{2}\rho V^2}$$

$$CDA_{\text{tail}} = \frac{D_{\text{tail}}}{\frac{1}{2}\rho V^2} \quad \dots \text{etc}$$

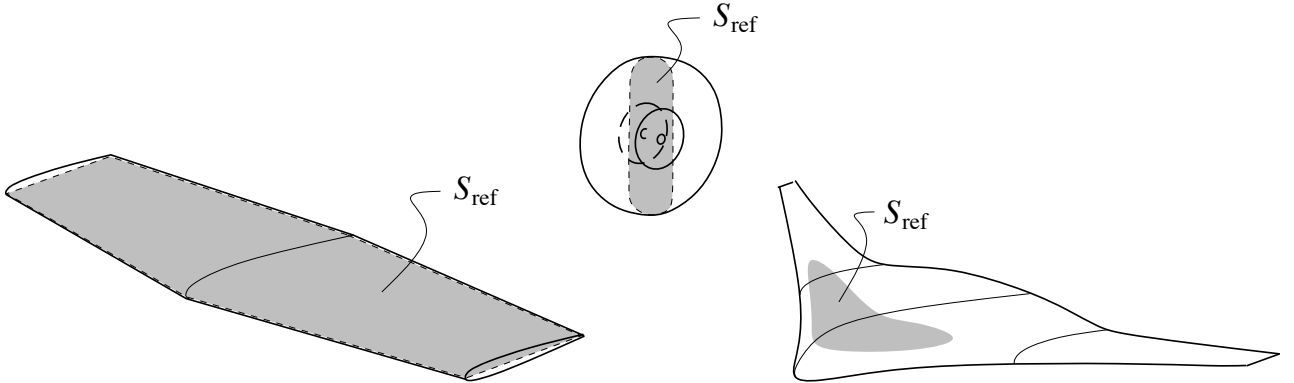
The summation (5) is called a *drag area buildup*.

Each component's drag area in (5) is estimated separately by whatever means are available. Typically, this will be the product of a drag coefficient  $C_D$ , and the reference area  $S_{\text{ref}}$  corresponding to that drag coefficient.

$$CDA_{\text{object}} = (C_D)_{\text{object}} (S_{\text{ref}})_{\text{object}}$$

For streamlined objects such as the tail surfaces,  $S_{\text{ref}}$  is typically the planform area. For bluff objects such as nacelles, wheels, etc,  $S_{\text{ref}}$  is typically the frontal area. For complex streamlined shapes, another approach is to use an average *skin friction coefficient* and the *wetted area*.

$$\begin{aligned} CDA_{\text{tail}} &= c_{d_{\text{tail}}} S_{\text{tail}} \\ CDA_{\text{wheel}} &= C_{D_{\text{wheel}}} S_{\text{wheel}} \\ CDA_{\text{shape}} &= C_f S_{\text{wet}} \end{aligned}$$



# Fluids – Lecture 11 Notes

1. Introduction to Compressible Flows
2. Thermodynamics Concepts

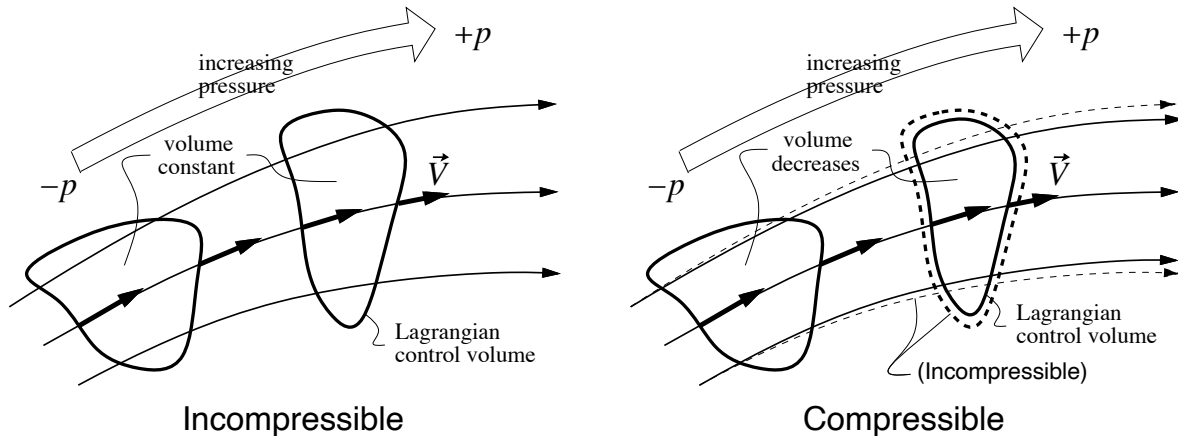
Reading: Anderson 7.1 – 7.2

## Introduction to Compressible Flows

### Definition and implications

A *compressible flow* is a flow in which the fluid density  $\rho$  varies significantly within the flowfield. Therefore,  $\rho(x, y, z)$  must now be treated as a field variable rather than simply a constant. Typically, significant density variations start to appear when the flow Mach number exceeds 0.3 or so. The effects become especially large when the Mach number approaches and exceeds unity.

The figure shows the behavior of a moving Lagrangian Control Volume (CV) which by definition surrounds a fixed mass of fluid  $m$ . In incompressible flow the density  $\rho$  does not change, so the CV's volume  $\mathcal{V} = m/\rho$  must remain constant. In the compressible flow case, the CV is squeezed or expanded significantly in response to pressure changes, with  $\rho$  changing in inverse proportion to  $\mathcal{V}$ . Since the CV follows the streamlines, changes in the CV's volume must be accompanied by changes in the streamlines as well. Above Mach 1, these volumetric changes dominate the streamline pattern.



Many of the relations developed for incompressible (i.e. low speed) flows must be revisited and modified. For example, the Bernoulli equation is no longer valid,

$$p + \frac{1}{2}\rho V^2 \neq \text{constant}$$

since  $\rho = \text{constant}$  was assumed in its derivation. However, concepts such as stagnation pressure  $p_o$  are still usable, but their definitions and relevant equations will be different from the low speed versions.

Some flow solution techniques used in incompressible flow problems will no longer be applicable to compressible flows. In particular, the technique of superposition will no longer be generally applicable, although it will still apply in some restricted situations.

### Perfect gas

A *perfect gas* is one whose individual molecules interact only via direct collisions, with no

other intermolecular forces present. For such a perfect gas, the properties  $p$ ,  $\rho$ , and the temperature  $T$  are related by the following *equation of state*

$$p = \rho RT$$

where  $R$  is the specific gas constant. For air,  $R = 287\text{J/kg}\cdot\text{K}^\circ$ . It is convenient at this point to define the *specific volume* as the limiting volume per unit mass,

$$v \equiv \lim_{\Delta\mathcal{V} \rightarrow 0} \frac{\Delta\mathcal{V}}{\Delta m} = \frac{1}{\rho}$$

which is merely the reciprocal of the density. In general, the nomenclature “specific X” is synonymous with “X per unit mass”. The equation of state can now be written as

$$pv = RT$$

which is the more familiar thermodynamic form.

The appearance of the temperature  $T$  in the equation of state means that it must vary within the flowfield. Therefore,  $T(x, y, z)$  must be treated as a new field variable in addition to  $\rho(x, y, z)$ . In the moving CV scenario above, the change in the CV’s volume is not only accompanied by a change in density, but by a change in temperature as well.

The appearance of the temperature also means that thermodynamics will need to be addressed. So in addition to the conservation of mass and momentum which were employed in low speed flows, we will now also need to consider the conservation of energy. The following table compares the variables and equations which come into play in the two cases.

	Incompressible flow	Compressible flow
variables:	$\vec{V}, p$	$\vec{V}, p, \rho, T$
equations:	mass, $\overrightarrow{\text{momentum}}$	mass, $\overrightarrow{\text{momentum}}$ , energy, state

## Thermodynamics Concepts

### Internal Energy and Enthalpy

The law of conservation of energy involves the concept of *internal energy*, which is the sum of the energies of all the molecules of a system. In fluid mechanics we employ the *specific internal energy*, denoted by  $e$ , which is defined for each point in the flowfield. A related quantity is the *specific enthalpy*, denoted by  $h$ , and related to the other variables by

$$h = e + pv$$

The units of  $e$  and  $h$  are  $(\text{velocity})^2$ , or  $\text{m}^2/\text{s}^2$  in SI units.

For a *calorically perfect gas*, which is an excellent model for air at moderate temperatures, both  $e$  and  $h$  are directly proportional to the temperature. Therefore we have

$$\begin{aligned} e &= c_v T \\ h &= c_p T \end{aligned}$$

where  $c_v$  and  $c_p$  are specific heats at constant volume and constant pressure, respectively.

$$h - e = pv = (c_p - c_v)T$$



and comparing to the equation of state, we see that

$$c_p - c_v = R$$

Defining the *ratio of specific heats*,  $\gamma \equiv c_p/c_v$ , we can with a bit of algebra write

$$c_v = \frac{1}{\gamma - 1} R$$

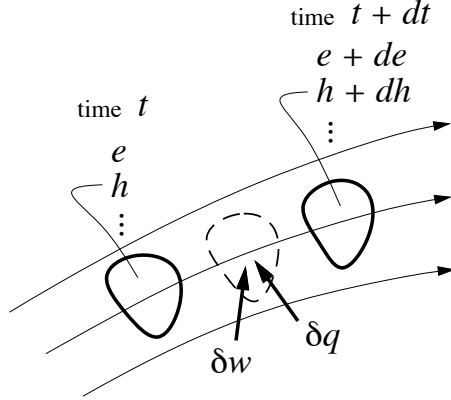
$$c_p = \frac{\gamma}{\gamma - 1} R$$

so that  $c_v$  and  $c_p$  can be replaced with the equivalent variables  $\gamma$  and  $R$ . For air, it is handy to remember that

$$\gamma = 1.4 \qquad \frac{1}{\gamma - 1} = 2.5 \qquad \frac{\gamma}{\gamma - 1} = 3.5 \qquad (\text{air})$$

### First Law of Thermodynamics

Consider a *thermodynamic system* consisting of a small Lagrangian control volume (CV) moving with the flow.



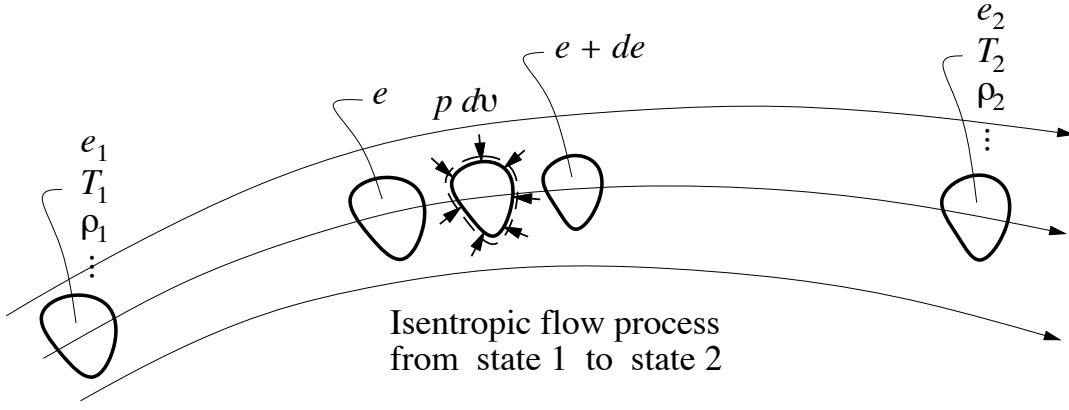
Over the short time interval  $dt$ , the CV undergoes a *process* where it receives work  $\delta w$  and heat  $\delta q$  from its surroundings, both per unit mass. This process results in changes in the state of the CV, described by the increments  $de$ ,  $dh$ ,  $dp \dots$ . The first law of thermodynamics for the process is

$$\delta q + \delta w = de \tag{1}$$

This states that whatever energy is added to the system, whether by heat or by work, it must appear as an increase in the internal energy of the system.

The first law only makes a statement about  $de$ . We can deduce the changes in the other state variables, such as  $dh$ ,  $dp$ ,  $\dots$  if we assume special types of processes.

1. *Adiabatic process*, where no heat is transferred, or  $\delta q = 0$ . This rules out heating of the CV via conduction through its boundary, or by combustion inside the CV.
2. *Reversible process*, no dissipation occurs, implying that work must be only via volumetric compression, or  $dw = -p dv$ . This rules out work done by friction forces.
3. *Isentropic process*, which is both adiabatic and reversible, implying  $-p dv = de$ .



### Isentropic relations

Aerodynamic flows are effectively inviscid outside of boundary layers. This implies they have negligible heat conduction and friction forces, and hence are isentropic. Therefore, along the pathline followed by the CV in the figure above, the isentropic version of the first law applies.

$$-p dv = de \quad (2)$$

This relation can be integrated after a few substitutions. First we note that

$$dv = d\left(\frac{1}{\rho}\right) = -\frac{d\rho}{\rho^2}$$

and with the perfect gas relation

$$de = c_v dT = \frac{1}{\gamma - 1} R dT$$

the isentropic first law (2) becomes

$$\begin{aligned} p \frac{d\rho}{\rho^2} &= \frac{1}{\gamma - 1} R dT \\ \frac{d\rho}{\rho} &= \frac{1}{\gamma - 1} \frac{\rho R}{p} dT \\ \frac{d\rho}{\rho} &= \frac{1}{\gamma - 1} \frac{dT}{T} \end{aligned}$$

The final form can now be integrated from any state 1 to any state 2 along the pathline.

$$\begin{aligned} \ln \rho &= \frac{1}{\gamma - 1} \ln T + \text{const.} \\ \rho &= \text{const.} \times T^{1/(\gamma-1)} \\ \frac{\rho_2}{\rho_1} &= \left(\frac{T_2}{T_1}\right)^{1/(\gamma-1)} \end{aligned} \quad (3)$$

From the equation of state we also have

$$\frac{\rho_2}{\rho_1} = \frac{p_2}{p_1} \frac{T_1}{T_2}$$

which when combined with (3) gives the alternative isentropic relation

$$\frac{p_2}{p_1} = \left(\frac{T_2}{T_1}\right)^{\gamma/(\gamma-1)} \quad (4)$$

# Fluids – Lecture 12 Notes

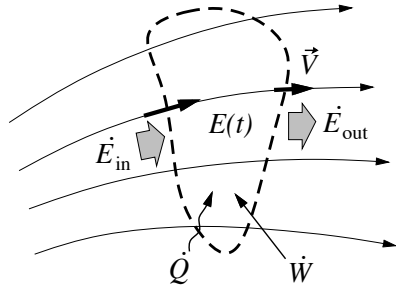
## 1. Energy Conservation

Reading: Anderson 2.7, 7.4, 7.5

## Energy Conservation

### Application to fixed finite control volume

The first law of thermodynamics for a fixed control volume undergoing a process is



$$dE = \delta Q + \delta W$$

$$\frac{dE}{dt} + \dot{E}_{\text{out}} - \dot{E}_{\text{in}} = \dot{Q} + \dot{W} \quad (1)$$

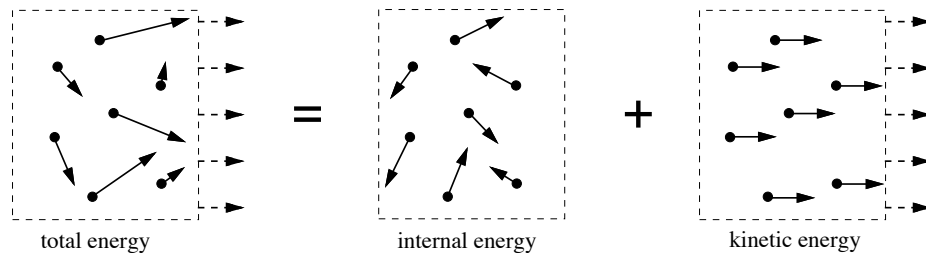
where the second rate form is obtained by dividing by the process time interval  $dt$ , and including the contribution of flow in and out of the volume.

### Total energy

In general, the work rate  $\dot{W}$  will go towards the kinetic energy as well as the internal energy of the fluid inside the CV, in some unknown proportion. This ambiguity is resolved by defining the *total specific energy*, which is simply the sum of internal and kinetic specific energies.

$$e_o = e + \frac{1}{2}V^2 = c_v T + \frac{1}{2}V^2$$

This is the overall energy/mass of the fluid seen by a fixed observer. The  $e$  part corresponds to the molecular motion, while the  $V^2/2$  part corresponds to the bulk motion.



We now define the overall system energy  $E$  to include the kinetic energy

$$E = \iiint \rho e_o dV$$

so that  $\dot{W}$  can now include all work.

### Energy flow

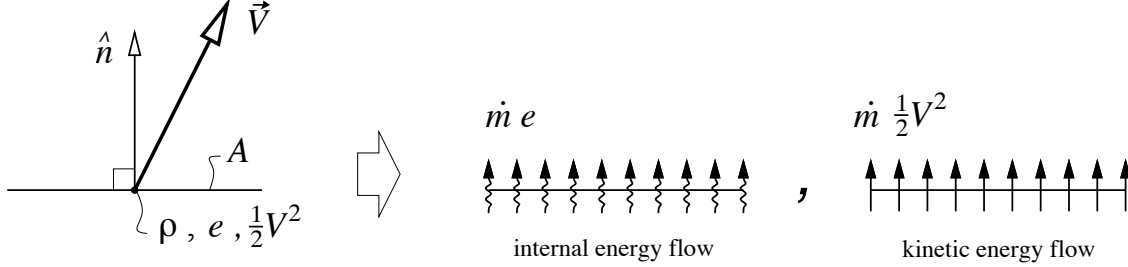
The  $\dot{E}_{\text{out}}$  and  $\dot{E}_{\text{in}}$  terms in equation (1) account for mass flow through the CV boundary, which carries not only momentum, but also thermal and kinetic energies. The *internal energy flow* and *kinetic energy flow* can be described as

$$\begin{aligned} \text{internal energy flow} &= (\text{mass flow}) \times (\text{internal energy/mass}) \\ \text{kinetic energy flow} &= (\text{mass flow}) \times (\text{kinetic energy/mass}) \end{aligned}$$

where the mass flow was defined earlier. The internal energy/mass is by definition the specific internal energy  $e$ , and the kinetic energy/mass is simply  $V^2/2$ . Therefore

$$\begin{aligned}\text{internal energy flow} &= \dot{m} e = \rho (\vec{V} \cdot \hat{n}) A e = \rho V_n A e \\ \text{kinetic energy flow} &= \dot{m} \frac{1}{2} V^2 = \rho (\vec{V} \cdot \hat{n}) A \frac{1}{2} V^2 = \rho V_n A \frac{1}{2} V^2\end{aligned}$$

where  $V_n = \vec{V} \cdot \hat{n}$ . Note that both types of energy flows are scalars.



The net total energy flow rate in and out of the volume is obtained by integrating the internal and kinetic energy flows over its entire surface.

$$\dot{E}_{\text{out}} - \dot{E}_{\text{in}} = \oint \rho (\vec{V} \cdot \hat{n}) \left( e + \frac{1}{2} V^2 \right) dA = \oint \rho (\vec{V} \cdot \hat{n}) e_o dA$$

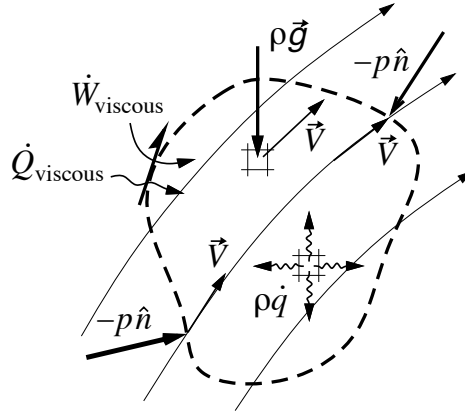
### Heat addition

Two types of heat addition can occur.

Body heating. This acts on fluid inside the volume. Examples are combustion, and internal absorption of radiation (e.g. microwaves). Whatever the source, the body heating is given by a specific heating rate  $\dot{q}$ , with units of power/mass.

$$\dot{Q}_{\text{body}} = \iiint \rho \dot{q} dV$$

Surface heating. The surface can transmit *heat flux* into or out of the volume. This is usually associated with viscous action, and like the viscous work rate it is complicated to write out. It will be simply called  $\dot{Q}_{\text{viscous}}$ .



### Work by applied forces

The work rate (or power) performed by a force  $\vec{F}$  applied to fluid moving at velocity  $\vec{V}$  is

$$\dot{W} = \vec{F} \cdot \vec{V}$$

We will consider two types of applied forces.

Body forces. These act on fluid inside the volume. The most common example is the gravity force, along the gravitational acceleration vector  $\vec{g}$ . The work rate done on the fluid inside the entire CV is

$$\dot{W}_{\text{gravity}} = \iiint \rho \vec{g} \cdot \vec{V} d\mathcal{V}$$

Surface forces. These act on the surface of the volume, and can be separated into pressure and viscous forces. The work rate done by the pressure is

$$\dot{W}_{\text{pressure}} = \oint -p \hat{n} \cdot \vec{V} dA$$

The work rate done by the viscous force is complicated to write out, and for now will simply be called  $\dot{W}_{\text{viscous}}$ .

### Integral Energy Equation

Substituting all the energy flow, heating, and work term definitions into equation (1) gives the *Integral Energy Equation*.

$$\begin{aligned} \frac{d}{dt} \iiint \rho e_o d\mathcal{V} + \oint \rho (\vec{V} \cdot \hat{n}) e_o dA = & \iiint \rho \dot{q} d\mathcal{V} + \oint -p \hat{n} \cdot \vec{V} dA + \iiint \rho \vec{g} \cdot \vec{V} d\mathcal{V} \\ & + \dot{Q}_{\text{viscous}} + \dot{W}_{\text{viscous}} \end{aligned} \quad (2)$$

### Total enthalpy

We now define the *total enthalpy* as

$$h_o = h + \frac{1}{2} V^2 = e + \frac{p}{\rho} + \frac{1}{2} V^2 = e_o + \frac{p}{\rho}$$

We can now combine the two surface integrals in equation (2) into one enthalpy-flow integral. The result is the simpler and more convenient *Integral Enthalpy Equation* which does no longer explicitly contains the pressure work term.

$$\frac{d}{dt} \iiint \rho e_o d\mathcal{V} + \oint \rho (\vec{V} \cdot \hat{n}) h_o dA = \iiint \rho \dot{q} d\mathcal{V} + \iiint \rho \vec{g} \cdot \vec{V} d\mathcal{V} + \dot{Q}_{\text{viscous}} + \dot{W}_{\text{viscous}} \quad (3)$$

In most applications we can assume steady flow, and also neglect gravity and viscous work. Equation (3) then simplifies to

$$\oint \rho (\vec{V} \cdot \hat{n}) h_o dA = \iiint \rho \dot{q} d\mathcal{V} + \dot{Q}_{\text{viscous}} \quad (4)$$

Along with the Integral Mass Equation and the Integral Momentum Equation, equation (4) can be applied to solve many thermal flow problems involving finite control volumes. The  $\dot{Q}_{\text{viscous}}$  term typically represents heating or cooling of the fluid by a solid wall.

### Differential Enthalpy Equation

The enthalpy-flow surface integral in equation (3) can be converted to a volume integral using Gauss's Theorem.

$$\oint \rho (\vec{V} \cdot \hat{n}) h_o dA = \iiint \nabla \cdot (\rho \vec{V} h_o) d\mathcal{V}$$

Omitting the viscous terms for simplicity, the integral enthalpy equation (3) can now be written strictly in terms of volume integrals.

$$\iiint \left[ \frac{\partial(\rho e_o)}{\partial t} + \nabla \cdot (\rho \vec{V} h_o) - \rho \dot{q} - \rho \vec{g} \cdot \vec{V} \right] d\mathcal{V} = 0$$

This relation must hold for *any* control volume whatsoever, and hence the whole quantity in the brackets must be zero at every point.

$$\frac{\partial(\rho e_o)}{\partial t} + \nabla \cdot (\rho \vec{V} h_o) = \rho \dot{q} + \rho \vec{g} \cdot \vec{V}$$

which applies at every point in the flowfield. Adding  $\partial p / \partial t$  to both sides and combining it on the left side gives the *Differential Enthalpy Equation* in “divergence form”.

$$\frac{\partial(\rho h_o)}{\partial t} + \nabla \cdot (\rho \vec{V} h_o) = \frac{\partial p}{\partial t} + \rho \dot{q} + \rho \vec{g} \cdot \vec{V} \quad (5)$$

We can recast this equation further by expanding the lefthand side terms.

$$h_o \left[ \frac{\partial \rho}{\partial t} + \nabla \cdot (\rho \vec{V}) \right] + \rho \left( \frac{\partial h_o}{\partial t} + \vec{V} \cdot \nabla h_o \right) = \frac{\partial p}{\partial t} + \rho \dot{q} + \rho \vec{g} \cdot \vec{V}$$

The quantity in the brackets is exactly zero by the mass continuity equation, and the quantity in the braces is simply  $Dh_o / Dt$ , so that the result can be written compactly as the *Differential Enthalpy Equation* in “convective form”.

$$\frac{Dh_o}{Dt} = \frac{1}{\rho} \frac{\partial p}{\partial t} + \dot{q} + \vec{g} \cdot \vec{V} \quad (6)$$

More specifically, equation (6) gives the rate of change of total enthalpy along a pathline, in terms of three simple terms.

### Steady, adiabatic flows

Assume the following three conditions are met:

Steady Flow. This implies that  $\partial p / \partial t = 0$

Adiabatic Flow. This implies that  $\dot{q} = 0$

Negligible gravity. This implies that we can ignore  $\vec{g} \cdot \vec{V}$

With these assumptions, equation (6) becomes simply

$$\frac{Dh_o}{Dt} = 0 \quad (7)$$

so that the total enthalpy is constant along a streamline. If all streamlines originate at a common upstream reservoir or uniform flow, which is the usual situation in external aerodynamic flows, then

$$h_o = h + \frac{1}{2} V^2 = \text{constant} \quad (8)$$

throughout the flowfield. Equation (8) in essence replaces the full differential enthalpy equation (5), which is an enormous simplification. Note also its similarity to the incompressible Bernoulli equation. However, equation (8) is more general, since it is valid for compressible flows, and is also valid in the presence of friction.

# Fluids – Lecture 13 Notes

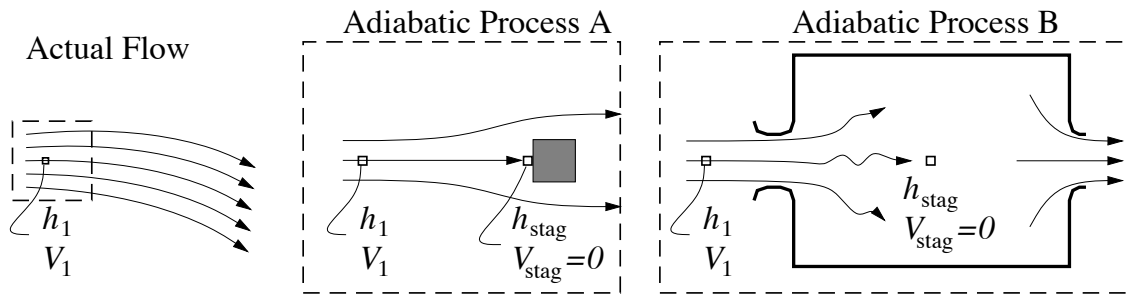
1. Stagnation Quantities
2. Introduction to Shock Waves

Reading: Anderson 7.5, 7.6

## Stagnation Quantities

### Adiabatic stagnation processes

An *adiabatic stagnation process* is one which brings a moving fluid element to rest adiabatically (without heat addition or removal). In the figure, a fluid element at station 1 in some flow being brought to rest by two hypothetical adiabatic processes. Process A is done by placing a blunt object in the flow, such that the fluid element reaches the stagnation point, where  $V = 0$ . Process B lets the fluid element flow into a large insulated chamber where it will mix with the stationary fluid there and thus come to rest.



The changes of  $h$  and  $V$  for either process are governed by the total enthalpy relation

$$h_o \equiv h + \frac{1}{2}V^2 = \text{constant}$$

derived previously. Therefore, we have

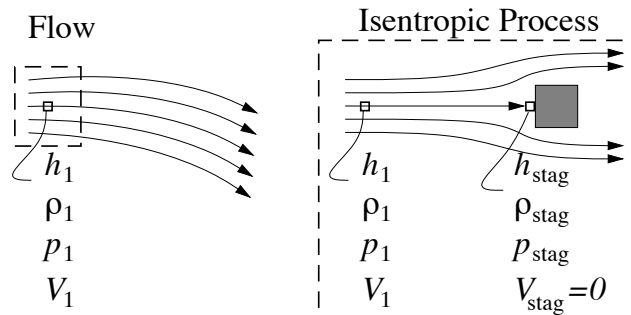
$$h_{o1} \equiv h_1 + \frac{1}{2}V_1^2 = h_{stag} + \frac{1}{2}V_{stag}^2 = h_{stag}$$

We see that at the end of the stagnation process,  $h_{stag}$  is equal to the total enthalpy  $h_{o1}$  at the beginning. For this reason, the terms *stagnation enthalpy* and *total enthalpy* are largely synonymous, although they are two distinct concepts.

The total enthalpy  $h_o$  on the streamline can therefore be measured by setting up an actual stagnation process, typically with a small obstruction like a small-scale version of Process A, and measuring the resulting temperature  $T_{stag}$ . One can then calculate  $h_o = h_{stag} = c_p T_{stag}$ .

### Isentropic stagnation processes

An *isentropic stagnation process*, is one which brings a moving fluid element to rest adiabatically and reversibly (without friction). Of the above figures, only Process A is of this type.



In addition to the total enthalpy relation

$$h_{o1} = h_{\text{stag}}$$

we now also have the isentropic relations between station 1 and the stagnation point.

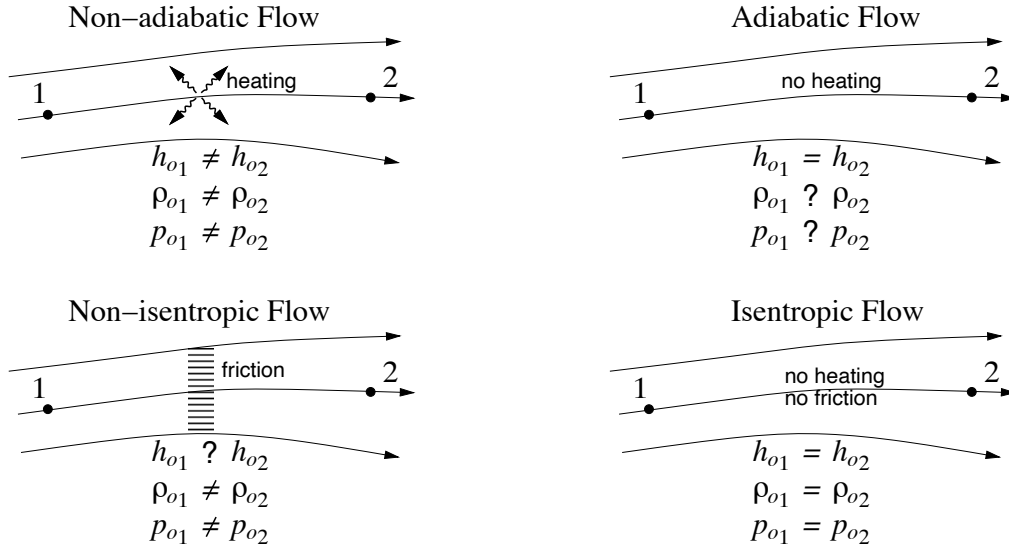
$$\begin{aligned}\frac{\rho_{\text{stag}}}{\rho_1} &= \left(\frac{T_{\text{stag}}}{T_1}\right)^{1/(\gamma-1)} = \left(\frac{h_{\text{stag}}}{h_1}\right)^{1/(\gamma-1)} \\ \frac{p_{\text{stag}}}{p_1} &= \left(\frac{T_{\text{stag}}}{T_1}\right)^{\gamma/(\gamma-1)} = \left(\frac{h_{\text{stag}}}{h_1}\right)^{\gamma/(\gamma-1)}\end{aligned}$$

Substituting  $h_{\text{stag}} = h_{o1}$ , and  $h_1 = h_{o1} - \frac{1}{2}V_1^2$ , we can now define the total density and total pressure at station 1 in terms of station 1 quantities.

$$\begin{aligned}\rho_{\text{stag}} \equiv \rho_{o1} &= \rho_1 \left(1 - \frac{V_1^2}{2h_{o1}}\right)^{-1/(\gamma-1)} \\ p_{\text{stag}} \equiv p_{o1} &= p_1 \left(1 - \frac{V_1^2}{2h_{o1}}\right)^{-\gamma/(\gamma-1)}\end{aligned}$$

### Relations along streamline

Any point along a streamline can be subjected to a hypothetical adiabatic or isentropic stagnation process in order to define the local total quantities  $h_o$ ,  $\rho_o$ , and  $p_o$ . Whether any two such points on a streamline have the same total quantities depends on whether a non-adiabatic or non-isentropic process occurred on the streamline between them. The figure shows four possible situations, resulting in equalities or inequalities between the two points on the streamline. The “?” relation in the non-isentropic and adiabatic cases indicates that the relation is unknown without additional information about the heating or friction, respectively.



For the adiabatic case, a unique total enthalpy  $h_o$  can be assigned to the whole streamline. Then for any point on the streamline we have

$$h = h_o - \frac{1}{2}V^2 \tag{1}$$



For the more restrictive isentropic case, a unique total density  $\rho_o$  and total pressure  $p_o$  can also be assigned to the whole streamline, which gives

$$\rho = \rho_o \left(1 - \frac{V^2}{2h_o}\right)^{1/(\gamma-1)} \quad (2)$$

$$p = p_o \left(1 - \frac{V^2}{2h_o}\right)^{\gamma/(\gamma-1)} \quad (3)$$

These equations are in effect a compressible-flow replacement for the incompressible Bernoulli equation.

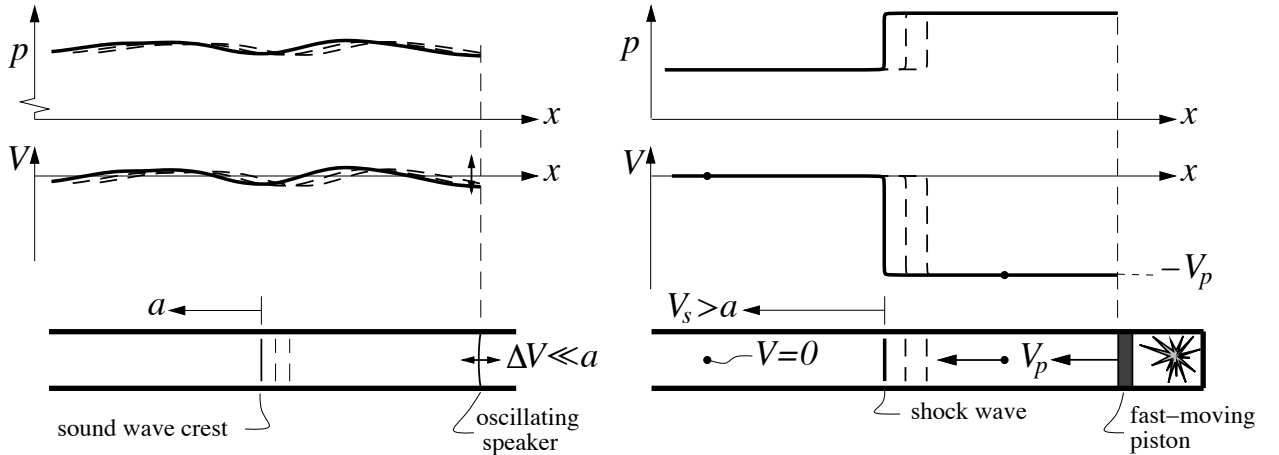
It's useful to note that only two of the three above equations are independent. Any one of them could be removed and replaced by the state equation.

$$p = \frac{\gamma - 1}{\gamma} \rho h$$

## Introduction to Shock Waves

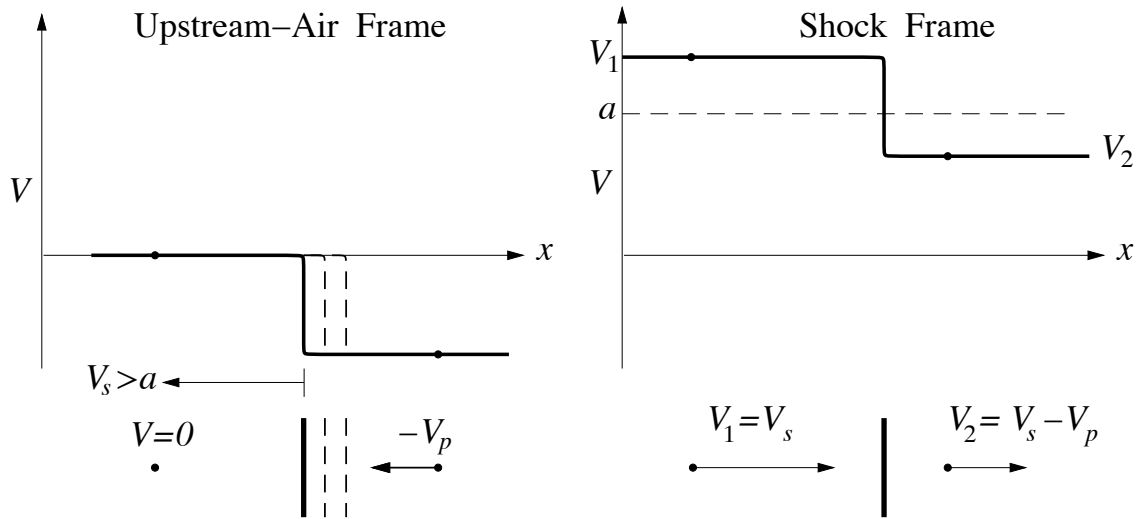
### Wave features

Compressibility of a fluid allows the existence of *waves*, which are variations in  $\rho$ ,  $p$ , and  $h$  (or temperature  $T$ ), which self-propagate through the fluid at some speed. Ordinary sound consists of very small variations which move at the speed of sound  $a$ , while a *shock wave* has a finite variation in flow quantities and moves at a larger speed  $V_s > a$ . The figure illustrates the difference in the two types of waves. The shock wave has a flow velocity behind it equal to the piston speed  $V_p$ , but the shock itself advances into the still air at a much higher speed  $V_s > a$ . The air properties  $\rho$ ,  $p$ , and  $h$  are all increased behind the shock.



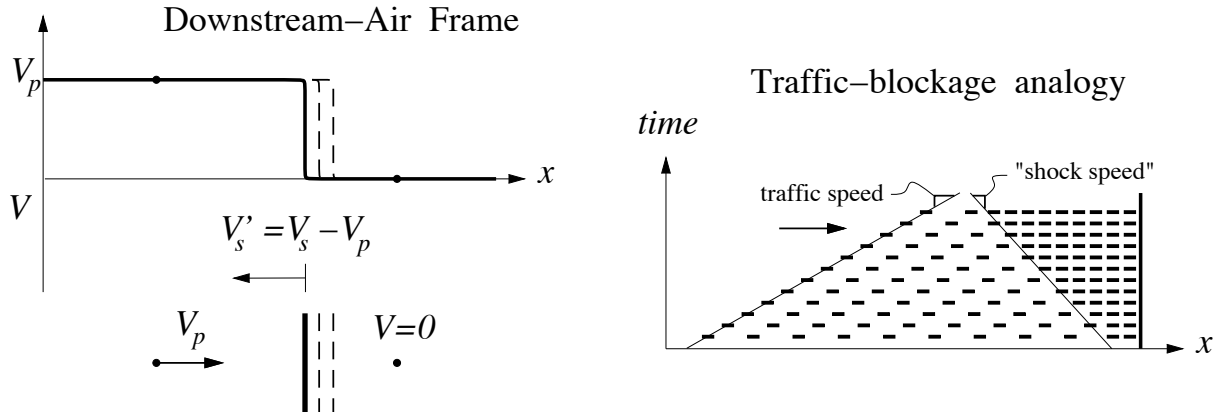
### Shock Frame

We now examine the piston shock flow in the frame of the shock, by shifting all the velocities by  $+V_s$ . In this frame the flow is steady, and is the most convenient frame for analyzing the shock. The upstream and downstream quantities are usually denoted by the subscripts  $( )_1$  and  $( )_2$ , respectively. The static air properties  $\rho$ ,  $p$ , and  $h$  are of course unchanged by this frame change.



### Downstream-Air Frame

An intuitive understanding of a shock wave is perhaps best obtained by looking at the situation yet again, in the downstream-air frame. The shock now propagates against the oncoming upstream flow. This situation is closely analogous to how a traffic blockage propagates backward against the oncoming traffic.



### Dissipation in Shock

The flow passing through a shock wave undergoes an adiabatic process, since there is no heat being supplied (there's nothing there to provide heat!). But because a shock wave is typically very thin — less than 1 micron at sea level — there are strong viscous forces acting on the fluid passing through it, so the process is irreversible. Therefore, the stagnation quantities have the following relations across a shock wave:

$$\begin{aligned} h_{o1} &= h_{o2} \\ \rho_{o1} &> \rho_{o2} \\ p_{o1} &> p_{o2} \end{aligned}$$

A more detailed analysis will quantify the inequalities.

# Fluids – Lecture 14 Notes

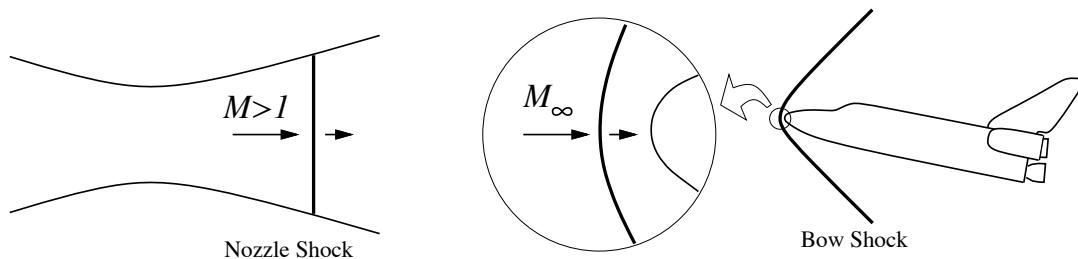
1. Normal Shock Waves
2. Speed of Sound

Reading: Anderson 8.1 – 8.3

## Normal Shock Waves

### Occurance of normal shock waves

A *normal shock wave* appears in many types of supersonic flows. Two examples are shown in the figure. Any blunt-nosed body in a supersonic flow will develop a curved *bow shock*, which is normal to the flow locally just ahead of the stagnation point. Another common example is a supersonic nozzle flow, which is typically found in a jet or rocket engine. A normal shock can appear in the diverging part of the nozzle under certain conditions.

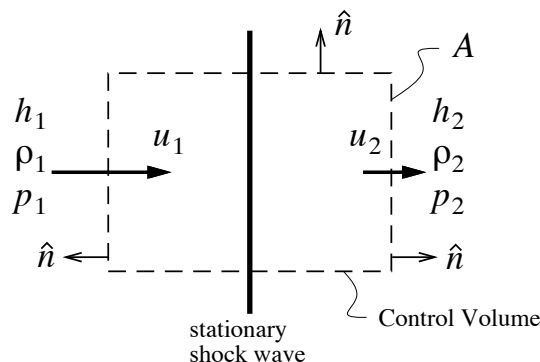


### Shock jump relations

We examine the flow in the frame in which the shock is stationary. The upstream and downstream flow properties are denoted by the subscripts  $()_1$  and  $()_2$  as shown in the figure. A control volume is defined straddling the shock. The flow in the shock has the following properties:

1. Flow is steady, so  $\partial()/\partial t = 0$  in all equations.
2. Flow is adiabatic, so  $\dot{q} = 0$ .
3. Body forces such as gravity are negligible, so  $\vec{g}$  is neglected.

The flow is also assumed irreversible due to viscous forces acting in the extremely large velocity gradients in the thin shock, although this doesn't explicitly influence the analysis. We now apply the integral conservation equations to the control volume. The flow is 1-dimensional in the  $x$ -direction normal to the shock, so that  $\vec{V} = u\hat{i}$ . There is no flow through the top and bottom boundaries, since  $\vec{V} \cdot \hat{n}$  there.



### Mass continuity

$$\begin{aligned}\oint \rho \vec{V} \cdot \hat{n} dA &= 0 \\ -\rho_1 u_1 A + \rho_2 u_2 A &= 0 \\ \rho_1 u_1 &= \rho_2 u_2\end{aligned}\tag{1}$$

### x-Momentum

$$\begin{aligned}\oint \rho \vec{V} \cdot \hat{n} u dA + \oint p \hat{n} \cdot \hat{i} dA &= 0 \\ -\rho_1 u_1^2 A + \rho_2 u_2^2 A - p_1 A + p_2 A &= 0 \\ \rho_1 u_1^2 + p_1 &= \rho_2 u_2^2 + p_2\end{aligned}\tag{2}$$

### Energy

$$\begin{aligned}\oint \rho \vec{V} \cdot \hat{n} h_o dA &= 0 \\ -\rho_1 u_1 h_{o1} A + \rho_2 u_2 h_{o2} A &= 0 \\ h_{o1} &= h_{o2} \\ h_1 + \frac{1}{2} u_1^2 &= h_2 + \frac{1}{2} u_2^2\end{aligned}\tag{3}$$

### Equation of State

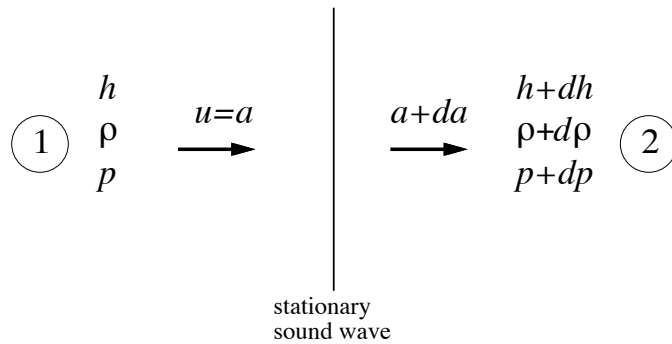
$$p_2 = \frac{\gamma - 1}{\gamma} \rho_2 h_2\tag{4}$$

Simplification of the energy equation (3) makes use of the mass equation (1). In most shock flow analysis situations, the upstream supersonic flow quantities at station 1 are known, either from the freestream conditions or from the flow about some upstream body. The four equations (1)–(4) then are sufficient to determine the four downstream flow quantities  $\rho_2$ ,  $u_2$ ,  $p_2$ , and  $h_2$ . The temperatures  $T_1$  and  $T_2$  can be considered additional variables, but for a perfect gas these are trivially related to  $h_1$  and  $h_2$  through  $h = c_p T$ .

## Speed of Sound

### Sound wave

Before solution of (1)–(4) is carried out for a general shock wave, we first consider an infinitesimally weak shock wave, also known as a *sound wave*. Because the velocity gradients and hence the viscous action is small, the flow process through the wave is *isentropic*.



Rather than treating the 1 and 2 variables, we instead examine their infinitesimal differences  $dh$ ,  $d\rho$ ,  $dp$ , .... We also define  $u$  for this case to be the speed of sound (yet unknown), and denote it with a separate symbol  $a$ . The objective here is to determine this  $a$  in terms of the other variables by applying equations (1) – (4).

### Speed of sound derivation

The mass equation (1) for the sound wave case becomes

$$\begin{aligned}\rho a &= (\rho + d\rho)(a + da) = \rho a + a d\rho + \rho da \\ da &= -\frac{a}{\rho} d\rho\end{aligned}\tag{5}$$

where the higher-order term  $d\rho da$  has been dropped. Similarly for  $x$ -momentum we have

$$\begin{aligned}\rho a^2 + p &= (\rho + d\rho)(a + da)^2 + (p + dp) = \rho a^2 + a^2 d\rho + 2a\rho da + p + dp \\ 0 &= 2a\rho da + a^2 d\rho + dp\end{aligned}\tag{6}$$

Using equation (5) to eliminate  $da$  from (6) gives

$$\begin{aligned}0 &= 2a\rho \left(-\frac{a}{\rho} d\rho\right) + a^2 d\rho + dp \\ 0 &= -a^2 d\rho + dp \\ a^2 &= \frac{dp}{d\rho}\end{aligned}\tag{7}$$

We could now relate  $p$  and  $\rho$  and thus get  $dp/d\rho$  using the energy and state equations (3) and (4). But an algebraically simpler approach is to use one of the isentropic relations instead, which are valid for this weak wave. The simplest relation for this purpose is

$$\begin{aligned}\frac{p_2}{p_1} &= \left(\frac{\rho_2}{\rho_1}\right)^\gamma \\ \text{or} \quad \frac{p + dp}{p} &= \left(\frac{\rho + d\rho}{\rho}\right)^\gamma \\ 1 + \frac{dp}{p} &= \left(1 + \frac{d\rho}{\rho}\right)^\gamma = 1 + \gamma \frac{d\rho}{\rho} + \text{h.o.t.} \\ \frac{dp}{p} &= \gamma \frac{d\rho}{\rho} \\ \frac{dp}{d\rho} &= \gamma \frac{p}{\rho} = \gamma RT\end{aligned}$$

Combining this with equation (7) gives the speed of sound as

$$a = \sqrt{\frac{\gamma p}{\rho}} = \sqrt{\gamma RT}$$

which can be seen to depend on the temperature alone.

# Fluids – Lecture 15 Notes

1. Mach Number Relations
2. Normal-Shock Properties

Reading: Anderson 8.4, 8.6

## Mach Number Relations

### Local Mach number

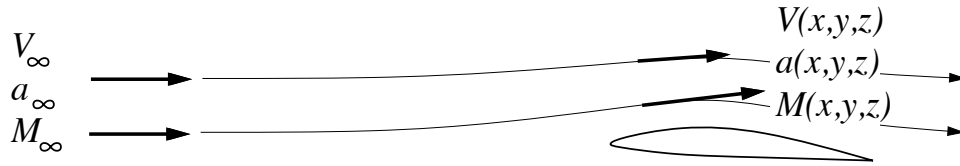
For a perfect gas, the speed of sound can be given in a number of ways.

$$a = \sqrt{\gamma RT} = \sqrt{\frac{\gamma p}{\rho}} = \sqrt{(\gamma-1) h} \quad (1)$$

The dimensionless *local Mach number* can then be defined.

$$M \equiv \frac{V}{a} = \sqrt{\frac{\rho(u^2 + v^2 + w^2)}{\gamma p}} = \sqrt{\frac{u^2 + v^2 + w^2}{(\gamma-1) h}}$$

It's important to note that this is a field variable  $M(x, y, z)$ , and is distinct from the freestream Mach number  $M_\infty$ . Likewise for  $V$  and  $a$ .



The local stagnation enthalpy can be given in terms of the static enthalpy and the Mach number, or in terms of the speed of sound and the Mach number.

$$h_o = h + \frac{1}{2}V^2 = h \left(1 + \frac{1}{2} \frac{V^2}{h}\right) = h \left(1 + \frac{\gamma-1}{2} M^2\right) = \frac{a^2}{\gamma-1} \left(1 + \frac{\gamma-1}{2} M^2\right) \quad (2)$$

This now allows the isentropic relations

$$\frac{p_o}{p} = \left(\frac{\rho_o}{\rho}\right)^\gamma = \left(\frac{h_o}{h}\right)^{\gamma/(\gamma-1)}$$

to be put in terms of the Mach number rather than the speed as before.

$$\begin{aligned} \frac{\rho_o}{\rho} &= \left(1 + \frac{\gamma-1}{2} M^2\right)^{1/(\gamma-1)} \\ \frac{p_o}{p} &= \left(1 + \frac{\gamma-1}{2} M^2\right)^{\gamma/(\gamma-1)} \end{aligned}$$

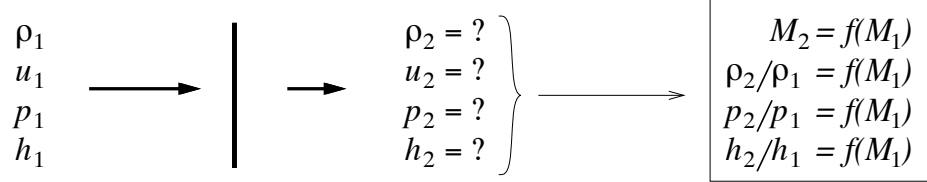
The following relation is also sometimes useful.

$$1 - \frac{V^2}{2h_o} = \left(1 + \frac{\gamma-1}{2} M^2\right)^{-1}$$

## Normal-Shock Properties

### Mach jump relations

We now seek to determine the properties  $\rho_2, u_2, p_2, h_2$  downstream of the shock, as functions of the known upstream properties  $\rho_1, u_1, p_1, h_1$ . In practice, it is sufficient and much more convenient to merely determine the downstream Mach number  $M_2$  and the variable ratios, since these are strictly functions of the upstream Mach number  $M_1$ .



The starting point is the normal shock equations obtained earlier, with  $V = u$  for this 1-D case. They are also known as the *Rankine-Hugoniot* shock equations.

$$\rho_1 u_1 = \rho_2 u_2 \quad (3)$$

$$\rho_1 u_1^2 + p_1 = \rho_2 u_2^2 + p_2 \quad (4)$$

$$h_1 + \frac{1}{2}u_1^2 = h_2 + \frac{1}{2}u_2^2 \quad (5)$$

$$p_2 = \frac{\gamma - 1}{\gamma} \rho_2 h_2 \quad (6)$$

Dividing the momentum equation (4) by the continuity equation (3) gives

$$\begin{aligned} u_1 + \frac{p_1}{\rho_1 u_1} &= u_2 + \frac{p_2}{\rho_2 u_2} \\ \text{or} \quad u_1 - u_2 &= \frac{1}{\gamma} \left( \frac{a_2^2}{u_2} - \frac{a_1^2}{u_1} \right) \end{aligned} \quad (7)$$

where we have substituted  $p/\rho = a^2/\gamma$  and rearranged the terms.

Now we make use of the energy equation (5). For algebraic convenience we first define the constant total enthalpy in terms of the known upstream quantities

$$h_1 + \frac{1}{2}u_1^2 \equiv h_o = h_2 + \frac{1}{2}u_2^2$$

which then gives  $a_1^2$  and  $a_2^2$  in terms of  $u_1$  and  $u_2$ , respectively.

$$\begin{aligned} a_1^2 &= (\gamma - 1)h_1 = (\gamma - 1) \left( h_o - \frac{1}{2}u_1^2 \right) \\ a_2^2 &= (\gamma - 1)h_2 = (\gamma - 1) \left( h_o - \frac{1}{2}u_2^2 \right) \end{aligned}$$

Substituting these energy relations into the combined momentum/mass relation (7) gives, after some further manipulation

$$u_1 - u_2 = \frac{\gamma - 1}{\gamma} \left( \frac{h_o}{u_2} - \frac{h_o}{u_1} + \frac{1}{2}(u_1 - u_2) \right)$$

Dividing by  $u_1 - u_2$  produces

$$1 = \frac{\gamma-1}{\gamma} \left( \frac{h_o}{u_1 u_2} + \frac{1}{2} \right) \quad (8)$$

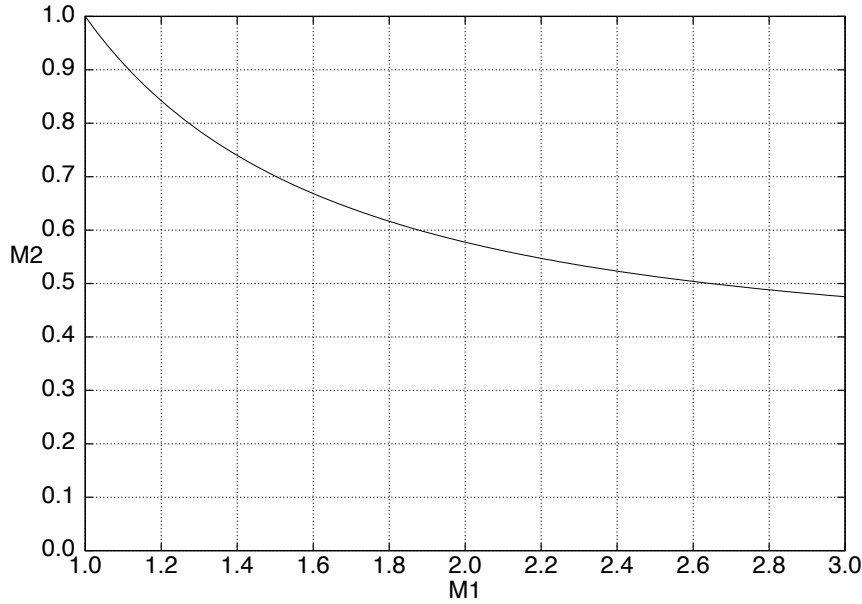
$$\begin{aligned} \frac{(\gamma-1)h_o}{u_1 u_2} &= \frac{\gamma+1}{2} \\ \frac{(\gamma-1)^2 h_o^2}{u_1^2 u_2^2} &= \left( \frac{\gamma+1}{2} \right)^2 \end{aligned} \quad (9)$$

Since  $h_o = h_{o1} = h_{o2}$ , we can write

$$(\gamma-1)^2 h_o^2 = (\gamma-1)h_{o1} (\gamma-1)h_{o2} = a_1^2 \left( 1 + \frac{\gamma-1}{2} M_1^2 \right) a_2^2 \left( 1 + \frac{\gamma-1}{2} M_2^2 \right)$$

and using this to eliminate  $h_o^2$  from equation (9), and solving for  $M_2$ , yields the desired  $M_2(M_1)$  function. This is shown plotted for  $\gamma = 1.4$ .

$$M_2^2 = \frac{1 + \frac{\gamma-1}{2} M_1^2}{\gamma M_1^2 - \frac{\gamma-1}{2}} \quad (10)$$



The  $M_1 \rightarrow 1^+$ ,  $M_2 \rightarrow 1^-$  limit corresponds to infinitesimal shock, or a sound wave. The  $M_2(M_1)$  function is not shown for  $M_1 < 1$ , since this would correspond to an “expansion shock” which is physically impossible based on irreversibility considerations.

### Static jump relations

The jumps in the static flow variables are now readily determined as ratios using the known  $M_2$ . From the mass equation (3) we have

$$\frac{\rho_2}{\rho_1} = \frac{u_1}{u_2} = \frac{u_1^2}{u_1 u_2}$$

From the Mach definition we have

$$u_1^2 = M_1^2 a_1^2 = M_1^2 \frac{(\gamma-1)h_o}{1 + \frac{\gamma-1}{2} M_1^2}$$



and from equation (8) we have

$$\frac{1}{u_1 u_2} = \frac{1}{(\gamma-1)h_o} \frac{\gamma+1}{2}$$

Combining these gives the shock density ratio in terms of  $M_1$  alone.

$$\frac{\rho_2}{\rho_1} = \frac{(\gamma+1)M_1^2}{2 + (\gamma-1)M_1^2} \quad (11)$$

The combination of the momentum equation (4) and mass equation (3) gives

$$p_2 - p_1 = \rho_1 u_1^2 - \rho_2 u_2^2 = \rho_1 u_1^2 \left(1 - \frac{u_2}{u_1}\right) = \rho_1 u_1^2 \left(1 - \frac{\rho_1}{\rho_2}\right)$$

which can be further simplified by using the general relation  $\rho u^2 = \gamma p M^2$ , dividing by  $p_1$ , and then using (11) to eliminate  $\rho_2/\rho_1$  in terms of  $M_1$ . The final result for the shock static pressure ratio is

$$\frac{p_2}{p_1} = 1 + \frac{2\gamma}{\gamma+1} (M_1^2 - 1) \quad (12)$$

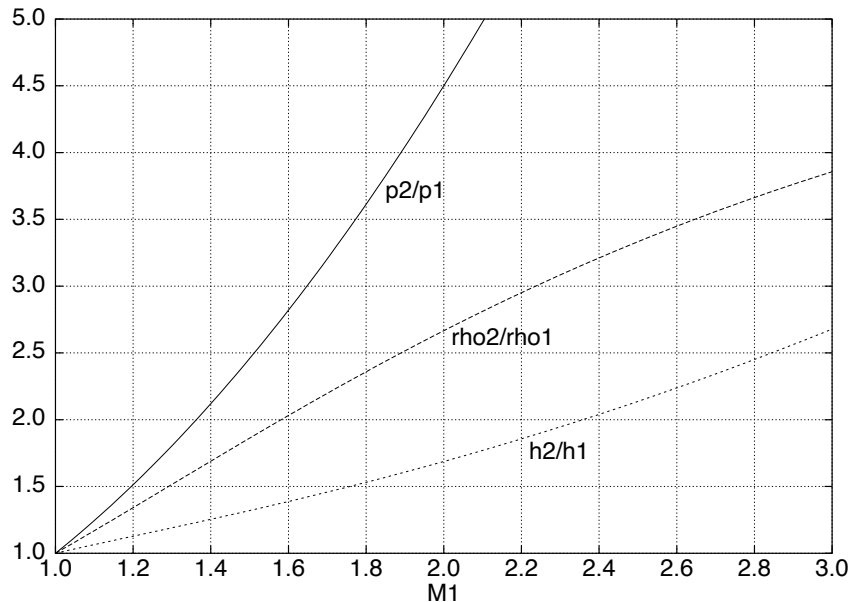
The static temperature or enthalpy ratio is now readily obtained from the pressure and density ratios via the state equation.

$$\frac{T_2}{T_1} = \frac{p_2 \rho_1}{p_1 \rho_2}$$

The result is

$$\frac{T_2}{T_1} = \frac{h_2}{h_1} = \left[1 + \frac{2\gamma}{\gamma+1} (M_1^2 - 1)\right] \frac{2 + (\gamma-1)M_1^2}{(\gamma+1)M_1^2} \quad (13)$$

The three static quantity ratios (11), (12), (13), are shown plotted versus  $M_1$ .



# Fluids – Lecture 16 Notes

1. Shock Losses
  2. Compressible-Flow Pitot Tube
- Reading: Anderson 8.6, 8.7

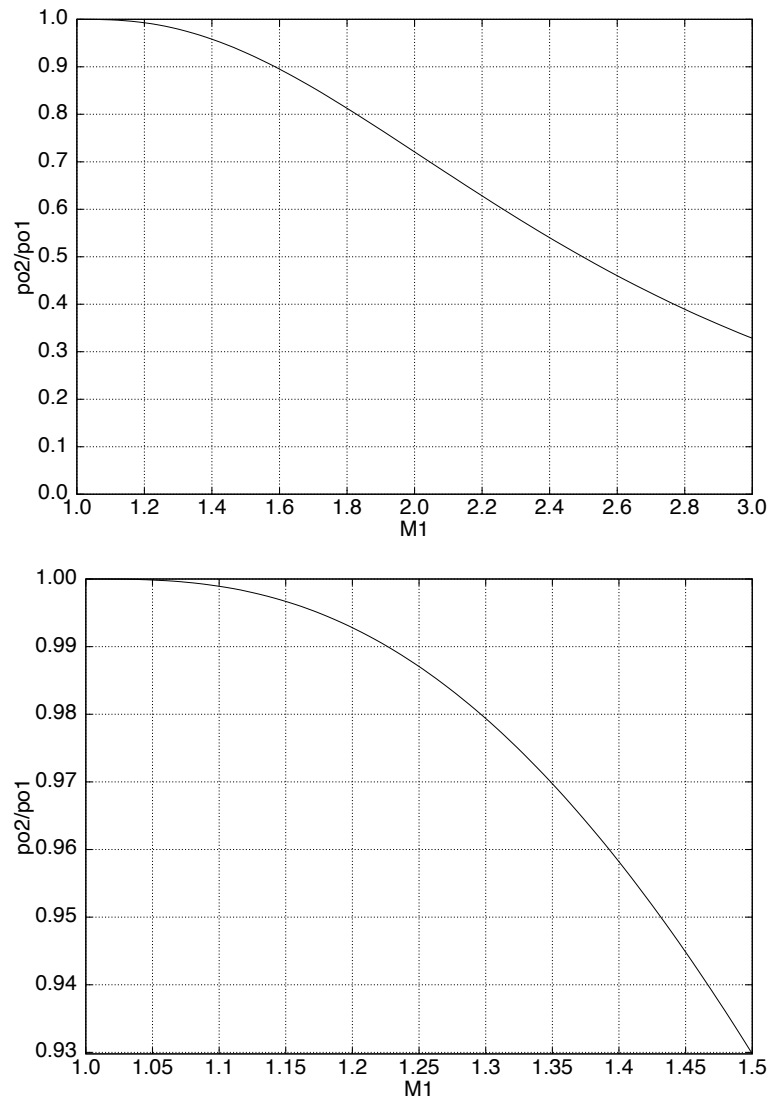
## Shock Losses

### Stagnation pressure jump relation

The stagnation pressure ratio across the shock is

$$\frac{p_{o2}}{p_{o1}} = \frac{p_2}{p_1} \left( \frac{1 + \frac{\gamma-1}{2} M_2^2}{1 + \frac{\gamma-1}{2} M_1^2} \right)^{\gamma/(\gamma-1)} \quad (1)$$

where both  $p_2/p_1$  and  $M_2$  are functions of the upstream Mach number  $M_1$ , as derived previously. The figures show the  $p_{o2}/p_{o1}$  ratio, with the second figure showing an expanded scale near  $M_1 \simeq 1$ .



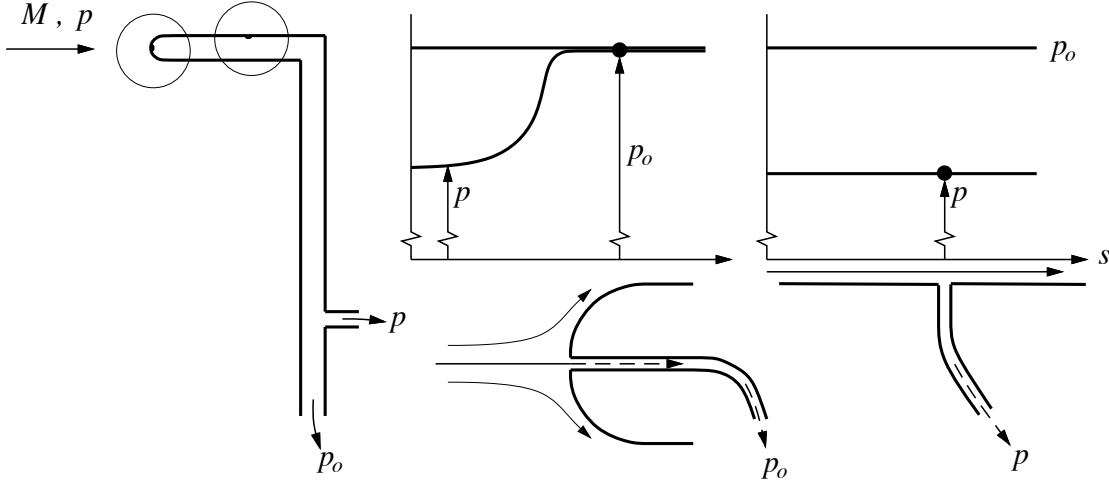
The fractional shock total-pressure loss  $1 - p_{o2}/p_{o1}$  is seen to be small for  $M_1$  close to unity, but increases rapidly for higher Mach numbers. Minimizing this loss is of great practical importance, since it cuts directly into the performance of supersonic air-breathing engines.

# Compressible-Flow Pitot Tube

## Subsonic pitot tube

A pitot tube in subsonic flow measures the local total pressure  $p_o$ . Together with a measurement of the static pressure  $p$ , the Mach number can be computed from the  $p_o/p$  ratio relation.

$$\begin{aligned}\frac{p_o}{p} &= \left(1 + \frac{\gamma-1}{2}M^2\right)^{\gamma/(\gamma-1)} \\ M^2 &= \frac{2}{\gamma-1} \left[ \left(\frac{p_o}{p}\right)^{(\gamma-1)/\gamma} - 1 \right]\end{aligned}\quad (2)$$



The pitot-static combination therefore constitutes a *Mach meter*. With  $M^2$  known, we can then also determine the dynamic pressure.

$$\frac{1}{2}\rho V^2 = \frac{\gamma}{2}pM^2 = \frac{\gamma}{\gamma-1}p \left[ \left(\frac{p_o}{p}\right)^{(\gamma-1)/\gamma} - 1 \right] \quad (3)$$

The velocity can be determined from

$$V^2 = a^2 M^2 = \frac{a_o^2 M^2}{1 + \frac{\gamma-1}{2}M^2}$$

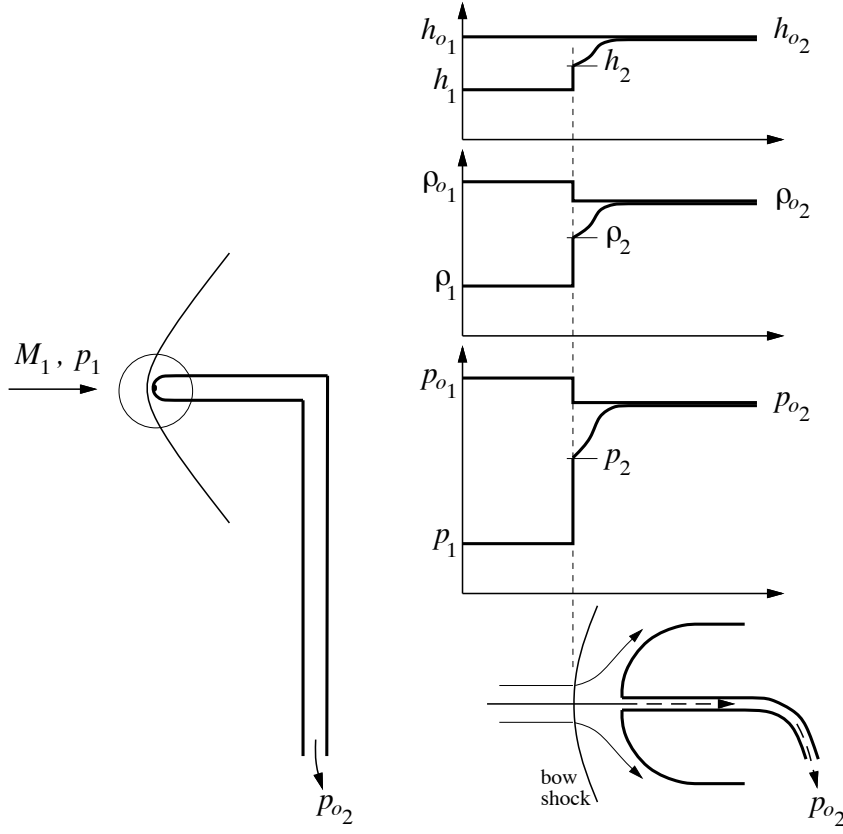
but this requires knowing either the static speed of sound  $a$ , or the stagnation speed of sound  $a_o$ . The latter can be obtained by measuring the stagnation temperature at the tip of the pitot probe.

## Supersonic pitot tube

A pitot probe in a supersonic stream will have a *bow shock* ahead of it. This complicates the flow measurement, since the bow shock will cause a drop in the total pressure, from  $p_{o1}$  to  $p_{o2}$ , the latter being sensed by the pitot port. It's useful to note that the shock will also cause a drop in  $\rho_o$ , but  $h_o$  will not change.

The pressures and Mach number immediately behind the shock are related by

$$\frac{p_{o2}}{p_2} = \left(1 + \frac{\gamma-1}{2}M_2^2\right)^{\gamma/(\gamma-1)}$$



In addition, we also have  $M_2$  and  $p_2/p_1$  as functions of  $M_1$  from the earlier normal-shock analysis. Combining these produces the relation between the  $p_{o2}$  measured by the pitot probe, the static  $p_1$ , and the required flow Mach number  $M_1$ . After some manipulation, the result is the *Rayleigh Pitot tube formula*.

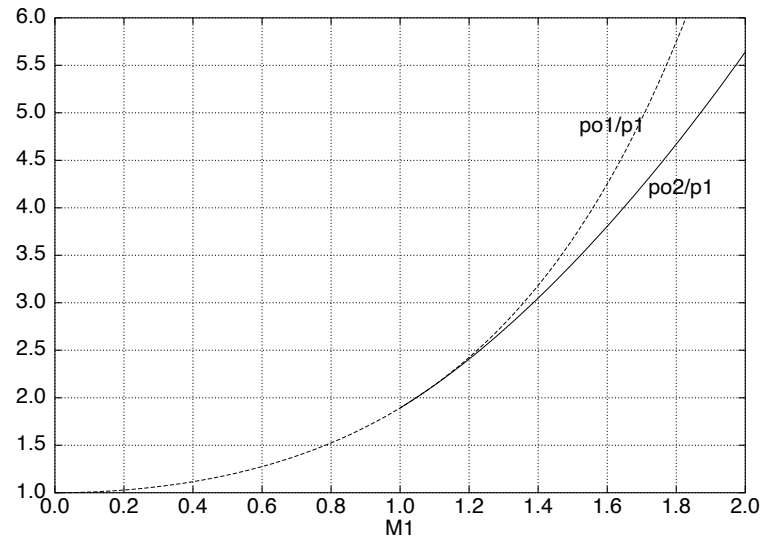
$$\frac{p_{o2}}{p_1} = \frac{p_{o2}}{p_2} \frac{p_2}{p_1} = \left( \frac{(\gamma+1)^2 M_1^2}{4\gamma M_1^2 - 2(\gamma-1)} \right)^{\gamma/(\gamma-1)} \frac{1 - \gamma + 2\gamma M_1^2}{\gamma+1} \quad (4)$$

The figure shows  $p_{o2}/p_1$  versus  $M_1$ , compared with the isentropic ratio  $p_{o1}/p_1$ .

$$\frac{p_{o1}}{p_1} = \left( 1 + \frac{\gamma-1}{2} M_1^2 \right)^{\gamma/(\gamma-1)} \quad (5)$$

Only the latter is plotted for  $M_1 < 1$ , where there is no bow shock, and so equation (4) does not apply. The effect of the pitot bow shock's total pressure loss, indicated by the difference  $p_{o1} - p_{o2}$ , becomes substantial at larger Mach numbers.

Ideally, we would like to have the pitot formula (4) give  $M_1$  as an explicit function of the pitot/static pressure ratio  $p_{o2}/p_1$ . However, this is not possible due to its complexity, so a numerical solution is required. The function is also readily available in table form.



# Fluids – Lecture 17 Notes

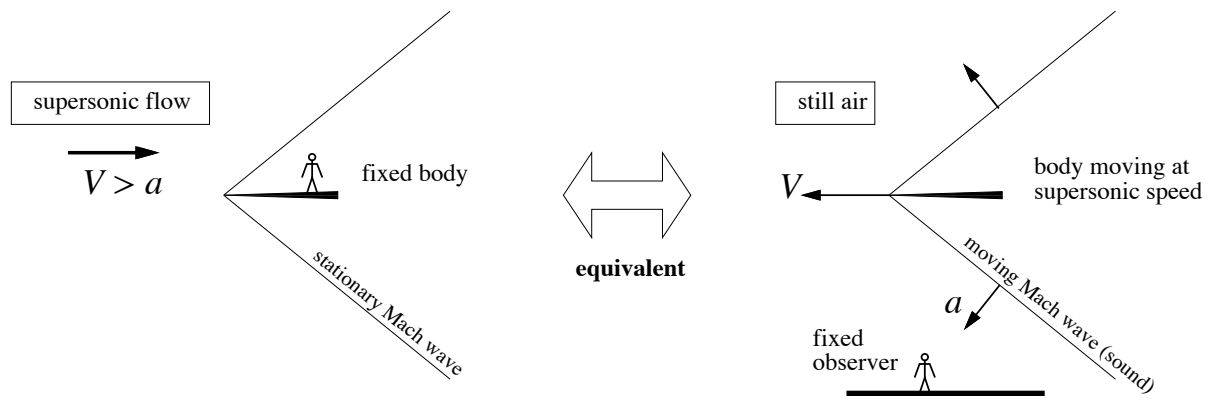
## 1. Oblique Waves

Reading: Anderson 9.1, 9.2

## Oblique Waves

### Mach waves

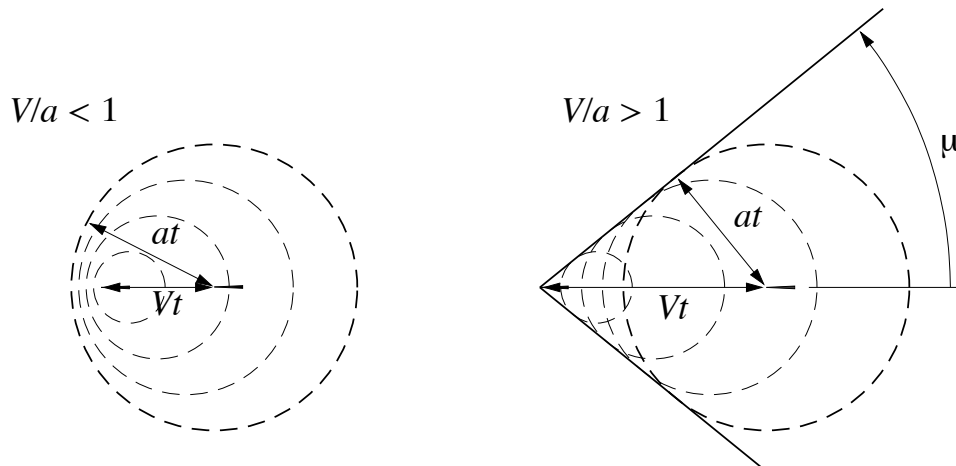
Small disturbances created by a slender body in a supersonic flow will propagate diagonally away as *Mach waves*. These consist of small isentropic variations in  $\rho$ ,  $V$ ,  $p$ , and  $h$ , and are loosely analogous to the water waves sent out by a speedboat. Mach waves appear stationary with respect to the object generating them, but when viewed relative to the still air, they are in fact indistinguishable from sound waves, and their normal-direction speed of propagation is equal to  $a$ , the speed of sound.



The angle  $\mu$  of a Mach wave relative to the flow direction is called the *Mach angle*. It can be determined by considering the wave to be the superposition of many pulses emitted by the body, each one producing a disturbance circle (in 2-D) or sphere (in 3-D) which expands at the speed of sound  $a$ . At some time interval  $t$  after the pulse is emitted, the radius of the circle will be  $at$ , while the body will travel a distance  $Vt$ . The Mach angle is then seen to be

$$\mu = \arcsin \frac{at}{Vt} = \arcsin \frac{1}{M}$$

which can be defined at any point in the flow. In the subsonic flow case where  $M = V/a < 1$  the expanding circles do not coalesce into a wave front, and the Mach angle is not defined.

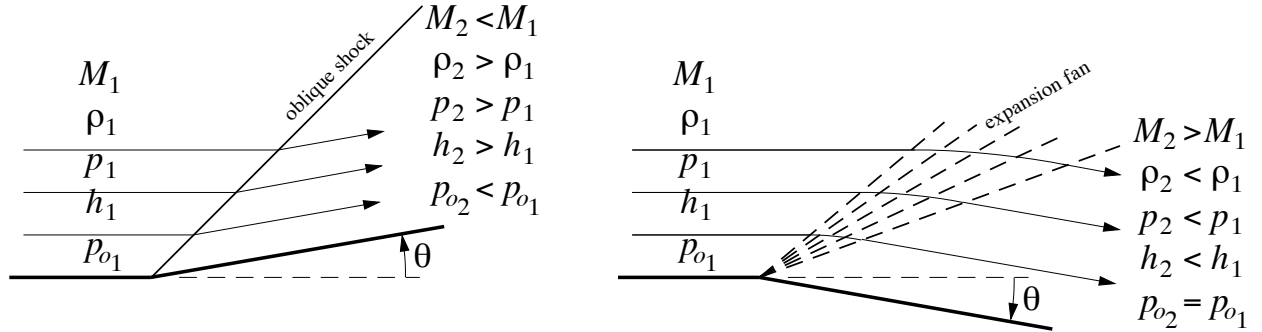


## Oblique shock and expansion waves

Mach waves can be either compression waves ( $p_2 > p_1$ ) or expansion waves ( $p_2 < p_1$ ), but in either case their strength is by definition very small ( $|p_2 - p_1| \ll p_1$ ). A body of finite thickness, however, will generate oblique waves of finite strength, and now we must distinguish between compression and expansion types. The simplest body shape for generating such waves is

- a concave corner, which generates an *oblique shock* (compression), or
- a convex corner, which generates an *expansion fan*.

The flow quantity changes across an oblique shock are in the same direction as across a



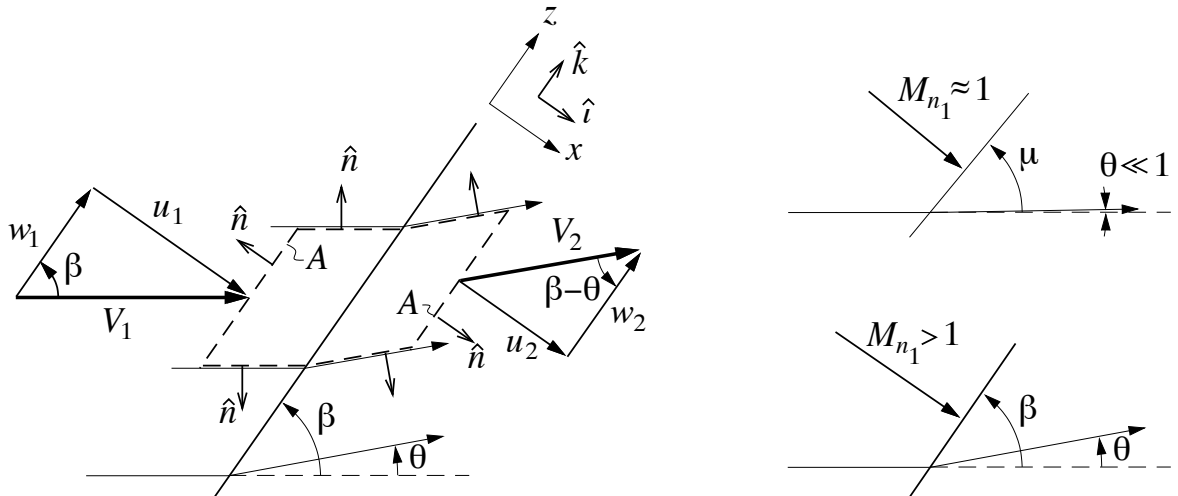
normal shock, and across an expansion fan they are in the opposite direction. One important difference is that  $p_o$  decreases across the shock, while the fan is isentropic, so that it has no loss of total pressure, and hence  $p_{o2} = p_{o1}$ .

## Oblique geometry and analysis

As with the normal shock case, a control volume analysis is applied to the oblique shock flow, using the control volume shown in the figure. The top and bottom boundaries are chosen to lie along streamlines so that only the boundaries parallel to the shock, with area  $A$ , have mass flow across them. Velocity components are taken in the  $x$ - $z$  coordinates normal and tangential to the shock, as shown. The tangential  $z$  axis is tilted from the upstream flow direction by the *wave angle*  $\beta$ , which is the same as the Mach angle  $\mu$  only if the shock is extremely weak. For a finite-strength shock,  $\beta > \mu$ . The upstream flow velocity components are

$$u_1 = V_1 \sin \beta$$

$$w_1 = V_1 \cos \beta$$



All the integral conservation equations are now applied to the control volume.

Mass continuity

$$\begin{aligned}\oint \rho \vec{V} \cdot \hat{n} dA &= 0 \\ -\rho_1 u_1 A + \rho_2 u_2 A &= 0 \\ \rho_1 u_1 &= \rho_2 u_2\end{aligned}\tag{1}$$

x-Momentum

$$\begin{aligned}\oint \rho \vec{V} \cdot \hat{n} u dA + \oint p \hat{n} \cdot \hat{i} dA &= 0 \\ -\rho_1 u_1^2 A + \rho_2 u_2^2 A - p_1 A + p_2 A &= 0 \\ \rho_1 u_1^2 + p_1 &= \rho_2 u_2^2 + p_2\end{aligned}\tag{2}$$

z-Momentum

$$\begin{aligned}\oint \rho \vec{V} \cdot \hat{n} w dA + \oint p \hat{n} \cdot \hat{k} dA &= 0 \\ -\rho_1 u_1 A w_1 + \rho_2 u_2 A w_2 &= 0 \\ w_1 &= w_2\end{aligned}\tag{3}$$

Energy

$$\begin{aligned}\oint \rho \vec{V} \cdot \hat{n} h_o dA &= 0 \\ -\rho_1 u_1 h_{o1} A + \rho_2 u_2 h_{o2} A &= 0 \\ h_{o1} &= h_{o2} \\ h_1 + \frac{1}{2} (u_1^2 + w_1^2) &= h_2 + \frac{1}{2} (u_2^2 + w_2^2) \\ h_1 + \frac{1}{2} u_1^2 &= h_2 + \frac{1}{2} u_2^2\end{aligned}\tag{4}$$

Equation of State

$$p_2 = \frac{\gamma - 1}{\gamma} \rho_2 h_2\tag{5}$$

Simplification of equation (3) makes use of (1) to eliminate  $\rho u A$  from both sides. Simplification of equation (4) makes use of (1) to eliminate  $\rho u A$  and then (3) to eliminate  $w$  from both sides.

### Oblique/normal shock equivalence

It is apparent that equations (1), (2), (4), (5) are in fact identical to the normal-shock equations derived earlier. The one addition  $z$ -momentum equation (3) simply states that the tangential velocity component doesn't change across a shock. This can be physically interpreted if we examine the oblique shock from the viewpoint of an observer moving with the everywhere-constant tangential velocity  $w = w_1 = w_2$ . As shown in the figure, the moving observer sees a normal shock with velocities  $u_1$ , and  $u_2$ . The static fluid properties  $p$ ,  $\rho$ ,  $h$ ,  $a$  are of course the same in both frames.

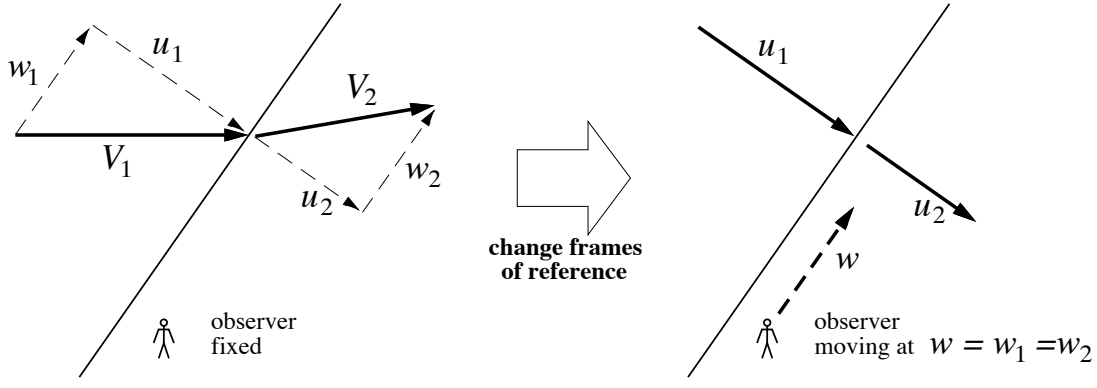
### Oblique shock relations

The effective equivalence between an oblique and a normal shock allows re-use of the already derived normal shock jump relations. We only need to construct the necessary transformation from one frame to the other.

First we define the *normal Mach number components* seen by the moving observer.

$$\begin{aligned}M_{n1} &\equiv \frac{u_1}{a_1} = \frac{V_1 \sin \beta}{a_1} = M_1 \sin \beta \\ M_{n2} &\equiv \frac{u_2}{a_2} = \frac{V_2 \sin(\beta - \theta)}{a_2} = M_2 \sin(\beta - \theta)\end{aligned}\tag{6}$$





These are then related via our previous normal-shock  $M_2 = f(M_1)$  relation, if we make the substitutions  $M_1 \rightarrow M_{n_1}$ ,  $M_2 \rightarrow M_{n_2}$ . The fixed-frame  $M_2$  then follows from geometry.

$$M_{n_2}^2 = \frac{1 + \frac{\gamma-1}{2} M_{n_1}^2}{\gamma M_{n_1}^2 - \frac{\gamma-1}{2}} \quad (7)$$

$$M_2 = \frac{M_{n_2}}{\sin(\beta - \theta)} \quad (8)$$

The static property ratios are likewise obtained using the previous normal-shock relations.

$$\frac{\rho_2}{\rho_1} = \frac{(\gamma+1)M_{n_1}^2}{2 + (\gamma-1)M_{n_1}^2} \quad (9)$$

$$\frac{p_2}{p_1} = 1 + \frac{2\gamma}{\gamma+1} (M_{n_1}^2 - 1) \quad (10)$$

$$\frac{h_2}{h_1} = \frac{p_2 \rho_1}{p_1 \rho_2} \quad (11)$$

$$\frac{p_{o2}}{p_{o1}} = \frac{p_2}{p_1} \left( \frac{h_1}{h_2} \right)^{\gamma/(\gamma-1)} \quad (12)$$

To allow application of the above relations, we still require the wave angle  $\beta$ . Using the result  $w_1 = w_2$ , the velocity triangles on the two sides of the shock can be related by

$$\frac{\tan(\beta - \theta)}{\tan \beta} = \frac{u_2}{u_1} = \frac{\rho_1}{\rho_2} = \frac{(\gamma+1)M_1^2 \sin^2 \beta}{2 + (\gamma-1)M_1^2 \sin^2 \beta}$$

Solving this for  $\theta$  gives

$$\tan \theta = \frac{2}{\tan \beta} \frac{M_1^2 \sin^2 \beta - 1}{M_1^2 (\gamma + \cos 2\beta) + 2} \quad (13)$$

which is an implicit definition of the function  $\beta(\theta, M_1)$ .

### Oblique-shock analysis: Summary

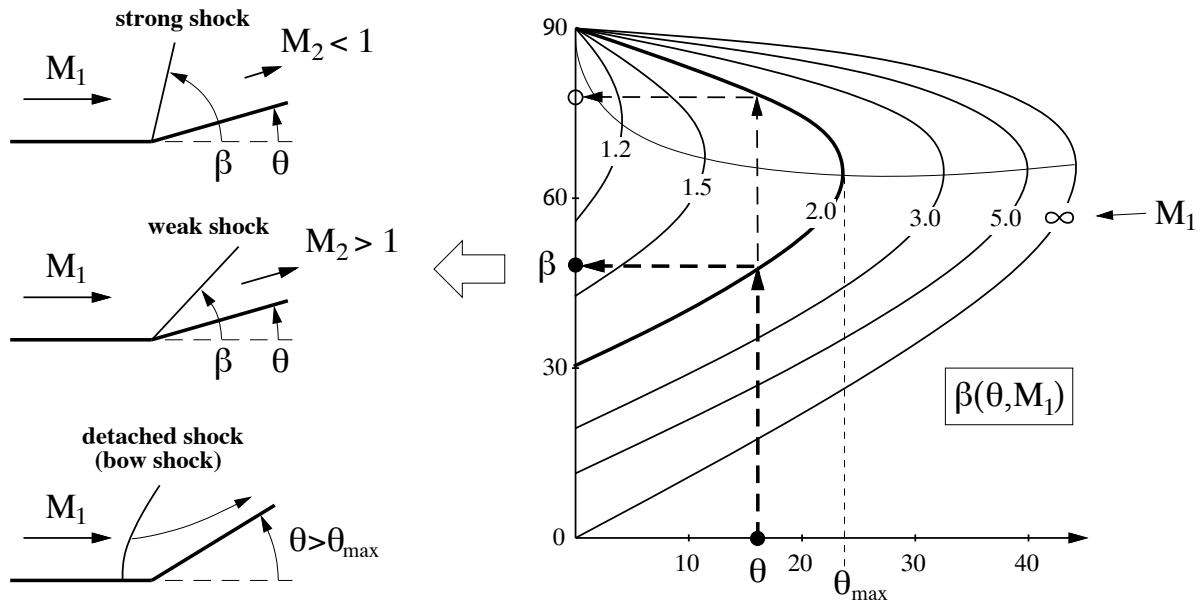
Starting from the known upstream Mach number  $M_1$  and the flow deflection angle (body surface angle)  $\theta$ , the oblique-shock analysis proceeds as follows.

$$\theta, M_1 \xrightarrow{\text{Eq.(13)}} \beta \xrightarrow{\text{Eq.(6)}} M_{n_1} \xrightarrow{\text{Eqs.(7)-(12)}} M_{n_2}, M_2, \frac{\rho_2}{\rho_1}, \frac{p_2}{p_1}, \frac{h_2}{h_1}, \frac{p_{o2}}{p_{o1}}$$

Use of equation (13) in the first step can be problematic, since it must be numerically solved to obtain the  $\beta(\theta, M_1)$  result. A convenient alternative is to obtain this result graphically,

from an oblique shock chart, illustrated in the figure below. The chart also reveals a number of important features:

1. There is a maximum turning angle  $\theta_{\max}$  for any given upstream Mach number  $M_1$ . If the wall angle exceeds this, or  $\theta > \theta_{\max}$ , no oblique shock is possible. Instead, a *detached shock* forms ahead of the concave corner. Such a detached shock is in fact the same as a bow shock discussed earlier.
2. If  $\theta < \theta_{\max}$ , two distinct oblique shocks with two different  $\beta$  angles are physically possible. The smaller  $\beta$  case is called a *weak shock*, and is the one most likely to occur in a typical supersonic flow. The larger  $\beta$  case is called a *strong shock*, and is unlikely to form over a straight-wall wedge. The strong shock has a subsonic flow behind it.
3. The strong-shock case in the limit  $\theta \rightarrow 0$  and  $\beta \rightarrow 90^\circ$ , in the upper-left corner of the oblique shock chart, corresponds to the normal-shock case.



# Fluids – Lecture 18 Notes

1. Prandtl-Meyer Waves
2. Shock-Expansion Theory (Supersonic Airfoils)

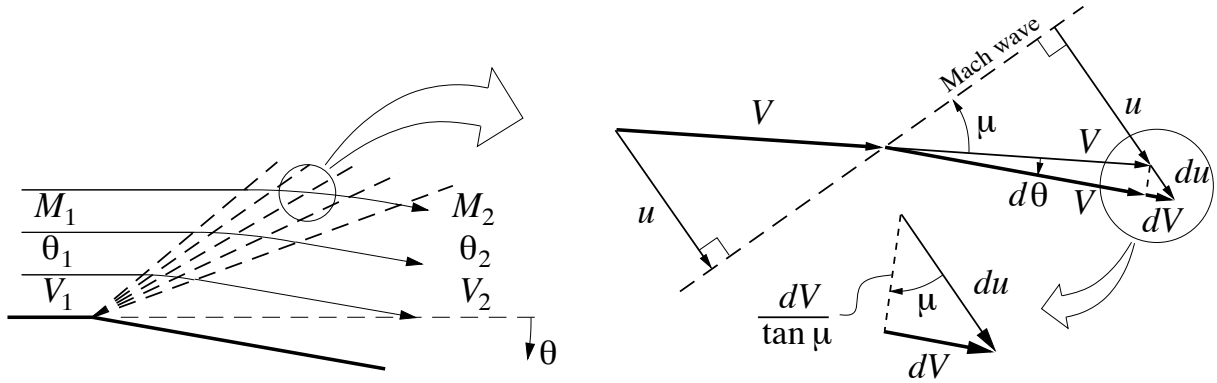
Reading: Anderson 9.6, 9.7

## Prandtl-Meyer Waves

### Wave flow relations

An expansion fan, sometimes also called a *Prandtl-Meyer expansion wave*, can be considered as a continuous sequence of infinitesimal Mach expansion waves. To analyze this continuous change, we will now consider the flow angle  $\theta$  to be a flowfield variable, like  $M$  or  $V$ .

Across each Mach wave of the fan, the flow direction changes by  $d\theta$ , while the speed changes by  $dV$ . Oblique-shock analysis dictates that only the normal velocity component  $u$  can change across any wave, so that  $dV$  must be entirely due to the normal-velocity change  $du$ .



From the  $u$ - $V$  and  $du$ - $dV$  velocity triangles, it is evident that  $d\theta$  and  $dV$  are related by

$$d\theta = \frac{dV}{\tan \mu} \frac{1}{V}$$

assuming  $d\theta$  is a small angle. With  $\sin \mu = 1/M$ , we have

$$\frac{1}{\tan \mu} = \frac{\cos \mu}{\sin \mu} = \frac{\sqrt{1 - \sin^2 \mu}}{\sin \mu} = \frac{\sqrt{1 - 1/M^2}}{1/M} = \sqrt{M^2 - 1}$$

and so the flow relation above becomes

$$d\theta = \sqrt{M^2 - 1} \frac{dV}{V} \quad (1)$$

This is a differential equation which relates a change  $d\theta$  in the flow angle to a change  $dV$  in the flow speed throughout the expansion fan.

### Prandtl-Meyer Function

The differential equation (1) can be integrated if we first express  $V$  in terms of  $M$ .

$$V = M a = M a_o \left( 1 + \frac{\gamma - 1}{2} M^2 \right)^{-1/2}$$

$$\begin{aligned}
\ln V &= \ln M + \ln a_o - \frac{1}{2} \ln \left( 1 + \frac{\gamma-1}{2} M^2 \right) \\
\frac{dV}{V} &= \frac{dM}{M} - \frac{1}{2} \left( 1 + \frac{\gamma-1}{2} M^2 \right)^{-1} \frac{\gamma-1}{2} 2M dM \\
\frac{dV}{V} &= \frac{1}{1 + \frac{\gamma-1}{2} M^2} \frac{dM}{M}
\end{aligned}$$

Equation (1) then becomes

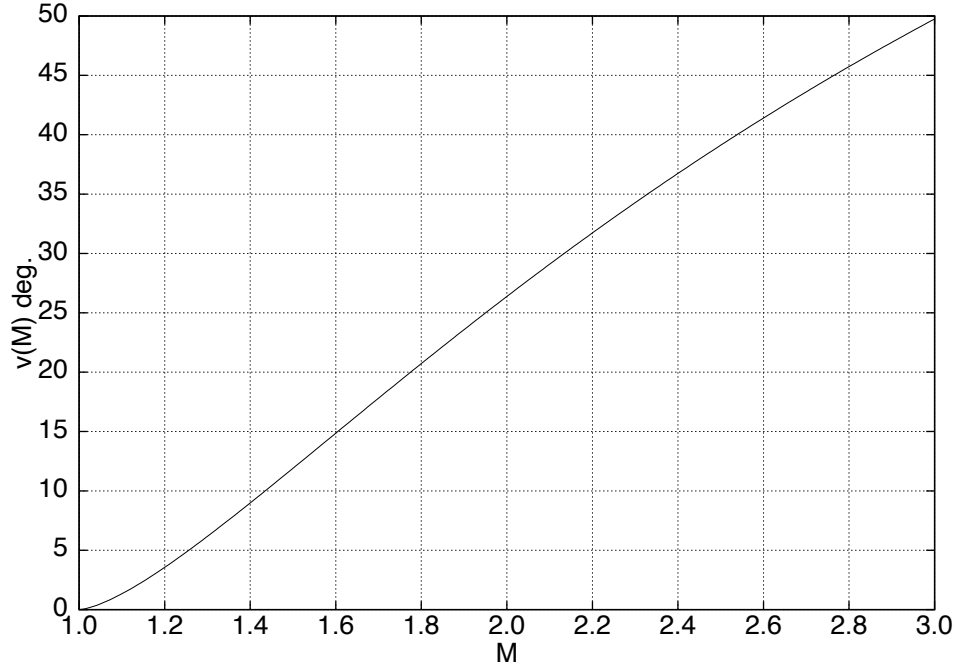
$$d\theta = \frac{\sqrt{M^2 - 1}}{1 + \frac{\gamma-1}{2} M^2} \frac{dM}{M} \quad (2)$$

which can now be integrated from any point 1 to any point 2 in the Prandtl-Meyer wave.

$$\begin{aligned}
\int_{\theta_1}^{\theta_2} d\theta &= \int_{M_1}^{M_2} \frac{\sqrt{M^2 - 1}}{1 + \frac{\gamma-1}{2} M^2} \frac{dM}{M} \\
\theta_2 - \theta_1 &= \nu(M_2) - \nu(M_1)
\end{aligned} \quad (3)$$

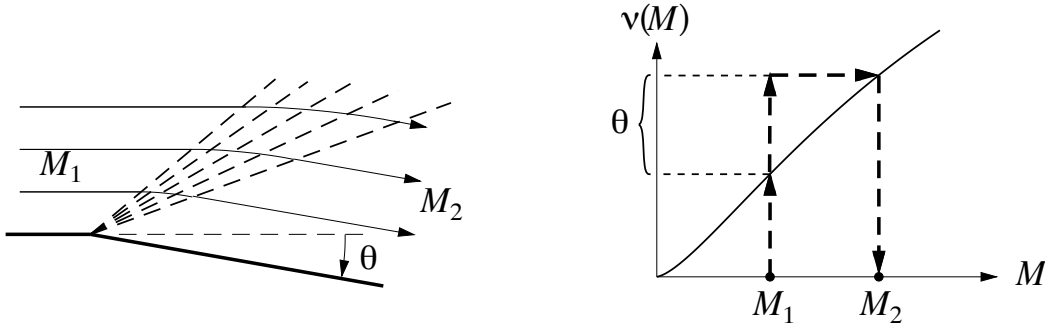
$$\text{where} \quad \nu(M) \equiv \sqrt{\frac{\gamma+1}{\gamma-1}} \arctan \sqrt{\frac{\gamma-1}{\gamma+1} (M^2 - 1)} - \arctan \sqrt{M^2 - 1} \quad (4)$$

Here,  $\nu(M)$  is called the *Prandtl-Meyer function*, and is shown plotted for  $\gamma = 1.4$ .



Equation (3) can be applied to any two points within an expansion fan, but the most common use is to relate the two flow conditions before and after the fan. Reverting back to our previous notation where  $\theta$  is the total turning of the corner, the relation between  $\theta$  and the upstream and downstream Mach number is

$$\theta = \nu(M_2) - \nu(M_1) \quad (5)$$



This can be considered an implicit definition of  $M_2(M_1, \theta)$ , which can be evaluated graphically using the  $\nu(M)$  function plot, as shown in the figure.

## Shock-Expansion Theory

The combination of oblique-shock relations and Prandtl-Meyer wave relations constitutes *Shock-Expansion Theory*, which can be used to determine the flow properties and forces for simple 2-D shapes in supersonic flow.

### Flat-plate supersonic airfoil

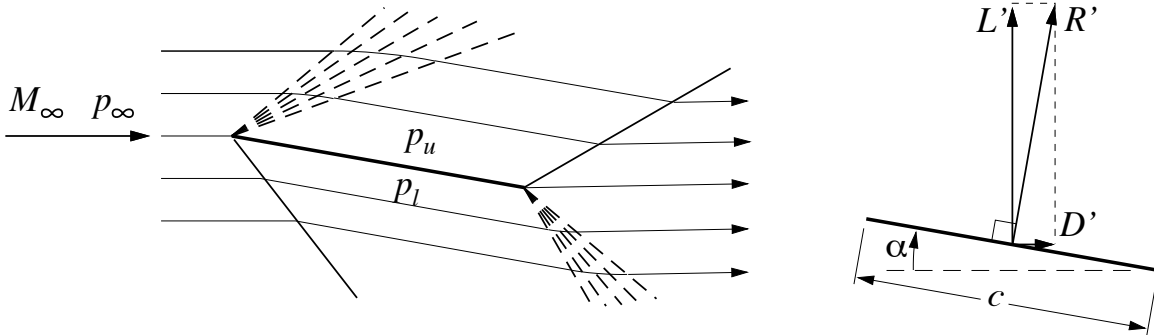
A flat plate is the simplest supersonic airfoil. When set at an angle of attack  $\alpha$ , the leading edge point effectively is a convex corner to the upper surface flow, with turning angle  $\theta = \alpha$ . The upper flow then passes through the resulting Prandtl-Meyer expansion, which increases its Mach number from  $M_1 = M_\infty$ , to a larger value  $M_2 = M_u$ . The latter is implicitly determined via the Prandtl-Meyer relation (5).

$$\alpha = \nu(M_u) - \nu(M_\infty) \quad \rightarrow \quad M_u(M_\infty, \alpha)$$

The corresponding upper-surface pressure is then given by the isentropic relation.

$$p_u = p_\infty \left( \frac{1 + \frac{\gamma-1}{2} M_\infty^2}{1 + \frac{\gamma-1}{2} M_u^2} \right)^{\gamma/(\gamma-1)}$$

Conversely, the leading edge is a concave corner to the bottom surface flow, which then sees a pressure rise through the resulting oblique shock. The lower-surface Mach number  $M_\ell$  and pressure  $p_\ell$  are obtained from oblique-shock relations, with  $M_1 = M_\infty$ ,  $\theta = \alpha$  as the inputs.



The pressure difference produces a resultant force/span  $R'$  acting normal to the plate, which can be resolved into lift and drag components.

$$\begin{aligned} R' &= (p_\ell - p_u) c \\ L' &= (p_\ell - p_u) c \cos \alpha \\ D' &= (p_\ell - p_u) c \sin \alpha \end{aligned}$$

It's worthwhile to note that this supersonic airfoil has a nonzero drag even though the flow is being assumed inviscid. Hence, d'Alembert's Paradox definitely does not apply to supersonic 2-D flow. The drag  $D'$  computed here is associated with the viscous dissipation occurring in the oblique shock waves, and hence is called *wave drag*. This wave drag is an additional drag component in supersonic flow, and must be added to the usual viscous friction drag, and also the induced drag in 3-D cases.

# Fluids – Lecture 19 Notes

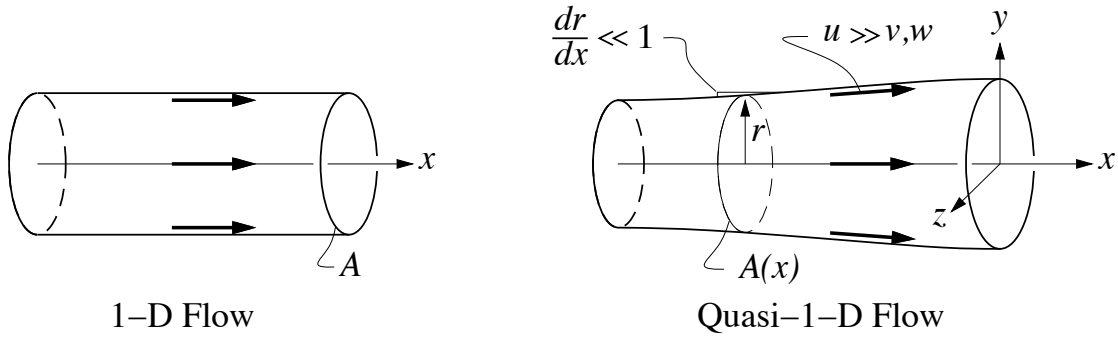
## 1. Compressible Channel Flow

Reading: Anderson 10.1, 10.2

## Compressible Channel Flow

### Quasi-1-D Flow

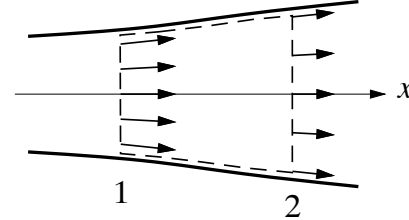
A *quasi-one-dimensional flow* is one in which all variables vary primarily along one direction, say  $x$ . A flow in a duct with slowly-varying area  $A(x)$  is the case of interest here. In practice this means that the slope of the duct walls is small. Also, the  $x$ -velocity component  $u$  dominates the  $y$  and  $z$ -components  $v$  and  $w$ .



### Governing equations

Application of the integral mass continuity equation to a segment of the duct bounded by any two  $x$  locations gives

$$\begin{aligned} \oint \rho \vec{V} \cdot \hat{n} dA &= 0 \\ -\rho_1 u_1 \iint_1 dA + \rho_2 u_2 \iint_2 dA &= 0 \\ -\rho_1 u_1 A_1 + \rho_2 u_2 A_2 &= 0 \end{aligned}$$



The quasi-1-D approximation is invoked in the second line, with  $u$  and  $\rho$  assumed constant on each cross-sectional area, so they can be taken out of the area integral.

Since stations 1 or 2 can be placed at any arbitrary location  $x$ , we can define the duct *mass flow* which is constant all along the duct, and relates the density, velocity, and area.

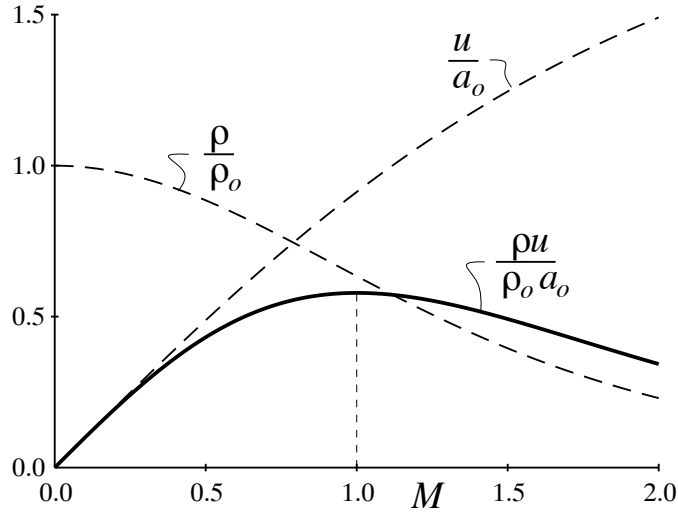
$$\rho(x) u(x) A(x) \equiv \dot{m} = \text{constant} \quad (1)$$

If we assume that the flow in the duct is isentropic, at least piecewise-isentropic between shocks, the stagnation density  $\rho_o$  and stagnation speed of sound  $a_o$  are both constant. This allows the normalized  $\rho$  and  $u$  to be given in terms of the Mach number alone.

$$\frac{\rho}{\rho_o} = \left(1 + \frac{\gamma-1}{2} M^2\right)^{-\frac{1}{\gamma-1}} \quad (2)$$

$$\frac{u}{a_o} = \frac{M a}{a_o} = M \left(1 + \frac{\gamma-1}{2} M^2\right)^{-\frac{1}{2}} \quad (3)$$

$$\frac{\rho u}{\rho_o a_o} = M \left(1 + \frac{\gamma-1}{2} M^2\right)^{-\frac{\gamma+1}{2(\gamma-1)}} \quad (4)$$



The figure shows these variables, along with the normalized *mass flux*, or  $\rho u$  product, all plotted versus Mach number.

The significance of  $\rho u$  is that it represents the inverse of the duct area, or

$$A \sim \frac{1}{\rho u}$$

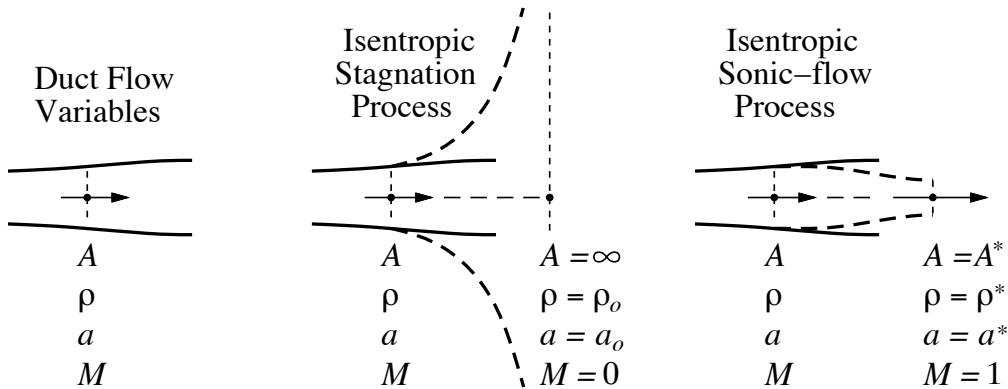
It is evident that the maximum possible mass flux occurs at a location where locally  $M = 1$ . This can be proven by computing

$$\frac{d}{dM} \left( \frac{\rho u}{\rho_o a_o} \right) = (1 - M^2) \left( 1 + \frac{\gamma - 1}{2} M^2 \right)^{-\frac{\gamma - 3}{2(\gamma - 1)}}$$

which is clearly zero at  $M = 1$ . Therefore, the duct must have a local minimum, or *throat*, wherever  $M = 1$ .

### Sonic conditions

In the development above, the stagnation conditions  $\rho_o$  and  $a_o$  were used to normalize the various quantities. For compressible duct flows, it is very convenient to also define *sonic conditions* which can serve as alternative normalizing quantities. These are defined by a hypothetical process where the flow is sent through a duct of progressively reduced area until  $M = 1$  is reached, shown in the figure along with the familiar stagnation process.



The resulting quantities at the hypothetical sonic throat are denoted by a  $()^*$  superscript. The advantage of the sonic-flow process is that it produces a well-defined *sonic throat area*



$A^*$ , while for the stagnation process  $A$  tends to infinity, and cannot be used for normalization. The ratios between the stagnation and sonic conditions are readily obtained from the usual isentropic relations, with  $M = 1$  plugged in. Numerical values are also given for  $\gamma = 1.4$ .

$$\begin{aligned}\frac{\rho^*}{\rho_o} &= \left(1 + \frac{\gamma-1}{2}\right)^{-\frac{1}{\gamma-1}} = 0.6339 \\ \frac{a^*}{a_o} &= \left(1 + \frac{\gamma-1}{2}\right)^{-\frac{1}{2}} = 0.9129 \\ \frac{p^*}{p_o} &= \left(1 + \frac{\gamma-1}{2}\right)^{-\frac{\gamma}{\gamma-1}} = 0.5283\end{aligned}$$

The sonic flow area  $A^*$  can be obtained from the constant mass flow equation (1). For the sonic-flow process we have

$$\dot{m} = \rho u A = \rho^* u^* A^*$$

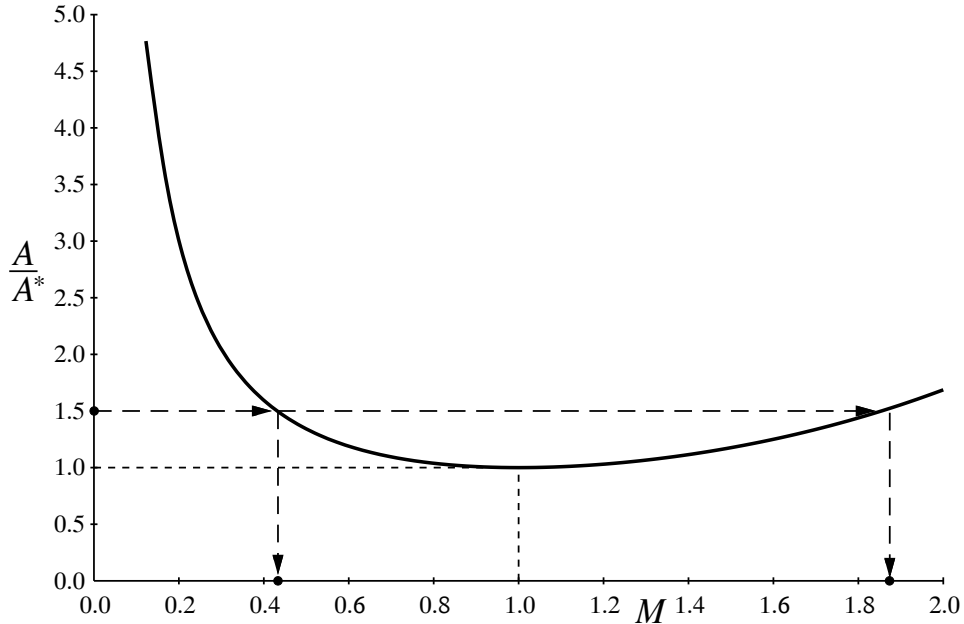
and we also note that  $u^* = a^*$  since  $M = 1$  at the sonic throat. Therefore,

$$\frac{A}{A^*} = \frac{\rho^* a^*}{\rho u} = \frac{\rho^* \rho_o}{\rho_o \rho} \frac{a^* a_o}{a_o u}$$

Using the previously-defined expressions produces

$$\frac{A}{A^*} = \frac{1}{M} \left[ \frac{2}{\gamma+1} \left( 1 + \frac{\gamma-1}{2} M^2 \right) \right]^{\frac{\gamma+1}{2(\gamma-1)}} \quad (5)$$

This is the *area-Mach relation*, which is plotted in the figure below for  $\gamma = 1.4$ , and is also available in tabulated form. It uniquely relates the local Mach number to the area ratio  $A/A^*$ , and can be used to “solve” compressible duct flow problems. If the duct geometry  $A(x)$  is given, and  $A^*$  is defined from the known duct mass flow and stagnation quantities, then  $M(x)$  can be determined using the graphical technique shown in the figure, or using the equivalent numerical table.



Once  $M(x)$  is determined, any remaining quantity of interest, such as  $\rho(x)$ ,  $u(x)$ ,  $p(x)$ , etc., can be computed from the isentropic or adiabatic relations such as (2) and (3).

Note that for any given area  $A(x)$ , two solutions are possible for the given mass flow: a subsonic solution with  $M < 1$ , and a supersonic solution with  $M > 1$ . Which solution corresponds to the actual flow depends on whether the flow upstream of that  $x$  location is subsonic or supersonic.

There is also the possibility of shock waves appearing in the duct. This introduces additional complications which will be considered later.

# Fluids – Lecture 20 Notes

## 1. Laval Nozzle Flows

Reading: Anderson 10.3

### Laval Nozzle Flows

#### Subsonic flow and choking

Consider a duct with a throat, connected at its inlet to a very large still air reservoir with total pressure and enthalpy  $p_r$ ,  $h_r$ . The duct exit is now subjected to an adjustable *exit static pressure*  $p_e$ , sometimes also called the *back pressure*. As  $p_e$  is gradually reduced from  $p_r$ , air will flow from the reservoir to the exit with a mass flow  $\dot{m}$ . We first note that the stagnation conditions are known from the reservoir values all along the duct.

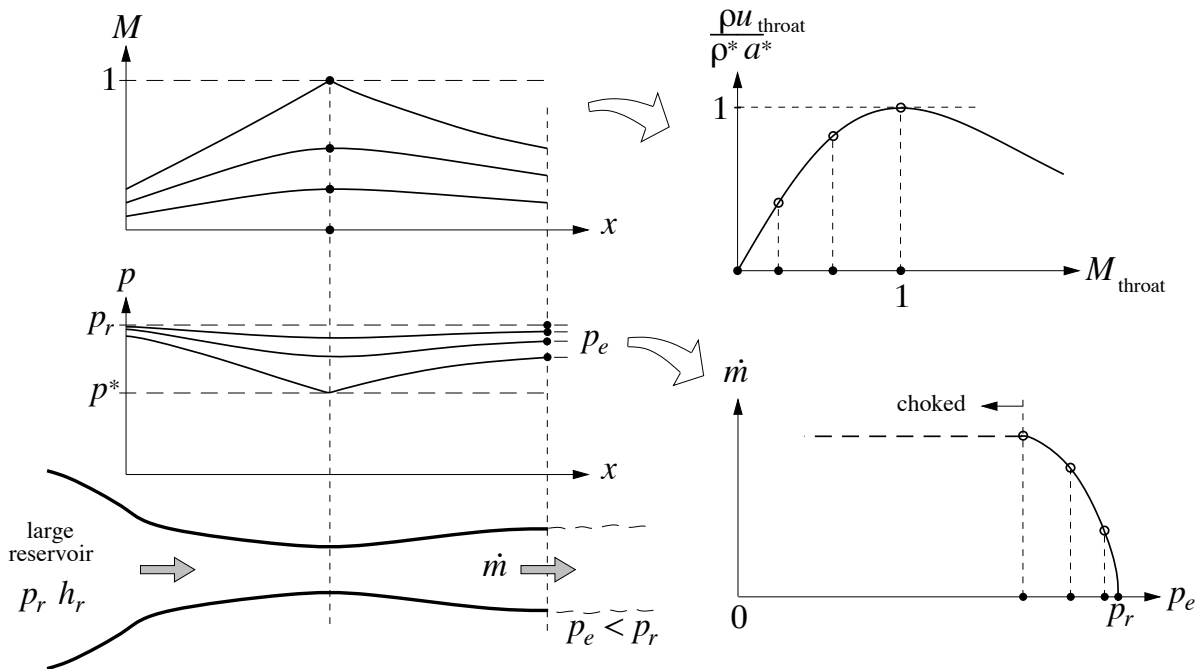
$$p_o = p_r \quad , \quad a_o^2 = (\gamma - 1)h_o = (\gamma - 1)h_r \quad , \quad \rho_o = \frac{\gamma p_o}{(\gamma - 1)h_o} = \frac{\gamma p_r}{(\gamma - 1)h_r}$$

If we assume isentropic flow,  $\dot{m}$  can be computed with the isentropic relations applied at the exit, using the known exit pressure  $p_e$  and known exit area  $A_e$ .

$$M_e^2 = \frac{2}{\gamma - 1} \left[ \left( \frac{p_o}{p_e} \right)^{\frac{\gamma - 1}{\gamma}} - 1 \right]$$

$$\dot{m} = \rho_e u_e A_e = \frac{\gamma p_o}{\sqrt{(\gamma - 1)h_o}} M_e \left( 1 + \frac{\gamma - 1}{2} M_e^2 \right)^{-\frac{\gamma + 1}{2(\gamma - 1)}} A_e \quad (1)$$

The observed relation between  $p_e$  and  $\dot{m}$  is shown on the bottom right in the figure. As  $p_e$  is reduced,  $\dot{m}$  will first increase, but at some point it will level off and remain constant even if  $p_e$  is reduced all the way to zero (vacuum). When  $\dot{m}$  no longer increases with a reduction in  $p_e$ , the duct is said to be *choked*.



If we examine the various flow properties along the duct, it is evident that the onset of choking coincides with the *throat* reaching  $M = 1$  locally. This also corresponds to the

mass flux  $\rho u$  at the throat reaching its maximum possible value  $\rho^* a^*$ , which is given by

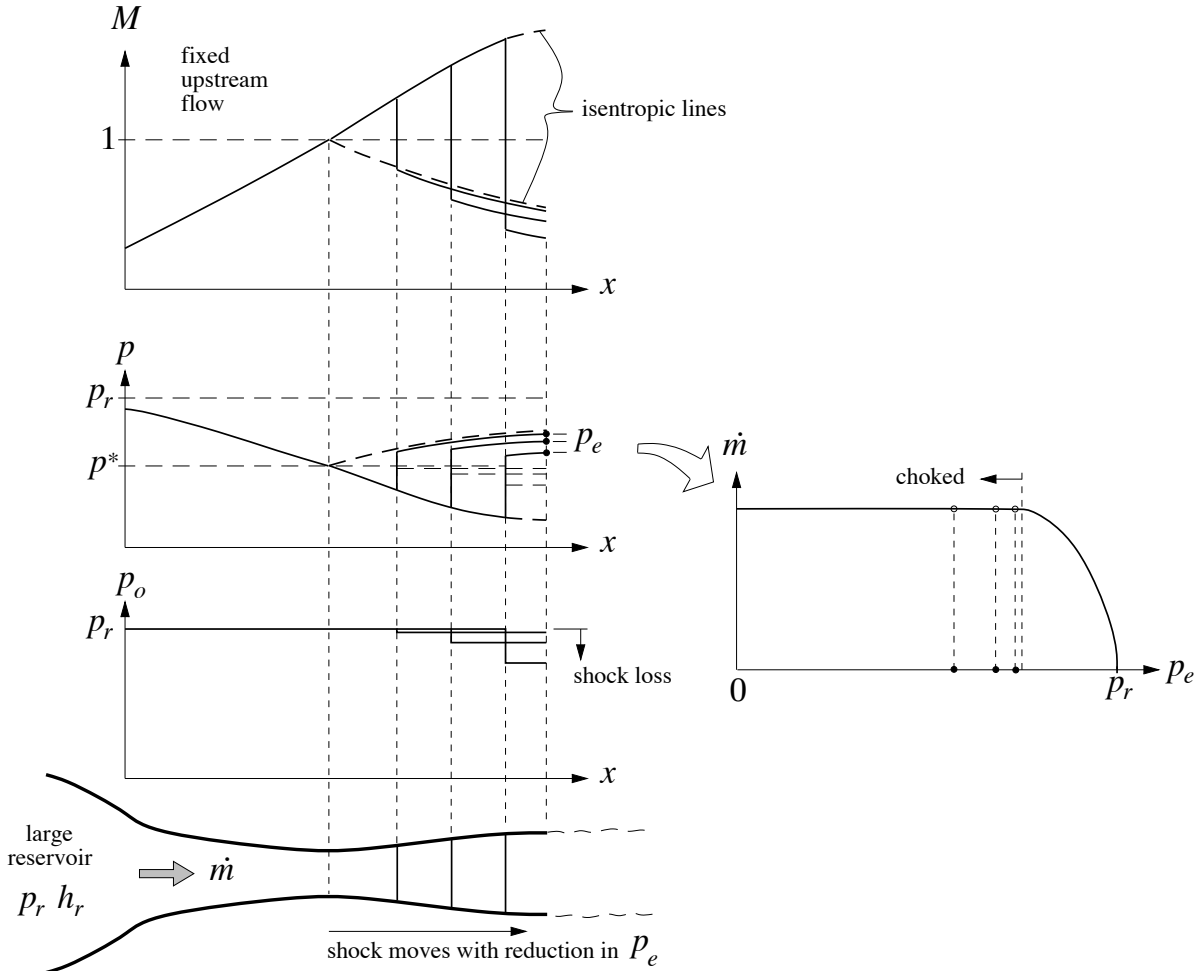
$$\rho^* a^* = \rho_o a_o \frac{\rho^* a^*}{\rho_o a_o} = \frac{\gamma p_r}{\sqrt{(\gamma-1)h_r}} \left(1 + \frac{\gamma-1}{2}\right)^{-\frac{\gamma+1}{2(\gamma-1)}} \quad (2)$$

Therefore, the only way to change the mass flow of a choked duct is to change the reservoir's total properties  $p_r$  and/or  $h_r$ .

### Choked flow with normal shock

When the back pressure is reduced below the level required to reach choking, a new flow pattern emerges, called a *Laval nozzle flow*, with the following important features:

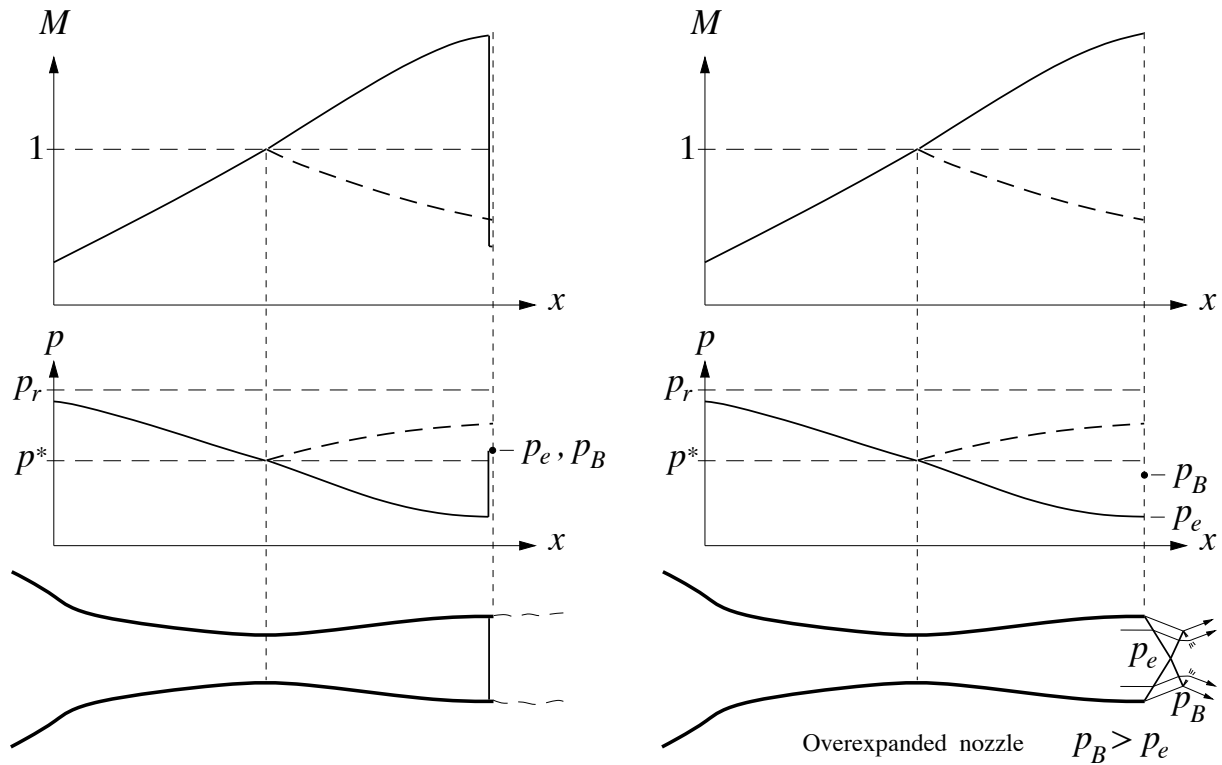
1. The flow upstream of the throat no longer changes with  $p_e$ , but remains the same as at the choking-onset condition. This is consistent with the mass flow being fixed.
2. The flow behind the throat becomes supersonic. The Mach number continues to increase and pressure to decrease as the area increases downstream.
3. A *normal shock* forms in the duct, and the flow behind the shock returns to subsonic. The Mach number then decreases and pressure increases towards  $p_e$  as the area increases.
4. The shock incurs a total pressure loss, so that  $p_o < p_r$  behind the shock all the way to the exit. Both  $p(x)$  and  $M(x)$  behind the shock are then lower than what they would be with isentropic flow at the onset of choking.



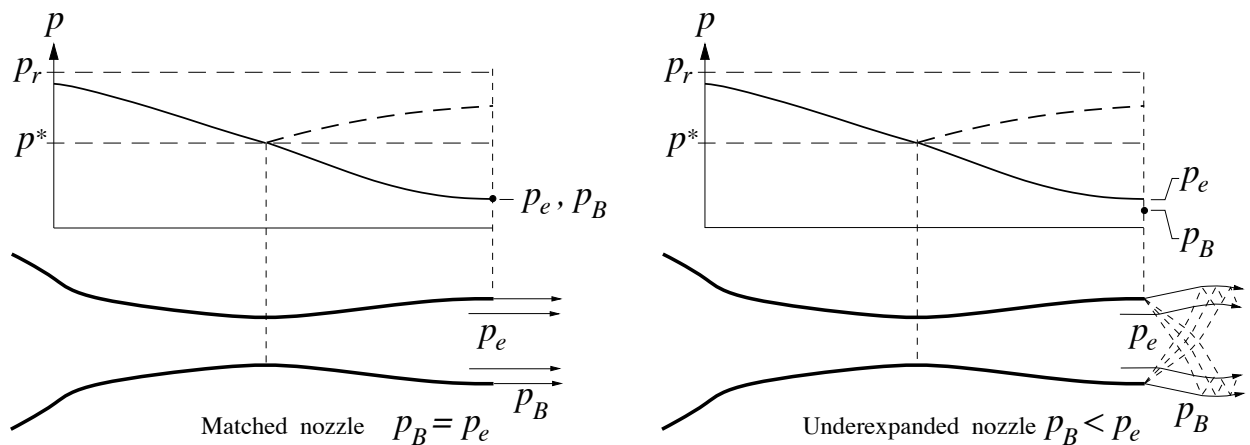
## Supersonic-exit flows

With sufficiently low back pressure, the shock can be moved back to nearly the exit plane. If the back pressure is reduced further, below the sonic pressure  $p^*$ , the exit flow becomes supersonic, leading to three possible types of exit flow. In these cases it is necessary to distinguish between the exit pressure  $p_e$  of the duct flow, and the back pressure  $p_B$  of the surrounding air, since these two pressures will in general no longer be the same.

Overexpanded nozzle flow. In this case,  $p_B < p^*$ , so the exit flow is supersonic, but  $p_B > p_e$ , so the flow must adjust to a higher pressure. This is done through oblique shocks attached to the duct nozzle edges. The streamline at the edge of the jet behaves much like a solid wall, whose turning angle adjusts itself so that the post-shock pressure is equal to  $p_B$ .



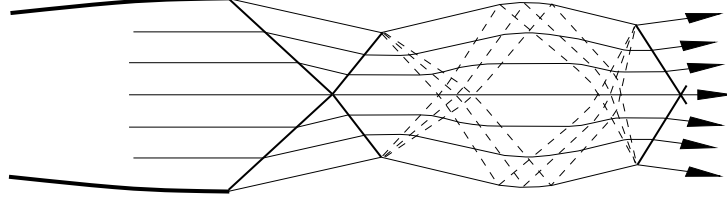
Matched nozzle flow. In this case, the back pressure is reduced further until  $p_B = p_e$ . The duct nozzle flow comes out at the same pressure as the surrounding air, and hence no turning takes place.



Underexpanded nozzle flow. In this case, the back pressure is reduced below the isentropic exit pressure, so that  $p_B < p_e$ . The duct nozzle flow must now expand to reach  $p_B$ , which is done through expansion fans attached to the duct nozzle edges.

### Jet shock diamonds

In the underexpanded and overexpanded nozzle flows, each initial oblique shock or expansion fan impinges on the opposite edge of the jet, turning the flow away or towards the centerline. The shock or expansion fan reflects off the edge, and propagates back to the other side, repeating the cycle until the jet dissipates through mixing. These flow patterns are known as *shock diamonds*, which are often visible in the exhaust of rocket or jet engines.



### Determination of Choked Nozzle Flows

A common flow problem is to determine the exit conditions and losses of a given choked nozzle with prescribed reservoir stagnation conditions  $p_r$ ,  $h_r$ , and a prescribed exit pressure  $p_e$ . We first note that the mass flow in this situation is known, and given by combining relation (2) with the fact that  $A^* = A_t$  for a choked throat.

$$\dot{m} = \rho^* a^* A_t = \frac{\gamma p_r}{\sqrt{(\gamma-1)h_r}} \left(1 + \frac{\gamma-1}{2}\right)^{-\frac{\gamma+1}{2(\gamma-1)}} A_t \quad (\text{choked}) \quad (3)$$

To then determine the exit conditions corresponding to this mass flow, we use the mass flow expression (1), but recast it in terms of the (known) exit static pressure rather than the (unknown) exit total pressure. We can also set  $h_o = h_r$  for adiabatic flow.

$$\dot{m} = \frac{\gamma p_e}{\sqrt{(\gamma-1)h_r}} M_e \left(1 + \frac{\gamma-1}{2} M_e^2\right)^{1/2} A_e \quad (\text{choked}) \quad (4)$$

Equating (3) and (4), and squaring the result, gives

$$M_e^2 \left(1 + \frac{\gamma-1}{2} M_e^2\right) = \left(\frac{p_r}{p_e} \frac{A_t}{A_e}\right)^2 \left(1 + \frac{\gamma-1}{2}\right)^{-\frac{\gamma+1}{\gamma-1}} \quad (\text{choked}) \quad (5)$$

This is a quadratic equation for  $M_e^2$ , which can be solved with a specified righthand side. The exit total pressure is then obtained via its definition.

$$p_{oe} = p_e \left(1 + \frac{\gamma-1}{2} M_e^2\right)^{\frac{\gamma}{\gamma-1}}$$

The overall nozzle total pressure ratio  $p_{oe}/p_r$  is due to the loss across the shock, so that

$$\frac{p_{oe}}{p_r} = \left(\frac{p_{o2}}{p_{o1}}\right)_{\text{shock}} = f(M_1) \quad (6)$$

where  $f(M_1)$  is the shock total pressure ratio function, also available in tabulated form. Equation (6) therefore implicitly determines  $M_1$  just in front of the shock, which together with the universal flow area function  $A/A^* = f(M)$  determines the nozzle area at the shock.